MECHANICAL DESIGN, CONTROL AND EVALUATION OF A PORTABLE REHABILITATION DEVICE FOR UPPER ARM

A Thesis

by

YUNYI WANG

Submitted to the Office of Graduate and Professional Studies of
Texas A&M University
in partial fulfillment of the requirements for the degree of

MASTER OF SCIENCE

Chair of Committee,	Sheng-Jen Hsieh
Committee Members,	John Buchanan
	Won-Jong Kim
Head of Department,	Andreas A. Polycarpou

May 2015

Major Subject: Mechanical Engineering

ABSTRACT

There is a need for functional and effective rehabilitation devices for humans with upper arm injuries. Existing devices are either too heavy, not portable, or do not have 4 degrees-of-freedom (DOF) on the forearm. In this research, a new mechanical mechanism and structure were proposed to cover the full range of wrist and forearm motions as much as possible without sacrificing portability. In addition, the proposed device would have 4 DOF including wrist flexion/extension and radial/ulnar deviation, forearm pronation/supination, and elbow flexion/extension motions. A prototype was developed using 3D printed parts weighing about 840 grams; by comparison, the lightest existing device weighs 2 kg. The portability of the proposed design can increase the flexibility of therapy programs. Experiments were carried out to evaluate the prototype based on workspace, backlash, accuracy, and repeatability. Compared to other devices, the prototype covers all 4 DOF and the motion range coverage ranges from 88% to 100%. These improvements allow the prototype to cover more complicated rehab motions and thereby facilitate performance of difficult daily activities such as rise from a chair and tie a scarf. Experiments results also suggest that the performance of the prototype is very accurate and repeatable. For example, the average backlash is about 1 mm, the accuracy of the device is about ±0.8 mm, and the repeatability is about 0.5 mm.

Future directions include (1) evaluate the effectiveness of the prototype with human subjects, (2) add a human centered sensory and computing device to monitor and provide customized rehabilitation motions.

ACKNOWLEDGEMENTS

I would like to thank my committee chair, Dr. Hsieh, and my committee members, Dr. Buchanan, and Dr. Kim for their guidance and support throughout the course of this research.

Thanks also go to all my friends and my parents for their love, big support, and encouragement throughout the course of my graduate studying in Texas A&M University.

NOMENCLATURE

DOF	Degree-of-Freedom
STDEV	Standard Deviation
CNC	Computer Numerical Control
FDM	Fused Deposition Modeling
ABS	Acrylonitrile Butadiene Styrene
PLA	Polylactic Acid
PWM	Pulse Width Modulation
PID	Proportional-Integral-Derivative
CPU	Central Processing Unit
LED	Light-Emitting Diode

TABLE OF CONTENTS

Page

Page

Page

LIST OF FIGURES

Page

Page

Page

Page

LIST OF TABLES

Page

LIST OF CHARTS

Page

1 INTRODUCTION

1.1 **Introduction**

Human upper limb motor disability caused by stroke or spinal cord injury can seriously reduce a patient's quality of life. Fortunately, studies indicate that post stroke patients still have motor adaptation or motor learning ability. Based on this motor learning mechanism, movements gained in specific training or therapy can be generalized to untrained tasks [1], [2]. In this way, patients' ability of doing daily activities can be improved by participating in some specifically designed therapy [3], [4]. Studies and research has also shown that robot-assisted rehabilitation or training has significant positive results for motor disability recovery [5] [6] [7] [8]. Therefore, different types of upper limb rehabilitation robots are being developed for robotic rehabilitation studies and robotic therapy. They are effective in motor learning [1] [9], and they are better for biomechanical and clinical measures than conventional therapy [10]. Some recent studies indicate that the repetitive movement exercise and training with specific motion patterns, rather than robotic assistance, is the primary stimulus to motor learning and recovery [11], [12], [13], [14]. Thus, more researchers have started studying rehabilitation effects with certain motion patterns for each joint.

Most existing rehabilitation robots for upper limb therapy are setup with grounded serial robots. They can provide different type of exercise for both shoulder and elbow by controlling the position and posture of user's hand. Thus, this type of rehabilitation device would be mentioned as end-effector type rehabilitation robots in this paper. Many clinic studies have proven the effectiveness of these types of rehabilitation methods. However, since the end-effector type robots provide exercise by just controlling patient's hand or forearm position and/or orientation, they lack abilities of controlling each joint's movement independently. Comparing to

end-effector type robots, exoskeleton type robots can provide better controlled moving patterns for each joint or even each degree of freedom without affecting other joints.

However, exoskeleton type rehabilitation robots show their restrictions in clinic study too. Most of these exoskeleton type rehabilitation robots have limited range of motion for the wrist. Also, their performance of combination motion of two degree of freedom of wrist is usually poorer than end-effector type rehabilitation robots. Besides, by definition of exoskeletons, all these type robots are supposed to be wearable and portable. Thus, it is obvious that heavy weight exoskeleton rehabilitation robots may affect its performance. Most of these defects are caused by robot's mechanical mechanism directly. Thus, a study of mechanical mechanism for upper limb exoskeleton type rehabilitation device is significance. For such motivation, this research will mainly focus on the mechanical mechanism of the upper limb rehabilitation device.

1.2 **Literature Review**

1.2.1 Overview of exist upper limb rehabilitation robots

There are so many rehabilitation robots have been developed for upper limb robotic therapy. Generally, they could be classified in two types: end-effector type and exoskeleton type. End-effector type rehabilitation systems are setup by special end-effector and grounded serial robots. They are usually big in size and heavy in weight. They provide arm exercise by controlling position and orientation of user's hand or forearm. End-effector robots are been widely used in rehabilitation study. Multi degree of freedom robot arms can control the position and orientation of the end point (hand or forearm) precisely. However these types of robots can only control the position and posture of one point, the provided exercise usually combines different motions of different joints. In order to study and control different motions of each joint

independently, more and more semi-exoskeleton or full exoskeleton type rehabilitation robots have been developed. Existing exoskeleton type rehabilitation devices have their limitations too. They are either not portable, do not have all 4 degree-of-freedom on forearm, or cannot cover full range of motion of each degree-of-freedom. Following sections present information about several well-known end-effector type rehabilitation robots and exoskeleton type rehabilitation robots.

1.2.2 End-effector type rehabilitation robots

MIT – MANUS is one of the earliest rehabilitation robots [15] [16]. This typical end effecter type robot was developed more than 20 years ago. . The patient is required to grab the handle of the robot. MANUS has a planar version and a vertical version. The planar version is a planar linkages structure robot with two active degrees of freedom. With this design, the end point of the robot can reach any position on its working surface. The vertical version has one degree of freedom. The handle bar is driven by a linear motor.

ADLER is a robotic therapy system developed for upper arm rehabilitation. In this project, the HapticMaster robot is been used [17]. HapticMaster is a cylindrical robot developed by the robot company – FCS Control Systems [18]. As any other cylindrical robot, HapticMaster has one rotary joint and two prismatic joints. The Approximate working volume of HapticMaster arm is 80 liters. In the ADLER therapy system, a Gimbal has been used as the end effector. The structure is like a Cardan joint. This Gimbal does not have any active degrees of freedom, but has three passive degrees of freedom. They are yaw relative to the HapticMaster arm, pitch relative to the Gimbal. The HapticMaster has been developed with sensitive force sensor. The force signal will be used for calculating the position, velocity, and acceleration. The HapticMaster use this information as feedback for its inner closed loop control. GENTLE/s

therapy system is almost the same as the ADLER system [19]. The only difference is that GENTLE/s uses a one active degree of freedom system and two passive degrees of freedom for the Gimbal Provided by FCS as the end effector.

Masahiro Takaiwa and his partner developed a wrist rehabilitation device and published their result in 2005 [20]. Their device is a parallel robot with six pneumatic cylinders basically. . The parallel robot, also known as parallel manipulator or Stewart platform, is a mechanical mechanism that uses several linear actuators to support one single moving platform. A typical parallel robot has six linear actuators paired both on a base plate and moving plate. A typical parallel robot has six degree of freedom. There are three Cartesian linear movements plus pitch, yaw, and roll. Thus, the parallel robot can control the position of a moving plate center very precisely in its 3D working space. Besides, because of its high rigidity, the parallel robot can provide high speed movement too. However, parallel robots have drawbacks too. Compared to serial robots, the working space is very limited for parallel robot. This is also a drawback of Takaiwa's project. The robot can only provide about 37% range of motion for forearm pronation and supination. Besides, the nonlinear behavior of the parallel robot also increases controlling difficulty.

UHD (Universal Haptic Drive) is a rehabilitation robot developed for arm and wrist. This is an end effector type rehabilitation robot [21]. The user is required to grab the handle on UHD. From a mechanical mechanism point of view, the UHD is a solid bar with a lockable cardan joint on it which can be swung in the X and Y direction. So the UHD has two active degrees of freedom and two passive degrees of freedom. However, the two active degrees of freedom are independent. It means that the bar can only swing along either X axis or Y axis, not in XY surface. When the cardan joint is locked, the UHD guides user's arm motion in either the X direction or the Y direction with -15° to +15°. When the cardan joint is unlocked and

assuming user's arm can stay at UHD's center line all the time, ± 15° bar swing can cause the handle bar rotate in ± 45°. A sliding mechanism is applied on the actuated bar to eliminate handle bar height change in operation. Since the actuated bar can only swing along either the X direction track or the Y direction of the track, the UHD can only provide one motion at a time. That is why the classification table shows 1+1+1+1 in "Exercisable arm DOF" column.

NeReBot is a rehabilitation robot for an upper arm [22]. There are three wires attached to the forearm support. By changing the length of three wires, the robot can manipulate the user's forearm posture. Thus it can provide forearm pronation and supination in a narrow range of motion, and a relatively wider range of motion for elbow flexion / extension and shoulder horizontal rotation. The PID controller is applied for the robot. But since no sensor is mentioned for detecting any information from user's arm, the interface between user and the manipulator is unclear. MariBot is a newer version of NeReBot. MariBot use the same mechanism for manipulating user's arm [23]. But MariBot added two more rotary joints on arm. These two degrees of freedom helps the MariBot adjust the position of forearm support. In this way, the MariBot can provide some range of motion for the shoulder in the vertical rotation.

MIME, stands for Mirror Image Movement Enabler, is a robotic therapy provider for elbow and shoulder [24]. Because the research group used an industry robot directly this program is famous for its study about mirror image movement, not the rehabilitation robot. In this program, a 6 DOF serial type articulated robot – PUMA 560 – is been used. The user's forearm is controlled by the robot. By controlling forearm's position and orientation, the robot can provide exercises for the elbow and shoulder easily. Like other end effector type robots, the PUMA 560 cannot control each joint's movement separately. Besides, since the PUMA 560 is a real industry robot, it can provide massive torque and speed. Thus, patient's safety becomes an issue.

Similarly to the MIME project, REHAROB robotic system used two industry robots instead of just one [25]. Two ABB industry robots are used in REHAROB system. One attaches to user's forearm, and the other one attaches to user's upper arm. By using two robots on same arm, forearm and upper arm's position and orientation could be controlled even more accurately. Also, elbow motion could be provided precisely. However, as mentioned above, patient's safety issue may become a big problem by using one or more powerful industry robots.

1.2.3 Exoskeleton type rehabilitation robots

CRAMER (Closed-chain Robot for Assisting in Manual Exercise and Rehabilitation) is a newly developed rehabilitation robot for the wrist and forearm [26]. The mechanical structure of the robot is relatively simple. There are two 2 DOF rods mounted in parallel. A Nintendo Wii remote is connected between two rods as a gripper for the user. However, since the griper is connected to the two rods passively, the lockup drawback may happen as mentioned in the paper. For the control system, the CRAMER is driven by four independent servo motors. As mentioned in the paper, the developer hasn't figured out the interface problem between Wii games and the CRAMER. Thus, the feedback signal from Wii remoter cannot be sent back to servo motors' controller. Besides, stroke patients or spinal cord injured patients may lack the ability to press buttons on Wii remoter which is another drawback of the CRAMER.

MentorTM is the rehabilitation robot specifically for the wrist [27]. It only has one degree of freedom which is wrist flexion and extension. The mechanical structure of the MentorTM is a planar linkage structure. Because of the characteristics of the planar linkages structure, the MentorTM can provide the coordinated motion of the fingers and wrist. The robot is driven by one pneumatic muscle actuator. By mounting a potentiometer on the pivot point, the controller can know the position of the wrist. Also, the EMG signal detected by sensors affects

the controller's decision making. Thus, the control system of MentorTM is a close loop system. Since fingers only have flexion and extension motion, very similar mechanical structure has been used in finger rehabilitation robots [28] [29].

Researcher Dustin Williams and his group at Massachusetts Institute of Technology developed a robot for wrist rehabilitation about 14 years ago [30]. This robot is one of the earliest wearable devices developed just for wrist and forearm pronation and supination. They used a curved slider for forearm pronation and supination, and a differential type side-mounted handle for two wrist degree of freedom. In this mechanical mechanism, wrist structure and forearm structure are independent. Two independent brushless motors drive two end bevel gears. With different combinations of rotation directions of two end bevel gears, the handle can provide flexion, extension, abduction, and adduction motions. Since the curve slide is not a full circle, the range of motion of pronation and supination is limited. However on the other hand this robot is very easy to wear due to the half ring curve slide design. The device used encoder as its position feedback sensor.

ARMin is a well-developed rehabilitation robot for arm [31]. ARMin is a semi-skeleton and semi-articulated robot. This 6 degree of freedom robotic arm can provide 3 shoulder degrees of freedom and 1 elbow degree of freedom. Shoulder motions are provided by the end-effector type articulated robotic arm, and the elbow structure is wearable. A two degree of freedom forearm extension could be attached on ARMin. It covers forearm pronation and supination, and wrist flexion and extension. The mechanical mechanism for forearm and wrist are independent. For forearm rotation, a semicircular slide guide has been used. It is driven by one independent actuator. A planar linkage structure, driven by a linear actuator, has been used for wrist flexion and extension.

ARMin II is the newer version of the ARMin robot [32]. ARMin II reduced two degree of freedom in articulated robotic arm part. Thus, ARMin II only uses a three degree of freedom articulated robot to simulate shoulder motions. Comparing to the ARMin range of motion of the shoulder, ARMin II has about the same range of motions for all three degrees of freedom. But the ARMin II articulated robotic arm's structure is simpler and lighter. Another semi-exoskeleton rehabilitation robot is called L-EXO [33]. Its structure is almost the same as ARMin II, but without wrist degree of freedom.

RUPERT is a newly developed wearable exoskeleton type rehabilitation robot for upper arms [34]. It covered four degrees of freedom. They are shoulder horizontal flexion and extension, elbow flexion and extension, forearm supination and pronation, and wrist flexion and extension. The mechanical structure of RUPERT is relatively simple. If four pneumatic muscle actuators are into consideration, the mechanical mechanism of RUPERT is the combination of four planar linkages structure. In this robot, potentiometers are used as position sensors in all joint axes. RUPERT uses pneumatic muscles as actuators. Thus, the robot includes a pneumatic system. In this device, a compressed air tank is used instead of an air compressor. It is worth mentioning that pneumatic muscles have been more and more commonly used in exoskeleton type robots. Comparing to other linear actuators, like linear motors and pneumatic cylinders, pneumatic muscles are flexible, lightweight, simple, and have a higher power to weight ratio. Japanese researcher H. Kobayashi and his partner developed a muscle suit without rigid frames for upper limbs [35].

The MAHI exoskeleton is specially designed for arm rehabilitation [36]. The robot has five degrees of freedom in total. It can cover all wrist motions, forearm motion, and elbow motion. The mechanical mechanism for elbow joint is a single pin type joint. The joint is driven directly by a motor. The forearm rotation mechanism is separated from the wrist mechanism too.

It is a smaller ring rotating inside a bigger ring. The mechanism for the wrist part is a parallel robot. Different to the parallel robot discussed above in Takaiwa's project, MAHI's parallel structure is a so called the 3-RPS platform. Since this is an exoskeleton type robot, MAHI uses rings instead of plates as base part and moving part of the parallel structure. The moving ring connected to actuators by ball joints, and the base ring connected to actuators by pin joints. With this design, the parallel structure has three degree of freedom. They are height change along Z axis, and two rotation about X and Y axes. Two rotational degree of freedom can be applied to provide wrist flexion / extension motions and radial / ulnar motions. Since the human arm does not have any prismatic movement, the height change movement of the parallel structure cannot provide motor exercise for the arm. But it is a good structure for user customized settings. Similar to other parallel robots, this 3-RPS parallel platform has limited working space too.

The RiceWrist is a modification of the MAHI [37]. RiceWrist only focuses on wrist motion and forearm motion, and it adopted all wrist and forearm designs from MAHI. However, the RiceWrist has a mechanical interface with MIME robot (PUMA 560). The RiceWrist-S is the newest version of RiceWrist [38]. The research group published their result in 2013. RiceWrist-S did not adopt parallel structure for wrist motion. Instead of using a parallel structure, the RiceWrist-S used a serial mechanism - two links driven by two motors. Therefore, the RiceWrist-S has wider range of motion for wrist.

Table 1.1 shows the classification of End-effector type rehabilitation robot. Table 1.2 and Table 1.3 shows the classification of exoskeleton type rehabilitation robot.

	DOF of the device (active)	DOF of the device (passive)	Exercisable arm DOF	Wrist flexion / extension	Wrist radial / ulnar	Forearm pronation / supination	Elbow flexion / extension	Shoulder	Control system	Notes
ADLER [17]	3	3	3				√	√	Close	Haptic Master robot
GENTLE/s [19]	4	2	3				√	√		
(PPM) [20]	6	0	3	√	√	√			Close	Parallel
UHD [21]	2	3	1+1+1+1	√		√	√		Close	One motion at a time
NeReBot [22]	3	0	3			√	√	√	Close (PD)	Wire manipulated
MariBot [23]	5	0	4			√	√	√	Close	Wire manipulated
MIME [24]	6	0	4				√	√	Close	PUMA 560
REHAROB [25]	6+6	0	5			√	√	√	Close	ABB industry
MIT-MANUS [15]	2	0	2				√	√	Close	

Table 1.1: Classification of End-effector type rehabilitation robots

	DOF of the device (active)	DOF of the device (passive)	Exercisable arm DOF	Wrist flexion	Wrist extension	Wrist radial	Wrist ulnar	Forearm pronation	Forearm supination	Elbow flexion / extension
CRAMER [26]	4	1	3	90°	70°	10°	15°	90°	85°	/
Mentor™ [27]	1	0	1	~ 50°	~55°	/	/	/	/	/
(ARFWR) [30]	3	0	3	50°	55°	20°	30°	76°	76°	/
ARMin [31]	6+2	0	6	45°	30°	/	/	70°	70°	5° - 119°
ARMin II [32]	6	0	6	50°	79°	/	/	90°	90°	0 - 135°
RUPERT [34]	4	0	4	60°	30°	/	/	45°	45°	0 - 125°
L-EXO [33]	5	0	5	/	/	/	/	90°	90°	0 - 105°
MAHI [36]	5	0	4	(42°)	(42°)	30°	30°	90°	90°	0 - 90°
RiceWrist [37]	4	0	3	42°	42°	> 19°	> 33°	90°	90°	/
RiceWrist-S [38]	3	0	3	60°	60°	35°	35°	90°	90°	/

Table 1.2: Classification of exoskeleton type rehabilitation robots I

	Control system	Feedback	Weight (on arm)	Portable	Note
CREAMER [26]	Open	Wii remote	1.5 kg	Grounded	No way to have clinical test
Mentor™ [27]	Close	Position (pot); EMG	TBD	Portable	Pneumatic muscle
(ARFWR) [30]	Close	Position (Encoder)	TBD	Grounded	Brushless motor
ARMin [31]	Close	Position (Encoder)	1.5 kg (forearm exoskeleton only)	Grounded	Forearm extension needed; 3 shoulder DOF included
ARMin II [32]	Close	Position (Encoder)	14.5 kg counterweight	Grounded	3 shoulder DOF included
RUPERT [34]	Close	Position (pot)	0.624 kg (upper arm)	Portable	1 shoulder DOF included
L-EXO [33]	Close	Force feedback	5 kg on arm	Grounded	3 shoulder DOF included
MAHI [36]	Close	Position (Encoder)	> 4 kg	Grounded	RiceWrist's original design
RiceWrist [37]	Close	Position (Encoder)	2 kg	Grounded	MIME interface
RiceWrist-S [38]	Close	Position (Encoder)	TBD	Grounded	Newer version of RiceWrist

Table 1.3: Classification of exoskeleton type rehabilitation robots II

1.3 **Research Problem**

A human arm has 7 degrees of freedom in total. They are shoulder vertical rotation, shoulder horizontal rotation, shoulder internal and external rotation, elbow flexion and extension, forearm pronation and supination, wrist flexion and extension, and wrist adduction and abduction. Since this research has been scoped to wrist, forearm, and elbow 4 degrees-of-freedom, any shoulder motions would not be discussed in this paper.

As mentioned above, exoskeleton type of rehabilitation robots is preferred for specific motion pattern study of neuro-rehabilitation. But listed existing exoskeleton type rehabilitation robots have some defects. They are either not portable; do not have all 4 degrees-of-freedom on forearm; or cannot cover full range of motion of some or all degrees-of-freedom. Limited coverage on degree-of-freedom and range of motion will restricted the development of training motion patterns. Also, a non-portable rehabilitation system will further restrict the time and location of physical therapy program.

1.4 **Research Objectives**

The aim of this research is to find a better mechanical mechanism which can provide more than 90% of full range of motions of wrist flexion/extension and radial/ulnar deviation, forearm pronation and supination, and elbow flexion and extension without sacrificing its portability.

Based on the biomechanical studies of human normal range of motions of wrist, forearm, and elbow [39] [40] [41] [42], the following Table 1.4 shows the quantified range of motion criteria of the problem stated above. Figure 1.1 shows proposed wrist's range of motion in figure.

	Wrist				Forearm		Elbow
	Flexion	Extension	Radial deviation	Ulnar deviation	Pronation	Supination	Flexion / Extension
Full ROM	0 - 85°/90°	0 - 75°/80°	0 - 15°/25°	0 - 35°/45°	0 - 70°	0 - 85°	0 - 145°
Functional ROM	0 - 54°	0 - 60°	0 - 17°	0 - 30°	0 – 50°	0 - 50°	30° - 130°
Objective	0 - 80°	0 - 80°	0 - 35°	0 - 35°	0 - 90°	0 - 90°	0 - 145°

Table 1.4: Normal, functional and proposed range of motion of wrist and elbow combination

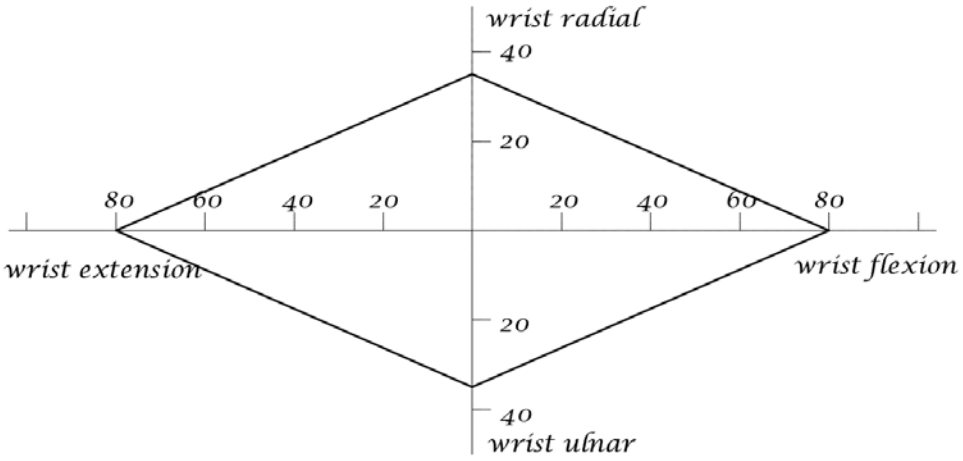

Figure 1.1: Wrist performance of proposed rehabilitation robot

For the weight of the rehabilitation robot, 1 kilogram on the arm is the aim of the proposed device. Besides, whether the device is portable or not is an important aim too. The criterion for satisfying this aim is to see if the device needs additional grounded support.

The scope of this research has been limited to the rehabilitation device's mechanism design, structure design, prototype making, and its performance tests. The prototype would not be commercial level equipment, and no clinic study or human subject experiments would be

included in this research. In addition, the budget and tool resources may become two other limitations for making the prototype. Main research processes are listed as following:

1) To study which mechanical mechanisms is proper for upper limb joints and develop a mechanical structure that can provide the desired range of motion of each joint.
2) To build a prototype for testing proposed mechanism and structure.
3) To develop a proper control systems which can make the device have the desired performance.
4) Test the prototype's performance without human subject.

1.5 **Research Assumptions**

The values of full range of motion are statistics result and varies based on subject's gender, race, age, and other factors. Thus, many organizations and researchers published slightly different ranges of each joint's motion. Table 1.5 listed several published motion ranges of wrist, forearm, and elbow. Centers for Disease Control and Prevention published results separately by gender and age, so their values are no included in the table. But their reference values are in similar ranges.

Normal ROM	Elbow extension/flexion	Forearm pronation/supination	Wrist extension/flexion	Wrist radial/ulnar
American Society for Surgery of the Hand	0/145°	70°/85°	70°/75°	20°/35°
Physical Therapy Merck Manual Professional	0/160°	90°/90°	70°/90°	25°/65°
American Academy of Orthopaedic Surgeons	0/150°	80°/80°	70°/80°	20°/30°
Orthopaedic Examination, Evaluation, and Intervention	0/150°	80°/80°	60°/60°	20°/30°
National Taiwan University	0/145°	70°/85°	80°/85° (avg)	20°/40° (avg)

Table 1.5: Several published normal range of motion reference values.

The definition of full range of motion in this paper will base on values in Table 1.5. Furthermore, the prototype would be built with non-flexible components. So the prototype may not fit every people. Therefore, the research has following assumptions:

1) Wrist's full range of motion is 0 - 70° for extension, 0 - 85° for flexion, 0 - 20° for radial deviation, and 0 - 35° for ulnar deviation.
2) Forearm's full range of motion is 0 - 80° for pronation, and 0 - 85° for supination.
3) Elbow's full range of motion is 0 - 145° for flexion.
4) The size of the prototype is based on developer's size.

1.6 **Anticipated Contributions and Results**

The proposed device accommodates 4 degrees-of-freedom: elbow flexion and extension, wrist flexion and extension and ulnar and radial, forearm pronation and supination. Comparing to other exoskeleton rehabilitation robots, the proposed device is a small sized, portable and light weight robot. It has low backlash, high accuracy, and high repeatability.

Because of the material selection, manufacturing method and accuracy of the assembling process, the final performance results may be poorer than expected. Though the prototype may fail in reaching full designed workspace, it should still provide wider range movement of wrist, forearm and elbow than most existing exoskeleton type rehabilitation robots.

2 MECHANISM DESIGN

The rehabilitation device designed in this research covers two joints (wrist and elbow) of the human upper arm. The combination of these two joints includes four degrees-of-freedom in total. In order to have a better result in the mechanism design, to understand kinematic structure of human's wrist and elbow would be the first step. Kinematics analysis of the wrist and elbow can be used as the main guide for the mechanism design of a fitting forearm rehabilitation device. Mechanism analysis and design will be discussed after the kinematics analysis in the anatomy of human wrist and elbow.

2.1 **Wrist and Forearm Mechanism Design**

2.1.1 Joint structure of the wrist complex

Based on the wrist joint anatomy, there are four different joints are considered at the wrist. They are radiocarpal joint, midcarpal joint, intercarpal joints and distalradioulnar joint (Figure 2.1). The radiocarpal joint is the joint between biconvex proximal row of the carpal bones and the end of the radius and articular disc. This joint involves wrist's flexion/ extension and radial/ ulnar motions. The degrees-of-freedom of this joint is equal to two. The rest position is wrist's slightly extension position. The midcarpal joints are joints between proximal row and distal row. The intercarpal joints are joints between carpal bones in the proximal row and distal row. In other words, midcarpal joints and intercarpal joints are joints between different carpal bones and each joint has slight motion which contributes to wrist flexion/extension and radial/ulnar motions. The distal radioulnar joint is the joint between the convex ulnar head and concave ulnar notch of the radius. This joint is a pivot type joint which is only involved in the forearm's pronation and supination. The degree-of-freedom of the distal radioulnar joint is equal

to one. Thus the wrist joint has two degrees-of-freedom. However, if the motion of distal radioulnar joint is considered and refer the wrist joint as the whole wrist complex, the degrees-of-freedom of the wrist can be considered as 3.

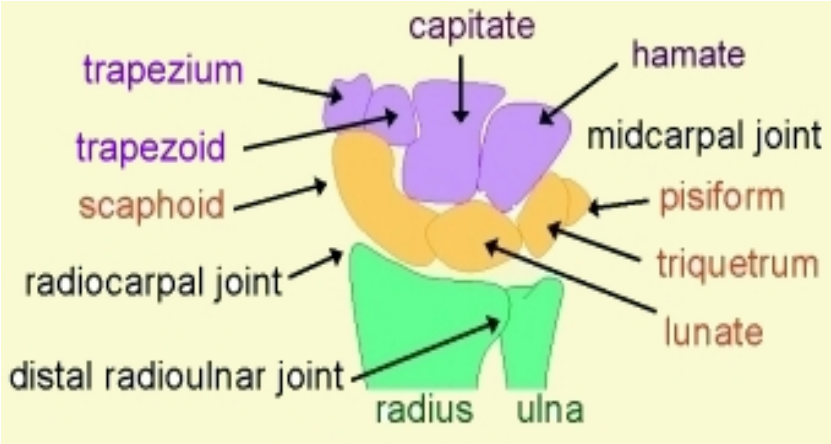

Figure 2.1: Anterior view of wrist complex

2.1.2 Kinematics of the wrist joint

2.1.2.1 Wrist flexion and extension

Both radiocarpal joint and midcarpal joint are involved in this motion. The radiocarpal joint contributes 67% of total motion in wrist extension but only about 40% in wrist flexion motion. The rotation axis is the frontal axis through the center of the capitate (in distal row). The range of motion is about 0 to 85/90 degree of flexion and 0 to 75/80 degree of extension. The range from 10 degree of flexion to 35 degree of extension is the functional range for wrist flexion/ extension.

2.1.2.2 Wrist radial and ulnar

All midcarpal joints, radiocarpal joints and intercarpal joints are involved in this motion where the midcarpal joints contribute most of the motion. The rotation axis is the line perpendicular to the palm plane through the intersection of the capitate and lunate (midcarpal joint). The range of motion is 0 to 15/25 degree of radial and 0 to 35/45 degree of ulnar.

2.1.3 Kinematics of forearm

Though both wrist joint and elbow joint are involved in forearm rotational motion, the forearm rotational degrees-of-freedom was considered more important in wrist mechanism design than elbow mechanism design. Because at the wrist end, there are two more degrees-of-freedom related to forearm rotational motion. But at the elbow end, only one more degree of freedom related to it. Thus, forearm kinematics analysis before wrist mechanism design is necessary.

With proximal radioulnar joint and humeroradial joint in elbow complex and the distal radioulnar joint in wrist complex, the forearm has pronation and supination motion. The axis of rotation passes through the center of the radial head and the distal ulnar head. Thus, this axis is not parallel to the forearm's longitude (Figure 2.2). The range of motion is about 0 to 70 degree of pronation and 0 to 85 degree of supination. The functional range is from 50 degree of pronation to 50 degree of supination.

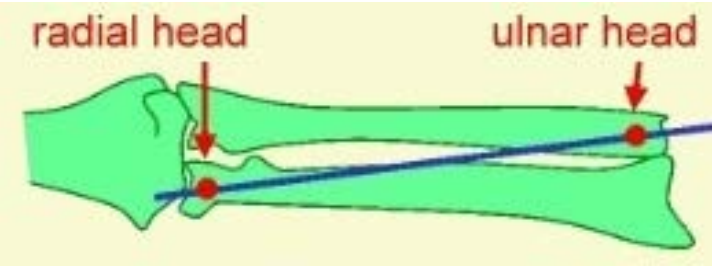

Figure 2.2: Anterior view of forearm. The blue line is the axis of forearm motions.

2.1.4 Mechanical expression of the wrist and forearm

From the kinematic analysis, we could know that the rotation axis of wrist flexion/extension and the rotation axis of wrist radial/ulnar are not intersecting in the same plane theoretically. The distance between these two rotation axes is about four millimeters [43]. Besides, the rotational axis of the forearm is not perfectly parallel to the longitude of arm. Therefore, these three axes are not perfectly perpendicular to each other and are not intersecting at one point. If all three axes are fixed in space, two degree of freedom wrist motions could be represented by a series of two revolute joints which are about four millimeters away, and the forearm rotation could be represented with another rotation joint (Figure 2.3).

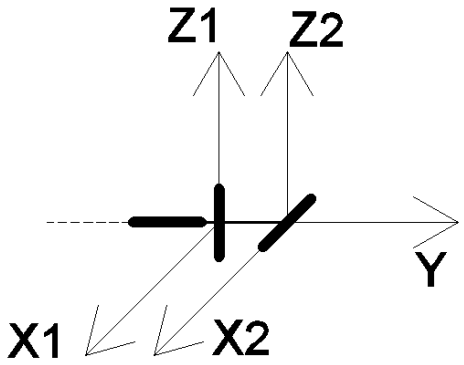

Figure 2.3: Mechanical representation of wrist joint.

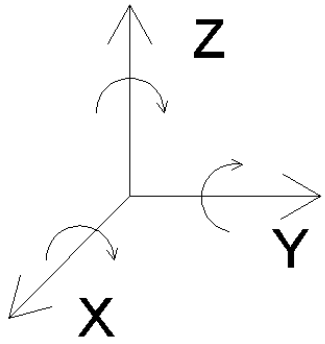

Figure 2.4: Spherical joint representation of wrist joint.

However, human bones are not connected by solid mechanical components. The location of each axis may change slightly because of the size of the arm or other factors. Besides, current study indicates that the location of rotational axis varies slightly with different rotation angles [44]. If we bring the concept of fuzzy logic to this problem, the mechanical expression would be considered to be a good expression if it can fully represent the performance of the joint. Therefore, it is safe to use a spherical joint, which has three rotational degrees-of-freedom, to represent the wrist and forearm complex (Figure 2.4).

2.1.5 Mechanical mechanism design for the wrist

It is obvious that the rehabilitation device can provide high quality exercise if it can fix the forearm and control the orientation of the hand properly. Since this research scoped down to a wearable device only, mechanism of end-effecter type rehabilitation robots (introduced in chapter 1) will not be discussed in the rest of this paper. For wearable devices, there are two ways for it to be mounted on a human arm: side-mount and through-mount. In this paper, all devices or parts for a one degree-of-freedom joint are defined as side-mount devices or parts. This is because that we could always find a position for the device where allowing device's rotation axis along the joint rotation axis. If the joint has two or more degrees of freedom, the side-mount configuration is defined as one where two or more rotation axes of the device do not fully coincide with the joint rotation axes, and the intersecting point of axes usually locates on the device. These types of mechanisms are usually mounted on the side of the arm. The through-mount configuration is defined as having two or more axes of movements of the device fully coinciding with the joint rotation axes, and the intersecting point of axes usually not locates on of the device. These types of mechanisms usually require the user to put their arm in or through

the device. The mechanism design would start with analysis of two different mounting configurations.

2.1.5.1 Side-mount mechanism

Side-mount is the most common and the easiest way to put an external mechanism on human. This method works perfect if the equipment is put on no degree-of-freedom body part or only one degree-of-freedom joint. All human joints are rotational joints. Thus, if the joint only has one degree-of-freedom, the device can always be set up along the rotation axis of the joint (Figure 2.5). For example, there are many commercial level elbow braces, knee braces or finger braces to help keep these joints moving properly. Elbow, knee, and finger joints (distal interphalangeal joints and proximal interphalangeal joints only) only have one rotational degree-of-freedom. All braces for these joints are mounted on the side of the appendage. So the rotation axis of the device is along the rotation axis of the joint. In this way, these braces can keep these joints rotating properly about their axes and help injured joints recover.

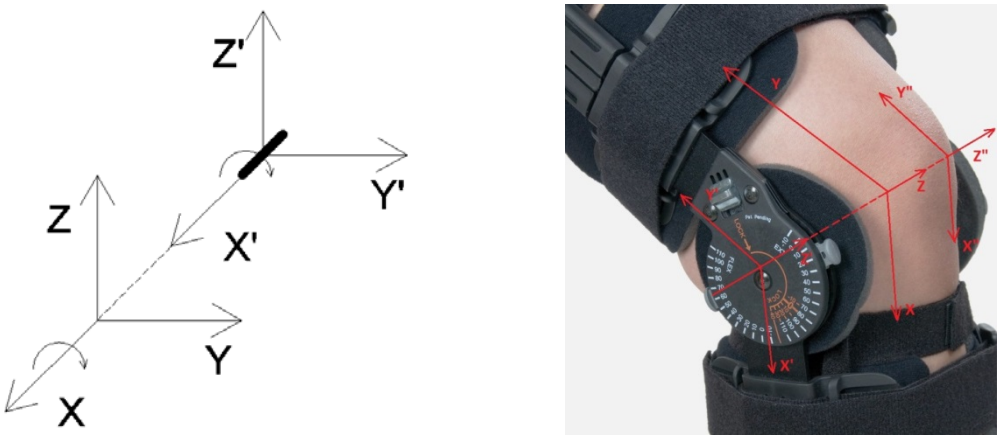

Figure 2.5: Rotational axis aligns joint axis, and an example.

However, there are few braces in market designed for shoulder, wrist, or ankle movements. These joints have two or more degrees-of-freedom and the intersecting point of rotation axes (or the points on the shortest distance path between rotation axes) is inside the joint (Figure 2.6). Since the device or accompanying parts cannot pass through the human body, there is no way for the side-mount device to find a position which allows all the rotation axes to coincide with joint rotation axes. For these joints, the main problem of the side-mount device is the link interference created by not aligning all the rotation axes with joint rotation axes.

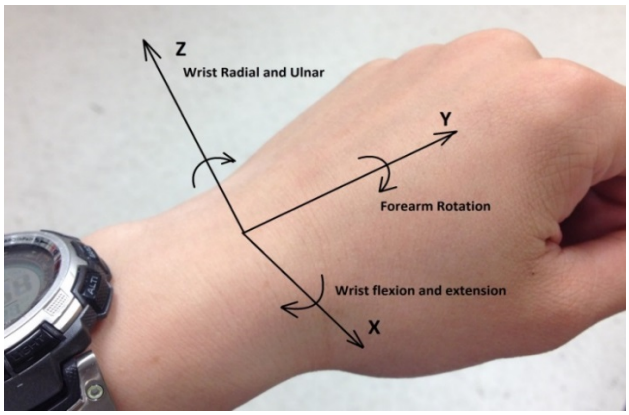

Figure 2.6: Coordinate system of wrist joint.

Link interference is mainly described as the distance change while the links rotate about the axis perpendicular to the plane which they are at. Also this is the main limitation of the range of rotation angle of the links. Figure 2.7 shows the problem caused by the link interference. Assuming two parallel links, link I and link II, are mounted on the frame by universal joints. They are placed on plane XY. Two rotation axes of both universal joints are along X axis and Z axis. The distance between these two links is defined as the minimal distance between any pair of points on the links. Assume the radius of link I is r1, and the radius of link II is r2. Assume the

distance between two universal joints is a. Then set a fixed point A on link I. The shortest distance path between two links, which through point A, will intersect link II at point B. If both links rotate about X axis with the same direction at the same rate, the distance d (d=a-r1-r2) between two links will not change. However, if links are rotating about Z axis, the distance d will decrease with the increasing of rotation angle Θ. The new distance will be d'=a*cos(Θ) -r1-r2. Therefore, the links will collide to each other if the distance d equal to or lower than zero. Since point A is fixed on link I, point B will move towards B' with the increasing of rotation angle Θ. BB'=a*sin(Θ). Actually, both links rotating about the X axis with the same direction at the same rate is the only special case which will not cause link interference.

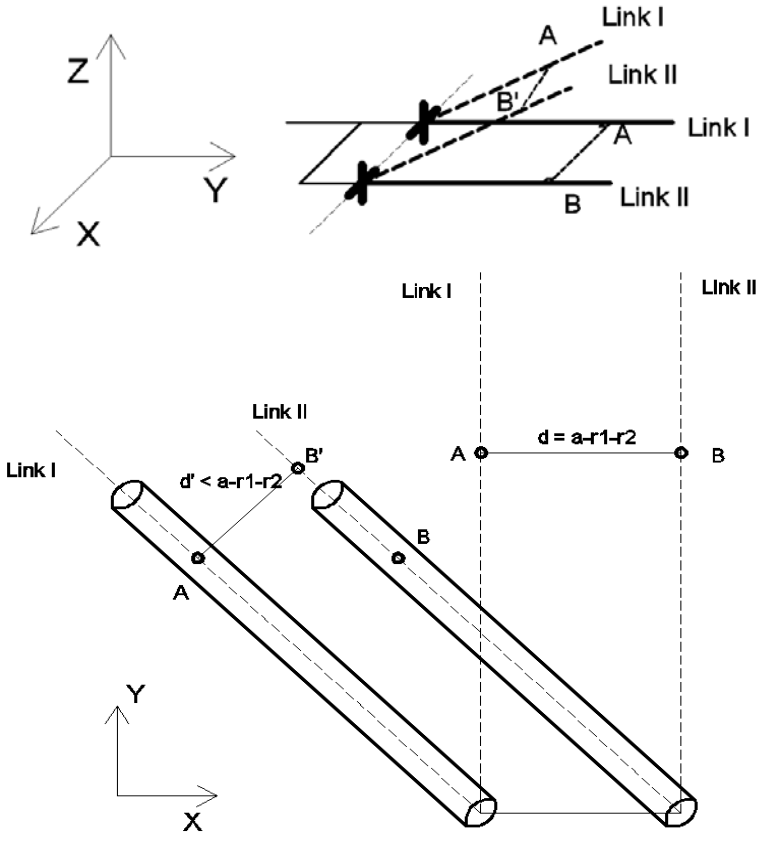

Figure 2.7: Example of link interference in 3D and in XY plane.

Assume link I represents the user's hand, and link II represents the rehabilitation device which is mounted on the side of the user's arm. The distance change between the user's hand and the device while doing the exercise will cause device to be unstable and user uncomfortable. The device needs another passive sliding mechanism be mounted on hand to solve the mount point (point B) movement problem. Clearly, the sliding mechanism will increase the complexity of the device and decrease the device stability when providing exercise. No matter where the hand locates, beside one link or between two links, the link interference cannot be eliminated. Even if the device uses a passive mechanical mechanism to keep the distance between two links, the mount point movement problem still exists. Therefore, a side-mount mechanism may not be a good choice for wrist joint, which has two degrees-of-freedom.

2.1.5.2 Through-mount mechanism

Through-mount mechanisms are especially for joints that have two or more degrees-of-freedom. Through-mount mechanisms allow the user to put their arm into the device structure. Thus, it requires the mechanism to have a rotation axes outside of the device and a coinciding rotational axes of the wrist joint. To meet this requirement, the spatial motion parallel robot, especially orientation manipulators, is the candidate of the wrist mechanism.

After decades of development on parallel robots, there are so many different types of parallel robot, both planar and spatial robots, have been introduced to the public. Theoretically, the six degrees-of-freedom robot can accomplish any motion in space. However, a human wrist joint doesn't have any ability to move linearly. Therefore in the wrist rehabilitation application, three translational degrees-of-freedom (heaving, swaying, and surging) are not necessary. By reducing three translational degrees-of-freedom, the parallel robot becomes a typical spatial orientation manipulator. A Spatial orientation manipulator is a type of parallel robot which

allows three rotations about one point in space. This characteristic of the orientation manipulator makes the through-mount mechanism a reality on the human wrist. Basically, there are three subgroups of spatial orientation manipulators. The first subgroup of orientation manipulator uses a passive constraint mechanism which only allows rotations of the moving platform or the end effecter. The most common passive constraint mechanism is the spherical joint which has three rotational degrees-of-freedom. Thus, the moving platform or the end effecter can only rotate about the spherical joint (Figure 2.8). The second subgroup is the spherical mechanism. There are three spherical chains that share the same point and lead the spherical mechanism (Figure 2.9). This mechanism is also known as the pointing mechanism. The center platform or end effecter can point to any direction in space. Another subgroup orientation robots use special configurations of passive joint axes to make the platform that only has rotational degrees of freedom (Figure 2.10). The Most common orientation manipulators in this subgroup have three UPU chains (or equivalent chains).

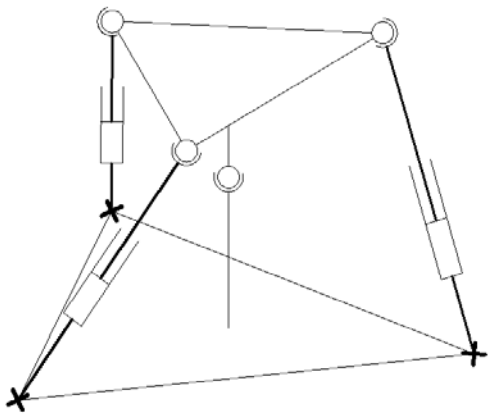

Figure 2.8: Orientation manipulator uses a passive constraint mechanism

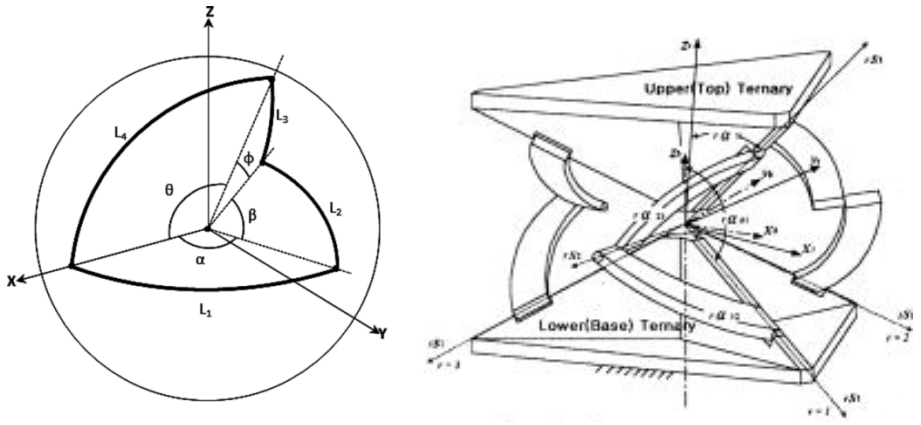

Figure 2.9: Spherical mechanism

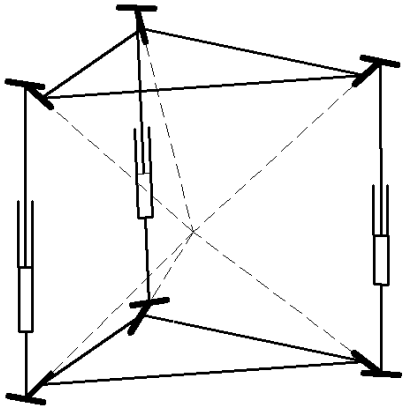

Figure 2.10: Orientation manipulator with special configurations of passive joint axes.

The workspace of the parallel robot used in industry is basically limited by the length of linear actuators or links, passive mechanical joint limits, and the link interference. But if we apply parallel robot configurations to wearable rehabilitation devices, there is one more limitation needs to be considered: the interference between moveable parts and the human body. All spatial orientation mechanisms have three degrees-of-freedom, which can represent all motions of the wrist and forearm. But if we take the arm in to consideration, all orientation mechanism in both the first subgroup and the third subgroup have interference with the arm

when making rotation about Z axis, which represents the forearm rotational motion. Without considering the passive joint limitation, link length limitation and assume the radius of links is zero, spatial orientation mechanisms in both first subgroup and third subgroup can rotate about the Z axis in the range of ±180° (Figure 2.11). However, all links need to cross the structure to realize this rotational motion. In industry, there is no problem, but in wearable rehabilitation devices it causes the interference with arm. Clearly, links cannot pass through the arm to make the moving platform rotate about Z axis. Therefore, the rotation about Z axis needs to be limited for all these spatial orientation mechanisms to become the wrist mechanism. For spatial orientation mechanisms in the first subgroup, the rotation about Z axis could be limited by replacing the spherical joint with a universal joint. For spatial orientation mechanisms in the third subgroup, the rotation about the Z axis could be limited by reducing one degree-of-freedom in each actuation chain. For example, the UPU chain (or equivalent chains) could be replaced by RPU chain (or equivalent chains).

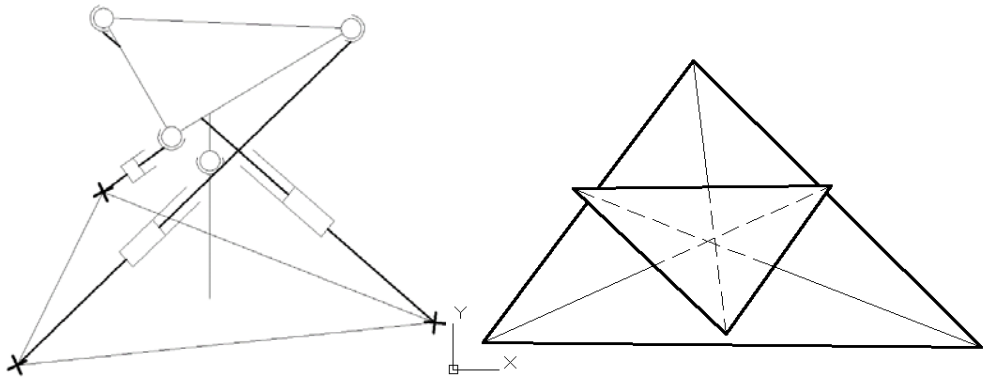

Figure 2.11: Example of link interference in 3D and in XY plane for the 1st and the 3rd subgroups.

The spherical mechanism (the second subgroup orientation mechanism) may or may not have interference with the user's arm if it is used as the wrist mechanism. If we can arrange each spherical chain cleverly, the spherical mechanism could be the perfect mechanism for the wrist and forearm mechanism. The spherical mechanism requires three precise rotary actuators, a firm structure, and a firm base. All these factors require a lot of space and will add a lot of weight on the spherical mechanism. These issues may not be a problem for any grounded or fixed wrist rehabilitation devices. However, since this research is scoped down to portable rehabilitation device for the whole arm, the bulky heavy wrist mechanism will need a stronger elbow mechanism to lift it and as a result make the whole device way too heavy to put on a human arm (the expected weight of the device is less than 1 kg as proposed in chapter 1). Therefore, the spherical mechanism would not be further considered as the wrist or forearm mechanism for this design. But, to find the best arrangement of all spherical chains and to reduce the weight of the mechanism could be the subject of future work of this rehabilitation device design.

Without taking the spherical mechanism into consideration, only orientation mechanisms with a passive constraint mechanism (the first subgroup) and orientation mechanisms with special configuration of passive joints (the third subgroup) could be applied as the wrist mechanism. The spatial orientation mechanism with special configuration of passive joints could be applied as wrist mechanism directly. There is an existing device that uses this orientation mechanism as the wrist mechanism: the RiceWrist. This grounded device uses three RPU chains to rotate the moving platform. The rotation point is on the moving platform plane. The only limitation of the mechanism is that the rotation range cannot cover the full range of wrist rotation. To avoid arm-link interference, we can replace the RPU chains to other equivalent chains, like RRU or even RRRR chains, to increase the rotational range. However, the mechanism would be twice bigger and much heavier to just expand the range slightly. Therefore,

to explore a new mechanism which can fit wrist mechanism and can cover more range of motions would be the main focus of this project.

2.1.5.3 Conflicts solving with TRIZ

As analyzed above, the orientation mechanism with a passive constraint mechanism was another good choice for a wrist mechanism. But the arm-link interference was still the biggest issue in the design. Before considering the passive joint limitation and link length limitation, arm-link interference needs to be eliminated. The first conflict was the interference between the passive constraint mechanism and the arm. The function of the passive constraint mechanism is to limit the rotational degrees-of-freedom of the moving platform and to fix the rotation point. As Figure 2.12 shows, the universal joint of the center mast fixed the rotation point at the universal joint, and allows only rotations about X and Y axes. However, the rotation point of the human wrist is inside the wrist. Obviously, it is impossible to place a mechanical mechanism inside the wrist to limit the motion of the device. In order to solve this problem, the TRIZ method (the theory of inventive problem solving) was used in this research. By using generalized engineering parameters to describe the conflict, the function of the center mast (limit the degree of freedom of the device) was translated to parameter #27 “Reliability”. The device’s motion would be more reliable with a passive constraint mechanism than without it. The wear-ability of the device was translated to parameter #33 “User friendliness”. In this case, parameter #33 is the one that should be improved, and parameter #27 “Reliability” would deteriorate due to the conflict. Solutions generated by the TRIZ relation matrix were solution #27 “Cheap short life instead of expensive longevity”, #17 “Principle of moving into a new dimension”, and #40“Using composite materials”. The solution #17 “Principle of moving into a new dimension” has been selected to solve this conflict. By applying this principle, the ball joint of the center

mast has been replaced by a universal joint, and the whole passive constraint mechanism has been enlarged until the arm can pass through (Figure 2.13). In this way, the passive constraint mechanism would not have an interference with the arm.

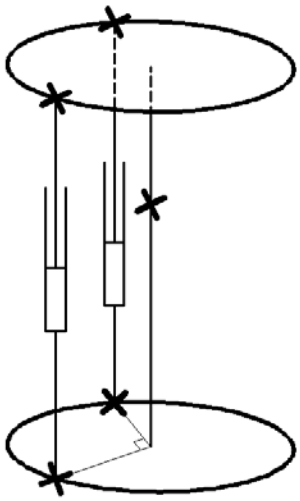

Figure 2.12: Wrist mechanism with universal joint as passive constraint.

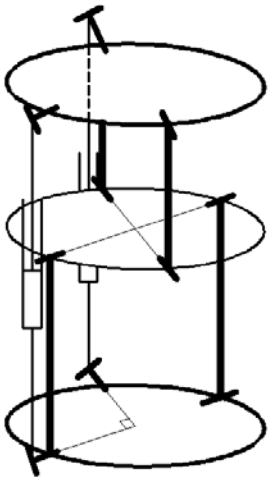

Figure 2.13: Wrist mechanism with modified passive constraint.

The second main conflict came from the mounting method of the wrist mechanism on the user's hand. Being a parallel mechanism, it requires all components to be rigid and firm, especially the moving platform. Without the rigid platform, the parallel mechanism cannot control the orientation of the moving platform or the end effecter precisely. If the rigidity of the platform decreases, the stability and the accuracy of the parallel mechanism will decrease sharply. However a human hand is not a rigid part. Soft tissues (like skin, muscle, and fat) are flexible. Thus, this conflict was straightforward. The demand of rigid platform was translated to the parameter #13 "stability of the object's composition". The fact that human hands are not rigid but flexible and soft could be translated to either "Flexibility" or "User Friendliness". If the

device uses a rigid platform, the flexibility of the hand would be minimized and the device would be considered as “not user friendly”. Therefore, the parameter #35 “Flexibility” or #33 “User Friendliness” should be improved. The parameter #13 “Stability of the object’s composition” deteriorated due to the conflict. Solutions generated by the TRIZ relationship matrix for these two cases were solutions #35 “Changing the aggregate state of an object”, #32 “The principle of using color”, #30 “Using flexible membranes and fine membranes”, #34 “The principle of discarding and regenerating parts”, and #2 “Principle of removal”. Solutions #35, #32, and #30 were obviously not suitable for this mechanism designing project. Besides, no part would fulfill its purpose and no longer needed during exercise providing process. Thus solution #2 was applied for this application. In this specific case, the moving platform has been removed by applying solution #2. By designing the mechanism in this way, all actuators of the parallel mechanism would be connected to the hand directly. In other words, the hand is to be used as a part of the parallel mechanism to minimize the flexibility of the mounting mechanism (Figure 2.14). This solution did make sense in this conflict, and how well this mechanism could perform was unknown. Testing after the structure design and manufacturing are necessary to determine the performance of the wrist mechanism.

Another conflict of the spatial orientation mechanism in rehabilitation applications was the interference between rigid links and arm. However, the rigid links were not required for the orientation mechanism with passive constraint mechanism. It is because that the rigid passive constraint mechanism already has limited motion patterns for the device. Therefore, the rigid links could be simply removed and replaced by flexible cable to avoid link-arm interference. The new wrist mechanism is shown in Figure 2.15.

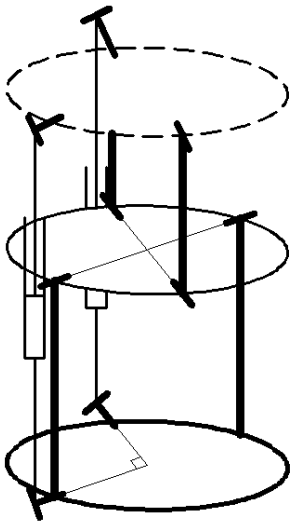

Figure 2.14: Wrist mechanism after the moving plate was removed.

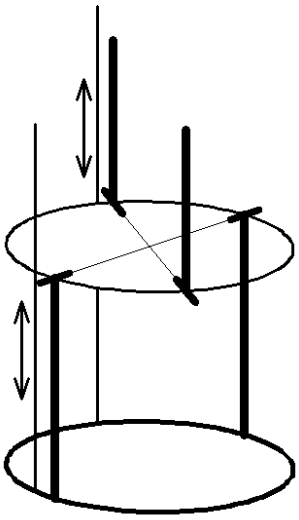

Figure 2.15: Wrist mechanism after the linear actuators was replaced by cables.

2.1.6 Mechanical mechanism design for the forearm rotation

A human forearm has one rotational degree-of-freedom. However, this motion requires both elbow joint and wrist joint to take part in. In general, the radioulnar joint glides anteriorly or posteriorly on the ulna for forearm rotation. So this rotational movement is more like a “twist motion” than “pivot rotation”. In order to imitate the “twist motion” of the forearm, the forearm mechanism has been designed to allow the wrist mechanism to rotate about the longitudinal axis of the forearm (Figure 2.16). The base platform of the wrist orientation mechanism would be the wrist-end of the forearm mechanism. The elbow-end of the forearm mechanism would be fixed on the forearm-end of the elbow revolute joint(s). Since the elbow-end of the forearm mechanism would be fixed with the elbow joint mechanism, this end would not be allowed to rotate. In contrast, the wrist-end would be controlled to rotate relative to the elbow-end, and about the longitudinal axis of the forearm. This mechanism doesn’t have any interference between the device and the arm.

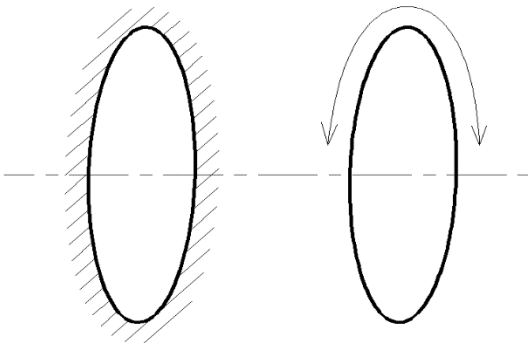

Figure 2.16: Forearm mechanism. Left ring is the elbow-end; right ring is the wrist-end.

2.1.7 Kinematic analysis of wrist orientation mechanism

2.1.7.1 Mechanism description

A complete kinematic analysis for the two degrees-of-freedom wrist mechanism was done in this part. There were four cables needed for controlling the wrist mechanism. But since cable cannot provide any pushing force, a pair of cables was needed to enable the device to rotate in two directions. Thus, the mechanism has two equivalent linear actuators. Since the number of actuators was equal to the moving platform's degree-of-freedom, this wrist mechanism is a modified fully parallel manipulator.

The connection type of the fixed point of a cable is a universal joint type, and the universal joint could be decomposed into two binary revolute joints. Besides, the cable operates the mechanism by pulling it. It is obvious that the length of the cable is changing while pulling the moving platform. Therefore, the wrist mechanism could be considered as two UPU or RRPRR kinematic structures. Position sensors would be available for measuring the rotational angle of the hand. So the forward kinematic analysis is not reported in this section. The workspace of this wrist mechanism was mainly limited by its structure and joints limitation.

Since the designed wrist mechanism was redesigned and modified especially for the wearable rehabilitation device, it is not a typical standard parallel manipulator. Based on the architecture of the wrist mechanism, the following assumptions were made for kinematic analysis:

1) The cable used in the mechanism can only provide pulling force. No pushing force could be provided at all.
2) When the cable is pulled by the moving platform, it can move and be bent freely.
3) All cables are identical. Joints on the base and the moving platform are identical.
4) The moving platform, which is the hand in this case, is rigid and firm.
5) The cable connections on the moving platform (i.e. hand) are firmly fixed.
6) Cables' end points on the base platform lie on the same plane which known as the reference plane.

2.1.7.2 Geometry of the wrist mechanism

Figure 2.17 shows the geometric model for the wrist mechanism. The base and the lower part of the passive constraint mechanism were one solid piece. Shortening or increasing the distance between the bass platform and the center of the passive constraint mechanism doesn't affect the kinematics of the structure at all. In order to simplify the analysis process, the distance between the center of the passive constraint mechanism and the base platform is been minimized. Thus, the reference plane was set on center ring of the passive constraint mechanism. The parameters used in the kinematics could be defined as:

$$l_b = ||\overrightarrow{CA_i}|| \,, \tag{2.1}$$

$$l_p = ||\overrightarrow{CP}|| \,, \tag{2.2}$$

$$l_d = ||\overrightarrow{PP_i}||_v \,, \tag{2.3}$$

$$l_k = ||\overrightarrow{PP_i}||_w \,, \tag{2.4}$$

In addition, C is the center of the reference plane; P is the center of the moving platform (i.e. hand); α is the angle between CA_2 and y axis; li are the lengths of cables for i = 1, 2; Pi are the endpoints of the cables on the moving platform; Ai are the endpoints of the cables on the fixed base platform. There are two coordinate systems defined for the analysis. The base coordinate system **{A}**: xyz is attached to the reference plane at point C. The z axis is perpendicular to the reference plane; the y axis is parallel to CA_2; the x axis is parallel to CA_1. So the angle α is always zero in this case. The second coordinate system **{B}**: uvw is attached to the center of the moving platform. The w axis is perpendicular to the moving platform plane. Thus, the position of the moving platform center P could be represented as:

$$^{A}\boldsymbol{P} = \begin{bmatrix} p_x & p_y & p_z \end{bmatrix}^T \tag{2.5}$$

Furthermore, the rotation matrix is used to represent the orientation of the end effecter with respect to the reference plane, using a pitch-roll-yaw representation:

$$^{A}\boldsymbol{R}_B = \boldsymbol{R}_z(\theta_z)\boldsymbol{R}_y(\theta_y)\boldsymbol{R}_x(\theta_x)$$

$$= \begin{bmatrix} \cos\theta_z \cos\theta_y & \cos\theta_z \sin\theta_y \sin\theta_x - \sin\theta_z \cos\theta_x & \cos\theta_z \sin\theta_y \cos\theta_x + \sin\theta_z \sin\theta_x \\ \sin\theta_z \cos\theta_y & \sin\theta_z \sin\theta_y \sin\theta_x + \cos\theta_z \cos\theta_x & \sin\theta_z \sin\theta_y \cos\theta_x - \cos\theta_z \sin\theta_x \\ -\sin\theta_y & \cos\theta_y \sin\theta_x & \cos\theta_y \cos\theta_x \end{bmatrix} \tag{2.6}$$

where θx, θy, and θz are the Euler angles of the moving platform denoting respect rotations about x, y, and z axes. Euler angles are a convenient method to represent the orientation of the

end effecter. However, it is not very easy for the kinematic analysis. Based on the characteristics of the modified universal joint type passive constraint mechanism in this structure, the rotations of the moving platform could be represented by uvw Euler angles:

$$\boldsymbol{R}_{uvw}(\theta_1\theta_2\theta_3) = \boldsymbol{R}_u(\theta_1)\boldsymbol{R}_v(\theta_2)\boldsymbol{R}_w(\theta_3)$$

$$= \begin{bmatrix} \cos\theta_3\cos\theta_2 & -\sin\theta_3\cos\theta_2 & \sin\theta_2 \\ \sin\theta_3\cos\theta_1 + \cos\theta_3\sin\theta_2\sin\theta_1 & \cos\theta_3\cos\theta_1 - \sin\theta_3\sin\theta_2\sin\theta_1 & -\cos\theta_2\sin\theta_1 \\ \sin\theta_3\sin\theta_1 - \cos\theta_3\sin\theta_2\cos\theta_1 & \cos\theta_3\sin\theta_1 + \sin\theta_3\sin\theta_2\cos\theta_1 & \cos\theta_2\cos\theta_1 \end{bmatrix} \tag{2.7}$$

So far, the position and the orientation of the moving platform (i.e. hand in this case) were completely defined.

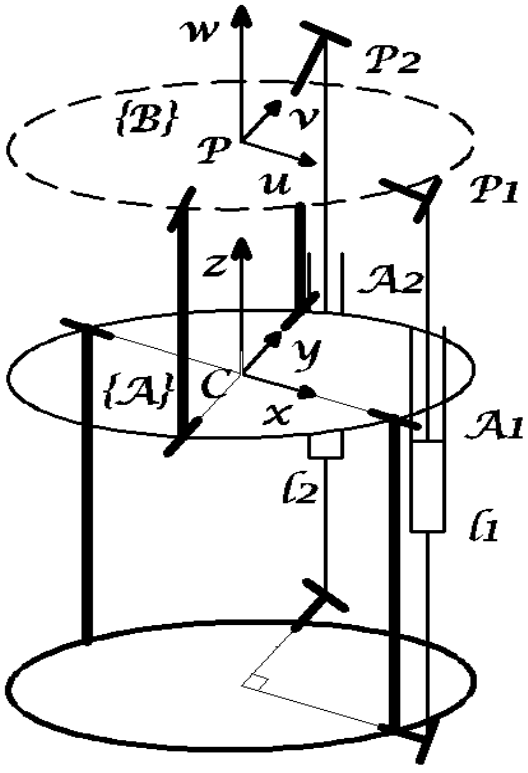

Figure 2.17: Geometry of the wrist mechanism.

2.1.7.3 Inverse kinematics

In the inverse kinematic analysis, the cable length li is solved by the function of rotation angle of the moving platform θ_1, θ_2, and θ_3. The loop-closure equation for each actuated cable is:

$$\boldsymbol{L}_i = l_i \hat{\boldsymbol{s}}_i = {}^A\boldsymbol{P} + {}^A\boldsymbol{R}_B \, {}^B\boldsymbol{P}_i - \boldsymbol{a}_i \tag{2.8}$$

which l_i is the length of i th cable, and $\hat{\boldsymbol{s}}_i$ is the unit vector pointing along the direction of the i th cable. ${}^A\mathbf{R}_B$ is the orientation matrix of the moving platform. Since the wrist mechanism only has two rotational degrees-of-freedom about x axis and y axis, so the θ_3 is zero:

$$\begin{aligned} {}^A\boldsymbol{R}_B &= \boldsymbol{R}_{uvw}(\theta_1\theta_2\theta_3) = \boldsymbol{R}_u(\theta_1)\boldsymbol{R}_v(\theta_2)\boldsymbol{R}_w(0) \\ &= \begin{bmatrix} \cos\theta_2 & 0 & \sin\theta_2 \\ \sin\theta_2 \sin\theta_1 & \cos\theta_1 & -\cos\theta_2 \sin\theta_1 \\ -\sin\theta_2 \sin\theta_1 & \sin\theta_1 & \cos\theta_2 \cos\theta_1 \end{bmatrix} \end{aligned} \tag{2.9}$$

and the moving platform center position vector ${}^A\mathbf{P}$ is rewritten in:

$${}^A\boldsymbol{P} = l_p[s_2 \quad -c_2 s_1 \quad c_2 c_1]^T \tag{2.10}$$

Moreover, vectors $\mathbf{a}_i$ denotes the end points of cables on base platform from the center point of the reference plane C, and vectors ${}^B\mathbf{P}_i$ denotes the end points of cables on the moving platform (i.e. the hand) from the center point of the moving platform plane P. Based on the given geometry of the wrist mechanism and the setup of coordination systems, we have:

$$a_1 = l_b[1 \quad 0 \quad 0]^T \tag{2.11}$$

$$a_2 = l_b[0 \quad 1 \quad 0]^T \tag{2.12}$$

and

$$^{B}\boldsymbol{P}_1 = [l_d \quad 0 \quad l_p - l_k]^T \tag{2.13}$$

$$^{B}\boldsymbol{P}_2 = [0 \quad l_d \quad l_p - l_k]^T \tag{2.14}$$

Thus, the lengths of cables, li, can be computed by dot multiplying equation 2.15 to it:

$$\boldsymbol{L}_i^T \boldsymbol{L}_i = l_i^2 = \left[{}^{A}\boldsymbol{P} + {}^{A}\boldsymbol{R}_B \, {}^{B}\boldsymbol{P}_i - \boldsymbol{a}_i \right]^T \left[{}^{A}\boldsymbol{P} + {}^{A}\boldsymbol{R}_B \, {}^{B}\boldsymbol{P}_i - \boldsymbol{a}_i \right] \tag{2.15}$$

2.2 **Elbow Mechanism Design**

2.2.1 Joint structure of the elbow complex

The elbow complex includes three joints. They are the humeroulnar joint, the humeroradial joint and the proximal radioulnar joint (Figure 2.18). The humeroulnar joint is the joint between humerus and ulna. It is the hinge type joint. So the degree-of-freedom of humeroulnar joint is equal to one. The motion of this joint is the elbow's flexion and extension. Its rest position is believed to be at 70 degree of elbow flexion and 10 degree of forearm supination. The humeroradial joint is the joint between humerus and radial head. The joint type is ball and socket. Thus, its degrees-of-freedom is equal to two. The motions are elbow flexion/extension and forearm pronation/supination. The third joint is proximal radioulnar joint. This joint is the joint between ulna and radial head. This joint is a pivot type joint. It only contributes to the forearm's pronation and supination. Its degree-of-freedom is equal to one. The rest position is believed to be at 70 degree of elbow flexion and 35 degree of forearm supination. Since the humeroradial joint and proximal radioulnar joint contributes forearm's pronation and supination, some scholars would claim the degree of freedom of the elbow joint is equal to two if they refer the elbow joint as the whole elbow complex. Usually, the elbow joint also has 10 to 15 degree of cubitus angle.

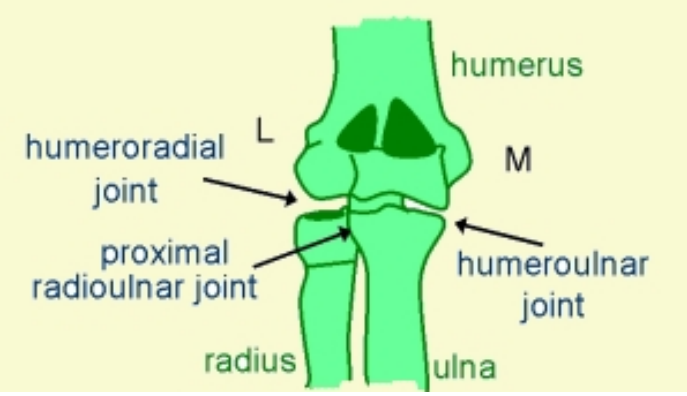

Figure 2.18: Anterior view of elbow complex.

2.2.2 Kinematics of the elbow joint

Both the humeroulnar joint and the humeroradial joint contribute to the elbow's flexion and extension. The rotation axis is close to the line which runs through the center of trochlea and the center of capitulum. Usually, this axis is not perpendicular to the humerus. The axis has a 4 to 8 degree of valgus to the lateral axis of the humerus. The range of motion of elbow flexion is 0 to 145 degree and the functional range is 30 to 130 degree.

2.2.3 Mechanical expression of the elbow joint

The elbow joint only has one rotational degree-of-freedom, and the joint motion is relatively independent from other joint. Therefore, one revolute joint can fully express the motion of the elbow.

2.2.4 Mechanical mechanism design for the elbow

Since elbow joint only has one degree-of-freedom, the side-mount type rotational mechanism can fully satisfy the elbow joint’s motion, as long as their rotational axes coincide.

So the mechanism of the elbow could be either one-side-mounted revolute joint or symmetrical mounted two revolute joints (Figure 2.5). The symmetrical mounted joints can provide better stability for forearm and wrist structure.

There were two main ways to actuate the mechanical revolute joint. The first way is to fix the frame and rotate the pivot. The second way is to adjust the distance between a non-center point on the frame and a non-center point on the pivot (the shortest line between these two points should not have an intersection with the rotation axis all the time). For the first way, it is better to mount the rotational actuator directly on the frame and rotate the pivot by the actuator. For the second way, any type of linear actuator could be directly applied on the pivot structure to shorten and extend the distance. As mentioned above, by considering the total weight on the wearable device, mounting actuators directly on the robot was not a good way to reduce the total weight. A linear actuator could not only be the pneumatic cylinder or linear electric motor, but could also be a cable or rod. By using cable driven or rod driven methods, the actuator could be removed from the elbow mechanism. Thus, the second actuation method was chosen for this application (Figure 2.19). Detailed elbow joint structure design would be discussed in next chapter.

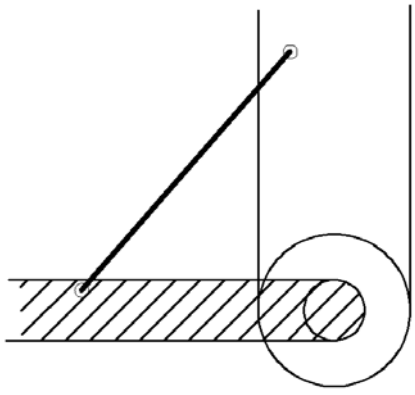

Figure 2.19: Elbow mechanism.

2.2.5 Kinematic analysis of wrist orientation mechanism

2.2.5.1 Mechanism description

Elbow mechanism is a one degree-of-freedom rotation joint. The linear actuator has the ability to provide both push and pull force. One end of the linear actuator was connected on the extension part of the frame with a revolute joint, and another end was connected on the extension part of the pivot with a revolute joint too. Two connection positions cannot locate at the center of the parts. They have to be located on the same side from the center line. Otherwise, they would create a dead-point while operating. If there is not momentum to break the dead-point, the joint cannot be rotated. In this way, the elbow mechanism becomes a slider-crank four-bar linkage mechanism.

2.2.5.2 Geometry of the wrist mechanism

Figure 2.20 shows a geometric model for the elbow mechanism. The parameters used in the kinematics are:

$$\left\|\overrightarrow{CA_1}\right\| = [l_1 \quad l_3]^T \tag{2.16}$$

$$\left\|\overrightarrow{CA_2}\right\| = [l_4 \quad l_2]^T \tag{2.17}$$

$$l = \left\|\overrightarrow{A_1A_2}\right\| \tag{2.18}$$

in which l is the length of the cable. In addition, the XY coordinate system is attached to the center point of the revolute joint C. A_1 is the fixed end-point of the cable on the pivot's extension; A_2 is the end-point of the cable on the frame. A is the angle of $\angle A_1CA_2$. l_1 is the distance on x axis from center point C to end-point A_1; l_2 is the distance on y axis from center

point C to end-point A_2; l_3 is the distance on y axis from center point C to end-point A_1; l_4 is the distance on x axis from center point C to end-point A_2;

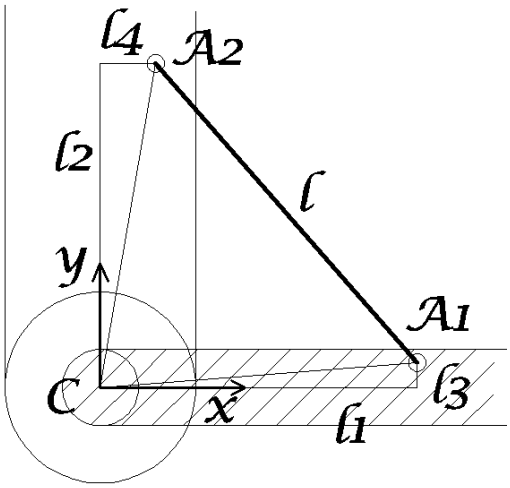

Figure 2.20: Geometry of the elbow mechanism.

2.2.5.3 Kinematics of the elbow mechanism

Based on the structure of the elbow mechanism, the close-loop equations for this elbow limb are:

$$\overrightarrow{CA_1} = \overrightarrow{l_1} + \overrightarrow{l_3} \tag{2.19}$$

$$\overrightarrow{CA_2} = \overrightarrow{l_2} + \overrightarrow{l_4} \tag{2.20}$$

$$\overrightarrow{A_1A_2} = \overrightarrow{CA_2} - \overrightarrow{CA_1} \tag{2.21}$$

Since end-points A1 and A2 are fixed on the parts, the length of $\overrightarrow{CA_1}$ and $\overrightarrow{CA_2}$ will be fixed:

$$\left\|\overrightarrow{CA_1}\right\| = \sqrt{{l_1}^2 + {l_3}^2} \tag{2.22}$$

$$\left\|\overrightarrow{CA_2}\right\| = \sqrt{{l_2}^2 + {l_4}^2} \tag{2.23}$$

Therefore, the relationship between the angle of $\angle A_1 C A_2$ and the length of cable is very straight forward. Apply law of cosines to this geometry,

$$\begin{aligned} l^2 &= \left\|\overrightarrow{CA_1}\right\|^2 + \left\|\overrightarrow{CA_2}\right\|^2 - 2\left\|\overrightarrow{CA_1}\right\|\left\|\overrightarrow{CA_2}\right\| \cos\alpha \\ &= {l_1}^2 + {l_3}^2 + {l_1}^2 + {l_3}^2 - 2\sqrt{\left({l_1}^2 + {l_3}^2\right)\left({l_2}^2 + {l_4}^2\right)} \cos\alpha \end{aligned} \tag{2.24}$$

Since the length of the cable cannot be a negative number, the relationship between l and α is linearly.

3 DEVICE STRUCTURE DESIGN AND FABRICATION

The mechanisms have been analyzed and designed in chapter 2, the following is to realize it and test it. In the current industry, designing is led by ideas but restricted by manufacturing ability. If the idea cannot be realized by current manufacturing methods, this idea is worthless and the design is considered a failure. Thus, the design has to stay under the limitations of current accessible manufacturing methods. Therefore, the material and the manufacturing methods for making the device need to be decided first. In following section, the drive method analysis and structure design for each part are provided.

3.1 **Material and Manufacturing Method for The Prototype**

The designed rehabilitation device does not perform any high speed or high accuracy motion, and is not used under high pressure or high temperature or any other extreme conditions. Thus, the device can use materials that do not exhibit exceptional mechanical properties. Since the device is aimed at specifics like light weight and portability, the main material for the device need to be considered on both weight basis and cost basis. So aluminum alloy and plastic (like ABS and PLA) would be two good choices for the described application.

The manufacturing method was limited to methods that can be provided by the Mechanical Department or Industry Distribution department of Texas A&M University machine shops. Because the machine shops of these two departments will be only two shops available for this project.

In general, there are two manufacturing methods accessible for this project. They are material removal methods and material accumulation methods. In accessible machine shops, the material removal methods refer to the material removal process by using manual or CNC lathe, mill, or other machine tools. The material accumulation methods refer to molding and plastic 3D

printing. Material removal methods are more common than any other manufacturing method. They are a good choice for making metal materials or high density plastics to usable parts in a relative fast pace and effective cost. However, since the accessible machine shops do not have high degree of freedom machining centers (4 or 5 axes CNC machining centers), the complexity of the parts was limited, and the difficulty or the manufacturing process was increased. Besides, due to the extremely low availability of CNC machine tools in accessible machine shops, basic manual machine tools were the main available tools for this project. Thus, the design was very restricted to accommodate machines available for use. Different molding processes are good choices for making complex parts. However, molding are usually be used for making high-volume of same part. Using molding to make few pieces or even just one piece of object is not cost-effective at all. Besides, making molds usually takes long time. Although, there are several relatively cost-effective and time-effective plastic molding process available for hobbies, it is better to avoid molding process for prototyping in order to reduce development cycle time and the cost. Based on the current available machine for the project, the 3D printing method mentioned above refers to the Fused Deposition Modeling (FDM) method. FDM is one of the rapid prototyping methods. It usually uses ABS (Acrylonitrile Butadiene Styrene), PLA (Polylactic Acid), Nylon, or similar materials. The FDM device heats the material to a semifluid state and extrudes them through the nozzle. Controlling by microchip, the nozzle moves following the two dimension CAD trajectory. The semifluid material cools down and becomes solid after being extruded. The nozzle extrudes material layer by layer based on the CAD model. With proper support structures while printing the object, the FDM device (3D printer) can make very complex objects or even sealed parts which cannot be made with conventional machine tools. The main drawback of the FDM method is the low adhesive strength between layers and lines. Since the extruded semifluid material is bonded to the previous extruded solid material, not

heated semifluid material, the present extruded material and the previous extruded material cannot be the same part. Thus, the 3D printed parts cannot be considered as a solid plastic part in theory. Because the adhesive strength between layers is usually a lot less than material's strength, so the mechanical properties of the part is mainly based on the adhesive strength between layers instead of the material properties. Besides, the adhesive strength between layers is affected by many factors, such as material's temperature, environment temperature, device vibration, and etc. Thus, the adhesive strength is very difficult to determine and it is so different from one place to another and from layer to layer. Therefore, the failure of the 3D printed part is really based on the location of the weakest adhesive point, and it is impossible to predict and simulate in computer currently. There are so many research groups doing researches about adhesive strength prediction and improving. But before the significant contribution is be made in this area, the main drawback of the 3D printed parts in this project is still unpredictable failure.

By considering all factors (cost, time, difficulty of fabricating process, and accessibility of the machine tool), the FDM method has been selected for making the main parts and all no load or little load parts for the rehabilitation device prototype. Other parts could be designed in simple structure and be made with manual machine tools. Due to the main drawback of the 3D printed parts, the prototype may have similar main drawback.

3.2 **Drive Method Selection for All Joints Mechanism**

All mechanisms designed in chapter 2 could be driven directly either by rotary actuators or linear actuators. However, the wrist mechanism was designed to be cable driven to reduce interference. Also, this project is aimed at portable rehabilitation device designing, so to minimize the weight of the device is the main consideration of the drive method selection. Adding any power transmission mechanism between actuators and objective device would make

the drive method from direct drive to indirect drive. By using the indirect drive method, actuators can be totally removed from the device. Thus, the indirect drive method is a good choice for approaching the light-weight aim of this project. Considering the power transmission mechanisms based on designed joint mechanisms, the cable drive is the best choice for this project because of its light weight and high efficiency in power transmission.

All actuators could be removed from the rehabilitation device by using the indirect drive method, but the actuators cannot be got rid of. Because the whole device needed to be designed as portable, the actuators and all other controlling systems could be carried by the user in a backpack manner. In that way, the power transmission mechanism between the controlling backpack and the device need to be flexible. Common power transmission mechanisms, like gearbox, chain, shafts etc., are firm and rigid and thus they cannot be used in this application. Cable or wire is another option for power transmission. Cable and wire are flexible themselves; however, just because of this characteristic, cable or wire can only provide pulling force. As a result, cable or wire can only transmit power between two points through the shortest distance path. Therefore, the normal cable or wire is not appropriate in this application. Flexible shaft and push-pull control cable are only two flexible power transmission mechanisms. Flexible shaft is designed to transmit rotational degree-of-freedom motion; and push-pull cable is designed to transmit translational degree-of-freedom motion. So the push-pull cable is the only option for power transmission purpose in this application.

The smallest push-pull cable available on the market is 3/64” diameter steel cable. Thus, the selected cable is the 3/64” (1.2mm) stainless steel, 1×19 strand dry condition cable. The minimum breaking strength is 375 lbs.

3.3 **Wrist Mechanism Structure Design**

The wrist mechanism has already been designed as a cable driven parallel mechanism without the moving platform, but with a giant passive constraint mechanism which can let the arm pass through. Thus, the focus of the wrist mechanism structure design is on the passive constraint mechanism.

As discussed in chapter 2, the passive constraint mechanism for the wrist mechanism is designed as a modified big universal join (Figure 2.15). The ring of the modified universal joint is placed over the wrist part, and rotates with the moving platform of the parallel mechanism (i.e. hand). Since the rotation axes of the ring has to coincide with the rotation axes of the wrist, it is impossible for the ring to rotate 90 degree from the default position. Otherwise, the ring has to move into the arm (Figure 3.1). Since the wrist radial and ulnar motions don't need 90 degree range, so the ring could be bent at the top and the bottom part to satisfy the full 90 degree range of wrist flexion and extension motions. However, this modification created a new conflict. Since the rotational axis of the radial and ulnar motions needs to be perpendicular to the rotational axis of the flexion and extension motions, the radial/ulnar motion's rotational axis has to be placed on the bent part. In this way, two rotational axes are separated, and they are impossible to coincide two wrist rotational axes. Although two wrist rotational axes are apart about 4 mm in theory, the height of the bent part on the ring has to be over 20 mm to fit the normal size of human arm. Therefore, this modification on the shape of the ring conflicts with the wrist mechanism.

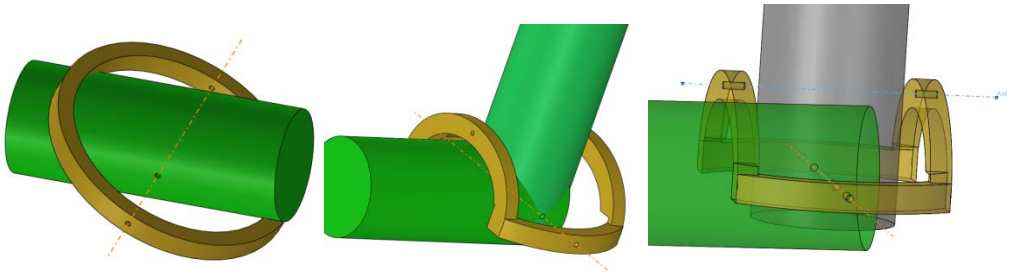

Figure 3.1: A failed design of the ring. Two rotational axes are apart due to the design.

The TRIZ method was used to try and solve the conflict. The shape of the ring was translated to the parameter #12 “Shape”, and the separation of two axes was translated to the parameter #27 “Reliability” or #37 “Difficulty to control”. Based on the TRIZ matrix, possible solutions which may fit this application were solution #1 “Principle of segmentation”, and #13 “Principle of opposite solution”. In order to keep the wrist mechanism controllable, the ring of the modified universal joint cannot have any extra degree of freedom. Thus, two possible solutions from TRIZ method don't help too much. This conflict was created by the bent part of the ring, but what if the ring did not have any bend modification? Let’s assume the radius of the ring is R, and the radius of arm is r (Figure 3.2). In addition, α is the angle between the ring and the line which perpendicular to the longitudinal axis of the arm, when the ring collides to the arm. Thus, the maximum rotation angle α has following relationship with ring radius: $\cos \alpha = r/R$. In this application, bigger α is better. It is clear that if r = R, the rotation angle α will be zero. If $R = \infty$, then α will be 90 degree. However, it is obvious that the radius of the ring cannot be infinity large. So the remaining thing is just to find a balance point between 1 and ∞ for r/R ratio.

Chart 3.1 shows the relationship between the angle α and R/r ratio. From the chat we can know that the maximum angle α increases rapidly from zero to 60 degree while R/r ratio increases from 1 to 2. After the R/r ratio reaches 3, the increase of α becomes slow. After the ratio reaches 4.5, α’s increasing is small enough to be ignored. The last three columns of the data

table indicate that the radius of the ring increased from 7 times of arm radius to 8 times, but the maximum rotation angle increased even less than 1 degree. Based on the analysis in chapter 2, the elbow flexion has the biggest range of motion. It is about 85 degree. The functional range of motion is much smaller than the full range. Different researches may indicate different functional range of motion, but none of them shows that the functional range of motion of wrist flexion is over 60 degree. Therefore, as long as the R/r ratio is bigger than 2, the mechanism can cover functional range of motion of wrist flexion and extension for sure. If R/r ratio is 3.5, the range of motion of the device can cover about 90 percent of the full range of motion of wrist flexion and extension. Taking every factor into consideration, select the R/r ratio around 3.5 is rational. Thus in this wrist mechanism, it is unworthy to give up mechanism's controllability, and reliability to just increase 10 degree more angle in one rotational degree of freedom. So the ring of the passive constraint mechanism will not be modified.

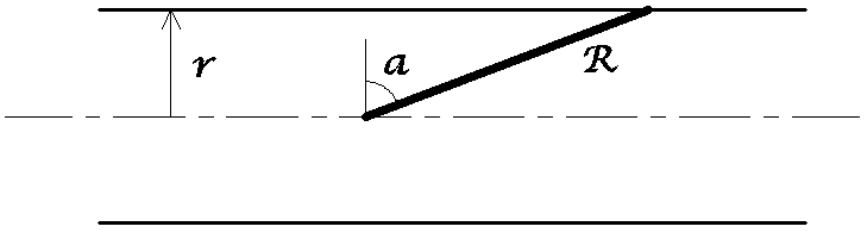

Figure 3.2: Geometry of ring structure.

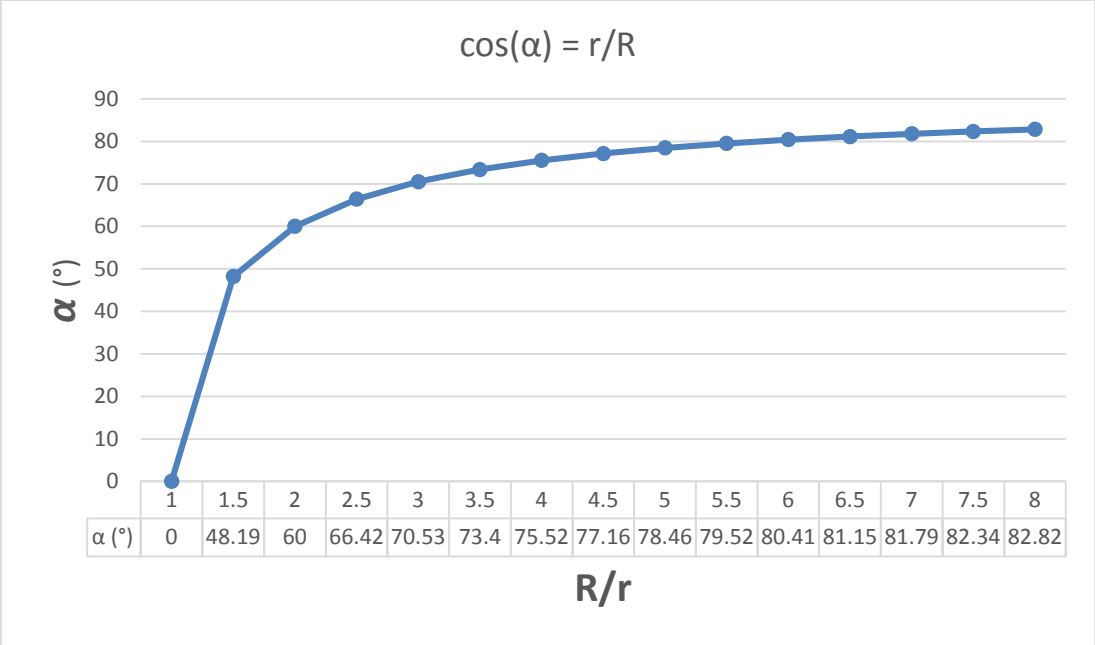

Chart 3.1: Relationship between α and R/r rate.

The CAD model of the ring is shown in Figure 3.3. Four revolute joints composed by bearings and shafts. The typical commercial type ball bearing's width is a lot smaller than its diameter. In order to increase the stability and reliability of the joints, a small bearing – shaft assembly is used in each joint (Figure 3.4). From the drawing we could know that the whole shaft-bearing assembly could be pulled out to the right. This is a safety design. In case of the device jammed or hurt the user while doing exercise, the upper part of the mechanism could be quick released from the hand. Therefore, the engineering tolerance of this shaft-bearing assemble are IT 9 interference fit (FN1) for bearing and the shaft, and IT 10 transition fit (RC1: close sliding fits or tighter) for the bearing and the frame. Technically, it is a wrong design for the shaft-bearing assembles. However, this design is specifically for this prototype based on the material and manufacturing method, and this design works perfect in this project. Therefore, this wrong design in industry is a proper design for this application. Theoretically, since the ring can

rotate about its two axes freely, no load will be applied on the ring while operating. So this part doesn't be analyzed in load simulation.

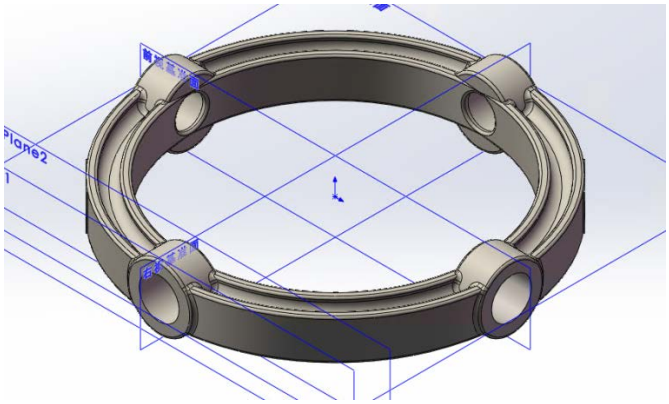

Figure 3.3: CAD model of the ring.

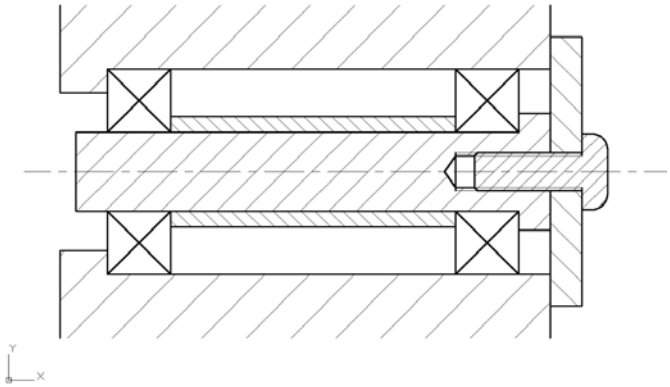

Figure 3.4: Drawing of the bearing-shaft assembly for the connection of the ring.

The upper part of the passive constraint mechanism should be connected to the moving platform. But based on the designed wrist mechanism, they will be connected to the hand directly. Figure 3.5 shows the structure design of the upper part of the modified universal joint. The ring shape structure at the top is designed for cable head connection. The flat surface under

the ring structure is designed to attach to the hand. The T shape design is in order to increase connection surface for better attachment. It is obvious that we cannot use screws to fix the part on hand or glue the part to hand. So an accessory is needed for attaching the part. In this project, a pair of tight gloves is used. The material of the gloves has no elasticity, and the gloves are chose as tight as possible. Velcro is used on the gloves and the device parts for quick release purpose. In this wrist application, two cables are used to control wrist flexion and extension. One cable pull the hand up for wrist extension and another cable pull the hand down for wrist flexion. If the resistance to passive movement of the wrist is applied to the device, the parts may deform or even fail because of the load. Thus, the load simulation is made for the upper parts assembly.

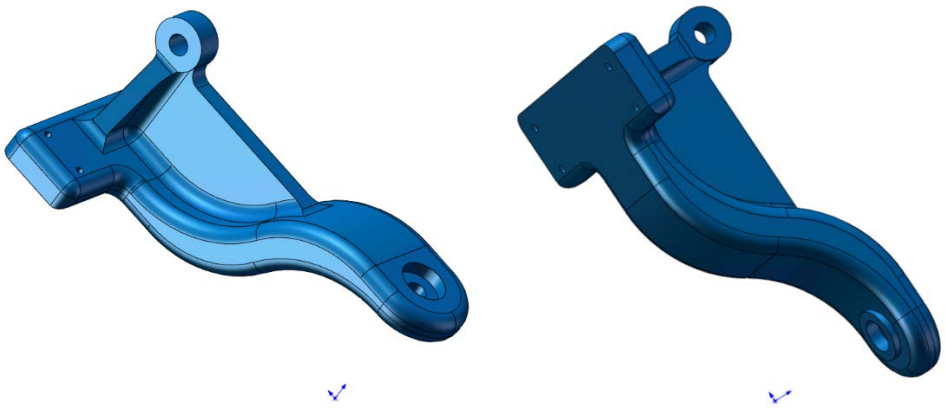

Figure 3.5: CAD model of the upper part of the modified universal joint.

Since the material of the part is ABS plastic. Unlike metals, plastic doesn't have the yield point. It means that plastic has little or no ductility comparing to metals. As the result, plastic almost doesn't have the deformation stage after the strength pass the yield point and before the part fails. Thus before the plastic part fails, the strength and displacements relationship could be considered as a linear relationship. Because of this property, plastics or

other brittle materials usually don't have any indication before they fail. This fact justifies the importance of the load simulation in part designing. Based on the property of plastic, the SolidWorks Finite Element Analysis Method Simulation Linear Stress Analysis is used for the load simulation. The SolidWorks Linear Stress Analysis has three basic assumptions:

1) The part under load deforms with small rotations and displacements.
2) The product loading is static and constant over time.
3) The material has a constant stress strain relationship.

Based on our application, we could know that these three assumptions are proper in the project.

The material used in simulation is ABS. The flexural modulus is used as elastic modulus in material properties setting. Furthermore, the flexural yield strength is used as yield strength. Material data applied is from SolidWorks data base. Density is 1020 kg/m3; tensile yield strength is 30 MPa; Flexural modulus is 2 GPa; Poisson's ratio is 0.394. Flexural yield strength data is from PROSPECTOR® []. It is from 54.8 MPa to 77.2 MPa at 73 °F. It is common for flexural strength to be higher than tensile strengths for the same material. But if the part only has defects on surfaces, flexural strength could be lower than tensile strengths. In this project, the fail standard is set based on following assumptions:

1) The material is homogeneous.
2) There are no defects in the material or on the surface of the part.
3) Plastic fibers are free from defects.

In order to increase safety factors, the "yield strength" of the simulation is either tensile yield strength or flexural yield strength, which has smaller value. In this case, the "yield strength" is equal to tensile yield strength, which is 30 MPa. Figure 3.6 and Figure 3.7 shows the simulation result. The part is fixed on the bearing-shaft assembly. The constant force is applied

on the ring structure on the right. The force direction is straight up along the y axis. The stress result indicates that the maximum strength is around the fixed point. When this maximum strength is close to the “yield strength”, the force applied is up to 30 N.

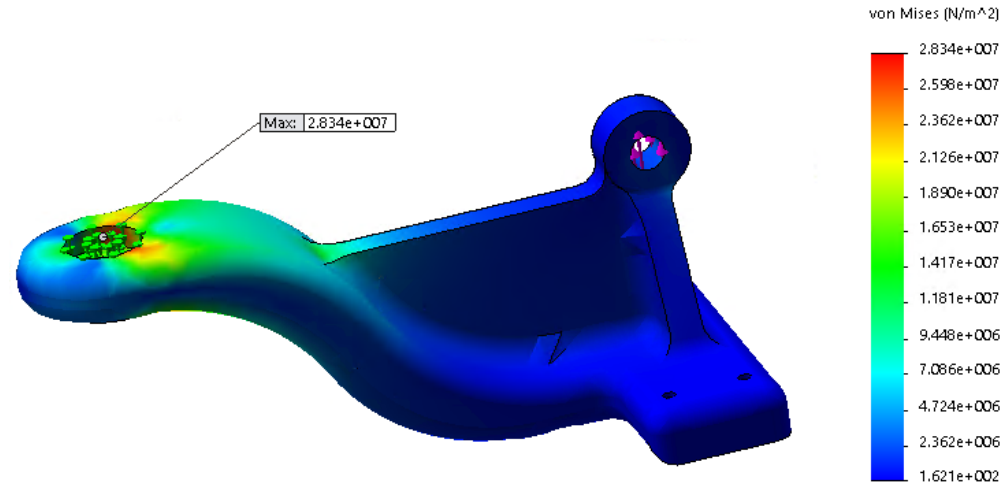

Figure 3.6: The load simulation stress result of the upper part of the wrist mechanism.

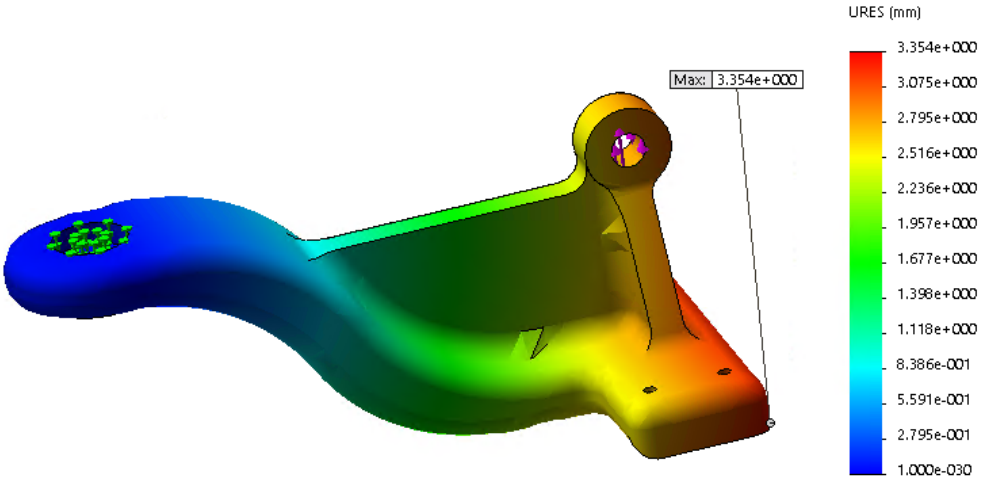

Figure 3.7: The load simulation displacement result of the upper part of the wrist mechanism.

The drive cable for wrist's radial and ulnar rotation will be connected on hand (glove) directly. By considering the comfort of the wearable robot, it is very important to find a proper point for actuating wrist radial and ulnar motions. Thus, instead of using two pulling cables, a push-pull rod is used on hand's ulna side to actuate wrist radial and ulnar motions. The lower part of the passive constraint mechanism will not get any load from wrist mechanism, and only functioning as a support for the whole passive constraint mechanism. Since this part will be connected to the forearm rotation mechanism, the detail structure design will be discussed in forearm structure designing part.

3.4 **Forearm Mechanism Structure Design**

Based on the analysis in chapter 2, the forces for making passive forearm rotation needs to be applied as close to the wrist end as possible. Based on the designed wrist mechanism and forearm mechanism, the forearm mechanism only has one rotational degree of freedom. The stationary portion of the forearm mechanism is fixed with elbow structure, and the cable driven rotary part is the support part of the passive constraint mechanism of the wrist mechanism. In this way, the forearm rotational motion is realized by rotating the whole wrist mechanism. Figure 3.8 shows the forearm structure. The cable connected on the rotary part and twined in its groove.

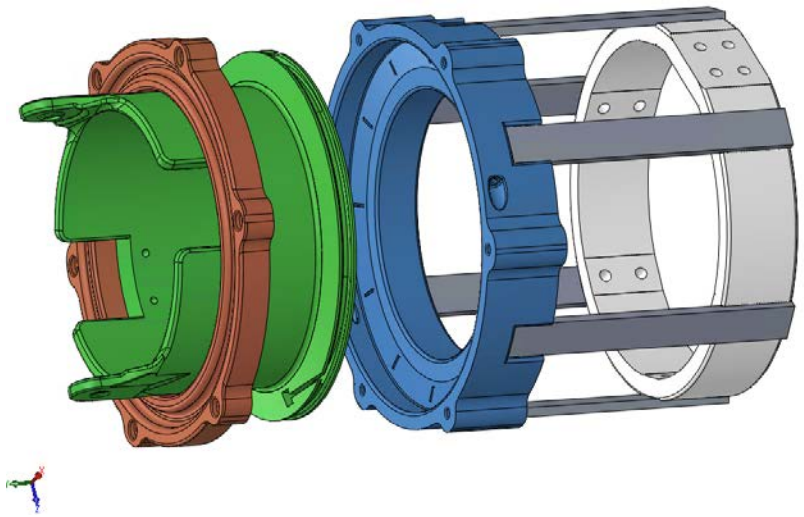

Figure 3.8: Forearm structure. Green part is the rotary part of the structure. Cables are twined on its groove, and the wrist structure is assembled on it. The right most part is connected with elbow structure.

Because part of the control cable (which is twined on the rotary part of the forearm mechanism) doesn't have the outside hose to limit its flexibility, this part of the control cable cannot provide any push force. Thus, two cables are needed for rotating the rotary part in two directions, although the push-pull control cable is used for transmitting the force from the actuator to the mechanism. The cable twining method is showing in Figure 3.9. Two cables are connected on the rotary part symmetrically, and twined in opposite direction. The outlets of the cable are on two sides of the stationary part. In this way, the rotary part can rotate 180 degree for each direction. The rotational degree can be modified by changing the arrangement of cable connection point and twining cycles. This mechanism is very similar as the motorcycle throttle control. The difference is in motorcycle throttle control mechanism, the throttle valve is cable pulled to open and spring back to close. The second cable is designed for safety reasons; i.e. when the spring cannot close the throttle by any reason, the cyclist can still roll the throttle

control bar back to close the throttle valve. In this application, spring back mechanism is not suitable because the rotation range is too big to have the spring back mechanism.

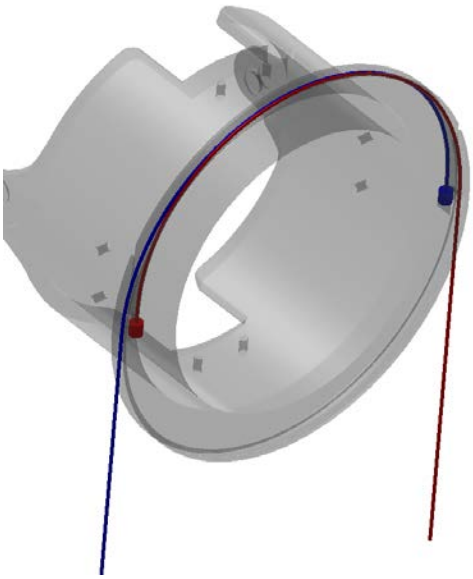

Figure 3.9: Rotary part cable twining method.

It is common sense that bearings help rotational parts rotate smoothly and stable. However for this application, the commercial bearings are not appropriate. For the rotary part's size (about 20 centimeter inner diameter), all type of commercial bearings are for heavy duty application. They are designed for high speed, heavy loads, high temperature, and they are heavy and big. For example, typical needle roller bearing which has 200 mm inner diameter has about 1500 KN load rating, and weighs about 16 kg. It is obvious that the typical ball bearing or other type of bearing with the same size is a lot heavier than needle roller bearing. Besides, if the bearing cannot rotate at a certain speed, it cannot generate enough heat to reduce the viscosity of the grease. As the result, the bearing increases the resistance instead and become the burden for

the device. In this forearm mechanism application, there is no load along the longitudinal axis, and the operation speed is lower than 1 rpm. Thus, the commercial bearing is obviously not proper for the forearm mechanism application. But the stability of the rotary part could be maintained by the structure designing. As showing in the Figure 3.10, the rotary part has the wedge shape disc at the bottom. The slope of the wedge shape disc matches the same angle slope of the stationary part. With sliding pieces in between stationary and rotary parts, which are mounted on the stationary part, the structure becomes a sleeve bearing. The angled slope creates radial force to keep the rotary part stay at the center. Because the operation speed is extremely low in this application, smooth surface and free running fits are good enough and are proper for this forearm mechanism application. Without using heavy grease, this structure will not create extra resistance.

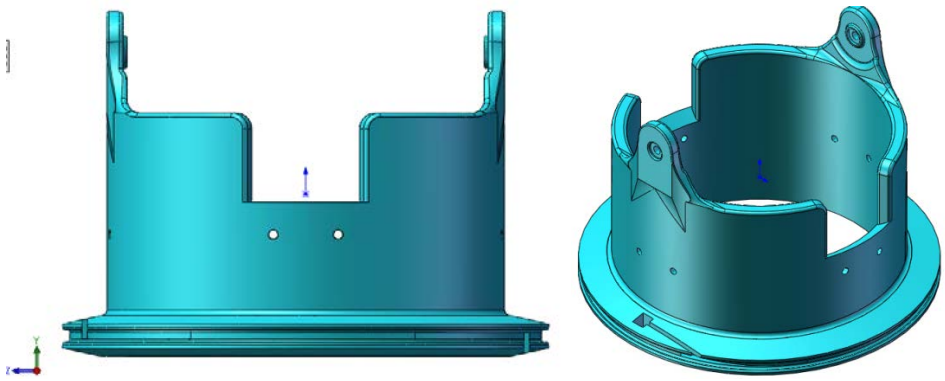

Figure 3.10: Rotary part of the forearm structure. The cable head is attached in the square on the bottom disc. The bottom disc has slope design to maintain the position of the part while operating.

The load simulation is shown in Figure 3.11 and Figure 3.12. All simulation conditions and assumptions are the same as simulation in wrist section. Cables are attached on the bottom disc, so the force is applied to the square place on the bottom disc. Two fixed points are top ring

structures which are assembled in bearing-shaft assemble. Since this is the rotary part inside the forearm structure, it has to maintain its position in the stationary part. Therefore, the degree of its displacement and deformation matters. If it displaces or deforms too much, it may crash into the stationary part and jam the whole mechanism. The stress result indicates that the maximum strength is at two fixed points. When this maximum strength is close to the “yield strength”, the force applied is up to 10 N. In this forearm structure, 10 N force applied on the bottom disc can generate 600 N·mm torque to user’s forearm. The displacement result indicates that the maximum displacement is about 1.1 mm under described conditions. The gap between the stationary part and rotary part (i.e. sleeve bearing’s tolerance) is designed to be 3 mm in total. Therefore, 1.1 mm maximum displacement is acceptable.

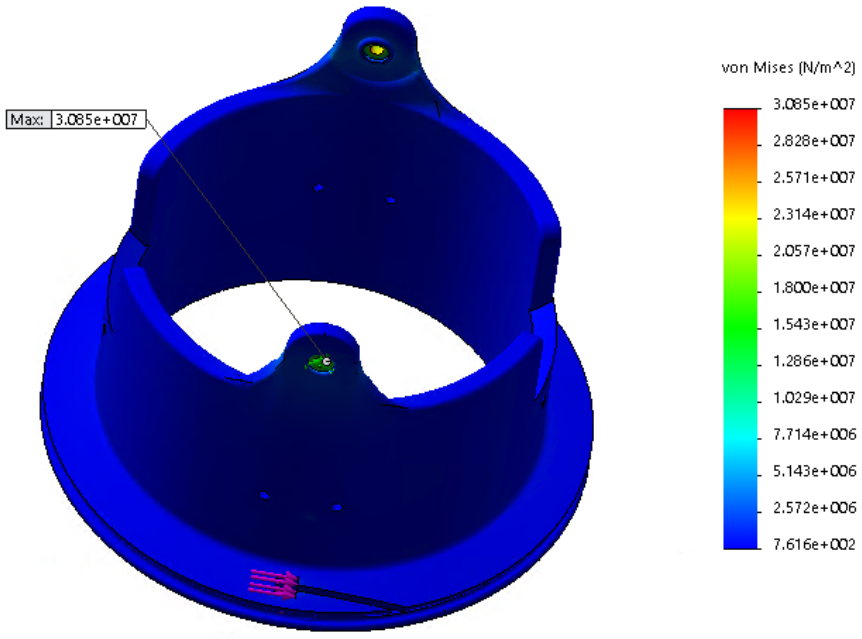

Figure 3.11: The load simulation stress result of the forearm rotary part.

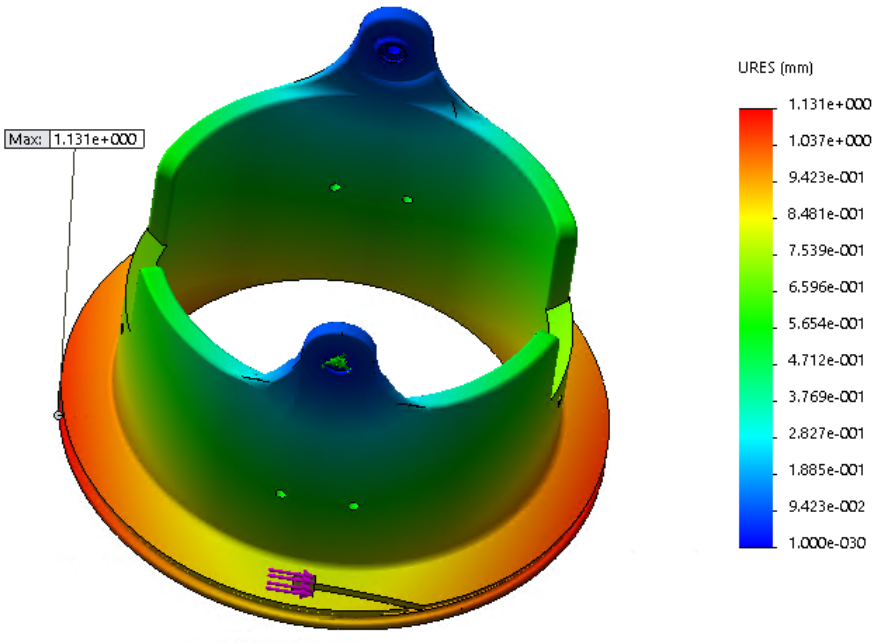

Figure 3.12: The load simulation displacement result of the forearm rotary part.

3.5 Elbow Mechanism Structure Design

Since the elbow joint only has one rotational degree of freedom, the mechanical revolute joint is the most similar and simplest structure which can represents the elbow joint. The mechanical revolute joint can be placed on anywhere as long as its rotation axis is along the rotation axis of elbow. This advantage makes the entire robot design more flexible in the elbow part. Since the robot is supposed to be small and light weight for a wearable design, the proper position for elbow structure is the place right beside the elbow.

As mentioned in chapter 2, there are two main ways to actuate the mechanical revolute joint. The rotational actuator could be used to rotate the joint directly; or the joint could be rotated by pulling the pivot part towards or push it away from the frame. From the mechanism point of view, the second actuating method is a planar four-bar linkage mechanism. In specific, it is an offset slider-cranks four-bar linkage mechanism (Figure 3.13). Typically, the linear

actuator, for example pneumatic cylinder or linear motor, is used directly to control the slider in the linkage mechanism. However, mounting actuators directly on the device is not a good way to reduce the weight for this project. So like the wrist mechanism, the same power transmission mechanism is used. An actuator controlled push-pull rod or two cables can be used to adjust the stroke. Also, an actuator controlled cable and spring back mechanism can be used to actuate this structure too.

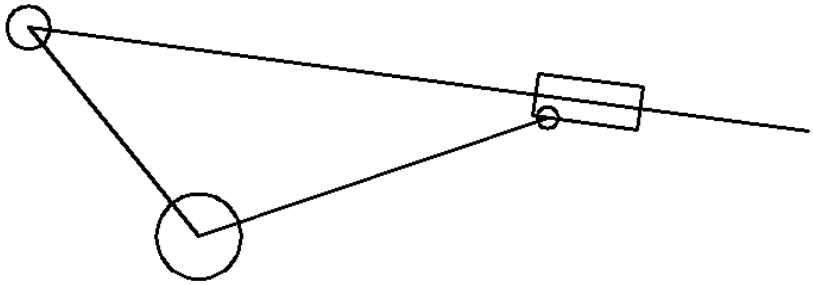

Figure 3.13: Offset slider-cranks four-bar linkage mechanism expression of the elbow structure.

By using the rod or cable to transfer the power, actuators can be removed to the control board. Because the push-pull rod is rigid, it is difficult to transfer the power from another direction. That means the actuator's output structure can be only mounted along the longitudinal axis of the rod. Thus, just like wrist mechanism and forearm mechanism, the push-pull cable is selected for transferring force form the actuator to the elbow mechanism. Though the cable cannot transfer compression force, the spring back mechanism can cover this shortcoming. Therefore, in order to simplify the structure, the electric actuator controlled cable pulled and spring back revolute joint mechanism is be used to express human's elbow flexion and extension motion. Figure 3.14 and Figure 3.15 shows the CAD model of the elbow structure. Figure 3.16

and Figure 3.17 show the result of load simulation. The spring back mechanism is designed as the part of the joint. The compression spring is used to store the energy. Thus, the default position of the wrist structure is fully extension position. The spring at this size can generate 2N force when it is compressed. Therefore, 2N force is applied in simulation.

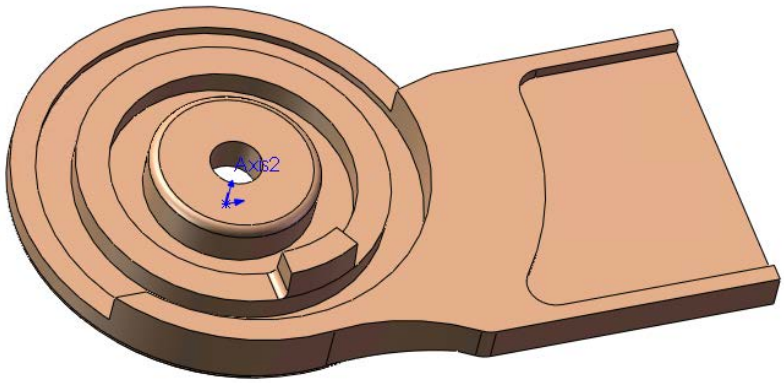

Figure 3.14: CAD model of the elbow structure with spring back design.

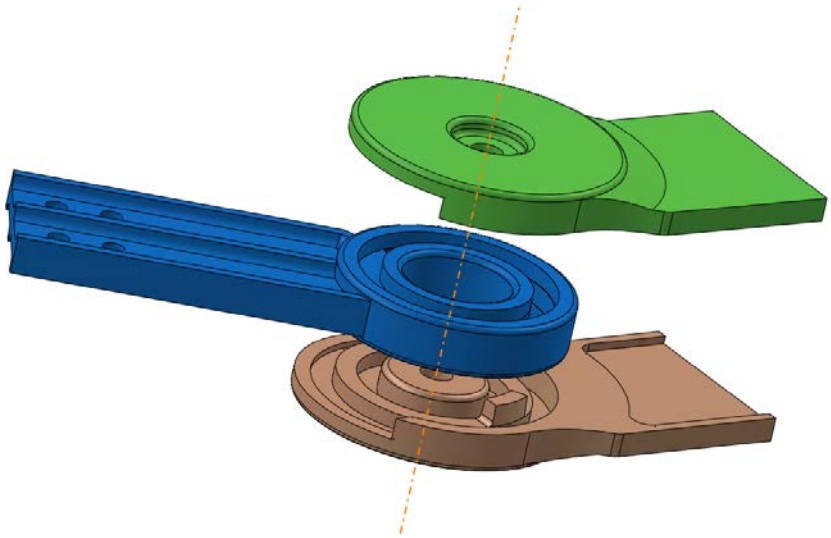

Figure 3.15: Elbow structure assembly's explosion view.

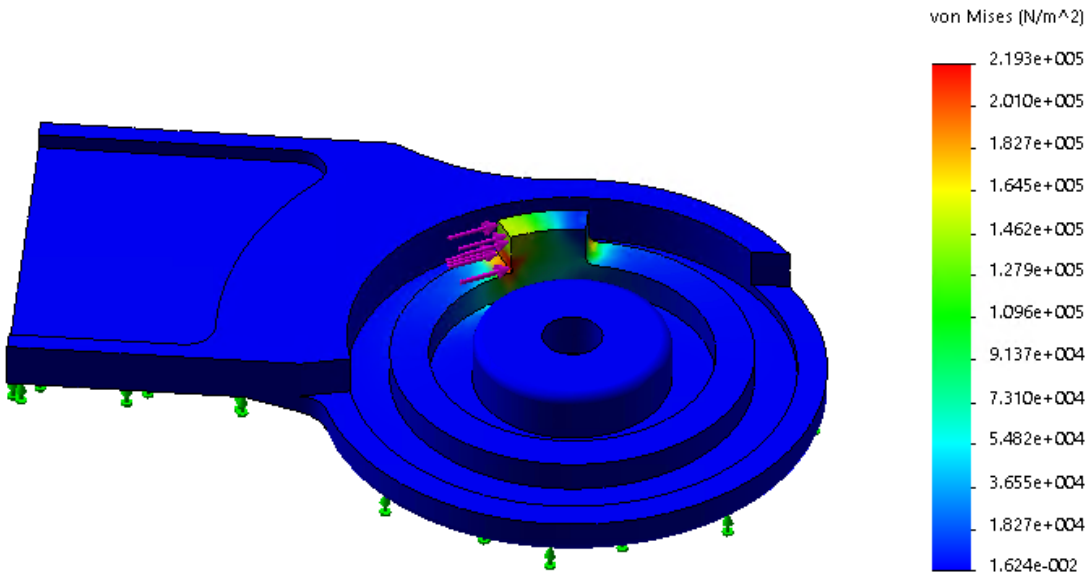

Figure 3.16: Load analysis stress result of the elbow structure.

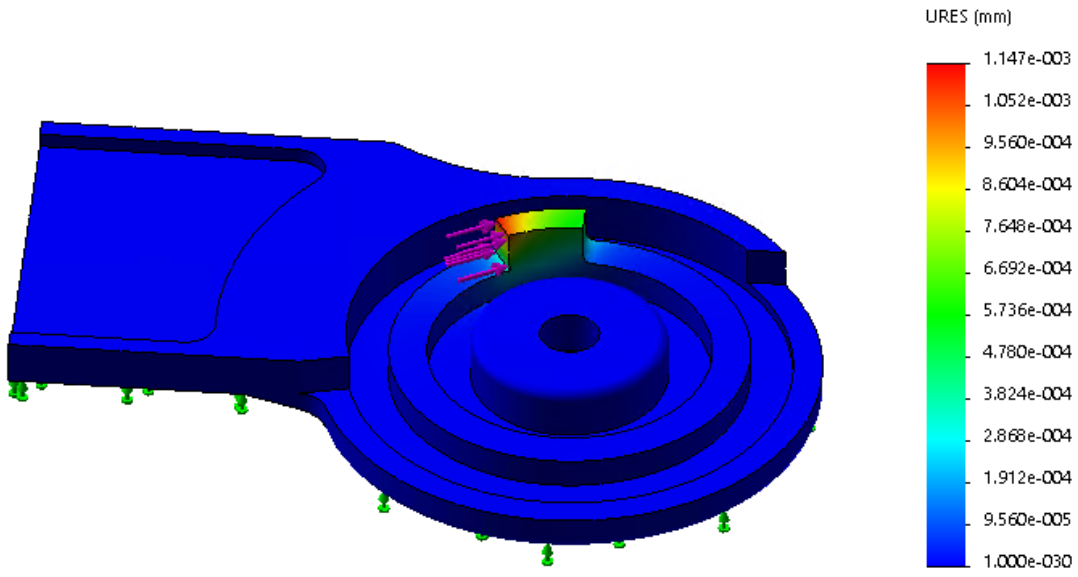

Figure 3.17: Load analysis displacement result of the elbow structure.

3.6 **The Rehabilitation Device Assembly**

Figure 3.18 shows the whole rehabilitation device assembly. Except bearings and shafts, all other parts are automatically made by 3D printer.

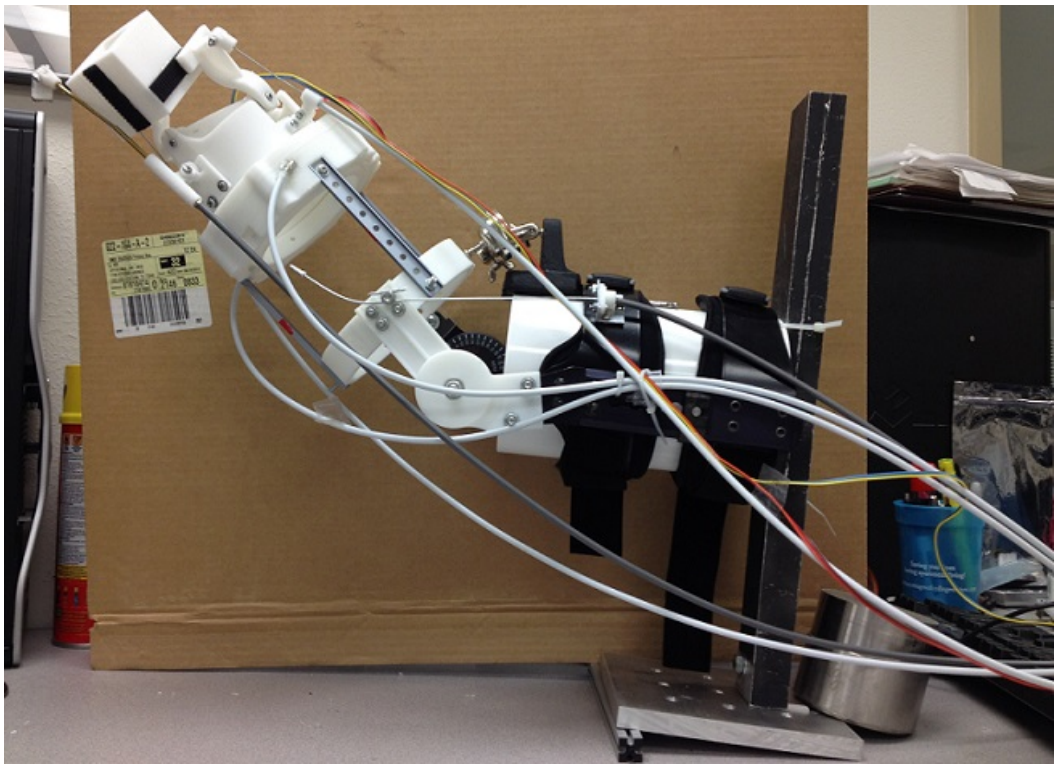

Figure 3.18: The rehabilitation device assembly.

4 CONTROL SYSTEM OF THE REHABILITATION DEVICE

Even after all parts were made and assembled together, the mechanism design and the structure design of the device still could not provide any anticipated motions without a control system. Thus, a control system was needed for the designed device. In this section, both hardware and software of the control system are reported.

4.1 **Actuating Method Selection**

There are many different power sources available in the current world. Among them, hydraulic drive system, pneumatic drive system, and electric drive systems are the most commonly used drive methods for mechanical devices. Additionally, these three drive methods are most popular in robotics. Selecting a proper drive system was the first step and also the most important step for control system design.

The hydraulic drive system uses pressurized hydraulic fluid to power hydraulic machinery. Basically, the hydraulic fluid is considered as incompressible. Thus, the hydraulic system can drive the machine precisely and at high operating speeds for both linear and rotational motions. Also, based on the basic principle of the hydraulic drive and Pascal's law, the hydraulic machine can provide extremely high force with very small input force. By using some special hydraulic fluid, which has low freezing point and high boiling point or little temperature sensitivity, the hydraulic system will still function well under extreme conditions. Therefore because of these advantages, the hydraulic drive system is usually used for heavy duty application and/or under extreme conditions. Aircraft hydraulics, submarine hydraulics, heavy duty mobile hydraulics and industrial hydraulics are some good examples.

Just as every coin has two sides, hydraulic drive systems also have some disadvantages. First of all, comparing to the simplest electronic motor drive system, the hydraulic drive system

is relatively a large and complex drive system. The system consists of at least three parts: the generator (the pump), control system (valves, filters, piping), and the actuator. However, the generator needs to be driven by another actuator, like an electric motor or an internal combustion engine. So this requirement makes the hydraulic drive system even more complex. In other words, the hydraulic drive system includes at least two systems: the hydraulic system itself, and the actuating system for the hydraulic generator. This creates a big and heavy system that does not support portability. In this research project, it is impossible for the user to carry the whole hydraulic drive system. Along with the previously stated vices, the hydraulic system requires professional routine maintenance. Just like any complex mechanical product, the hydraulic drive system may malfunction without proper routine maintenance. Last, usually the whole hydraulic system costs a lot of money.

In applications like aircraft, submarine, or industry heavy duty machinery, high strength, high accuracy, high speed, high durability, and ability to work under extreme conditions are most important things. Also, sometimes there is a group of technicians maintaining the whole machinery system. Thus, disadvantages mentioned above are not a big problem and the hydraulic drive system could be the best drive method in such applications. However, in this research project, high strength and high speed are not necessary. The device will only be used indoor under normal conditions. But it does require light weight, low maintenance, and low cost. Therefore, all advantages of the hydraulic drive system become pointless, and all disadvantages are strengthened in this wearable rehabilitation device designing project.

The pneumatic drive system is very similar to the hydraulic drive system. Instead of using pressurized liquid, it uses pressurized gas to power linear or rotational pneumatic actuators. The pneumatic system usually uses compressed air or compressed inert gases as the power source. Since the gas is compressible, usually the pneumatic actuators cannot provide

motions as accurate and fast as the hydraulic actuators. On the other hand, the air can be compressed to absorb shocks. Also the compressed air or inert gas is a lot safer and cleaner than flammable hydraulic oil. The pneumatic drive system still needs several components to work: the compressed air source (compressor or stored compressed air), control system (valves, piping), and the actuator. Unlike the hydraulic generator, the pneumatic generator (i.e. the air compressor) can generate compressed air by itself. Thus, the second actuating system is not necessary in a pneumatic drive system. Besides, the air compressor could be replaced by a refillable compressed air tank. As a result, the pneumatic drive system doesn't require extra electric power or any other power source.

In comparison to the hydraulic drive system, pneumatic valves and actuators are cheaper and easier to get from the market. As well, the pneumatic system usually applies lower pressure than hydraulic systems (most pneumatic applications use pressure around 100 psi; on the other hand, hydraulic applications use pressure from 1,000 psi up to 10,000 psi). It offers a simplified whole system and increased safety. In addition, since the compressed air is environment friendly, the pneumatic drive system doesn't have to be a close system like a hydraulic system. The pneumatic drive system could be designed as a close system, open system, or mixed system. This characteristic creates a lot of flexibility to the pneumatic drive system design. Many different kinds of pneumatic actuators in the market maximize the flexibility of the pneumatic drive system design. There is a variety of linear and rotational actuators in different sizes which have various levels of load capability, and stroke or speed. Currently, the pneumatic muscle has been used extensively in low load applications. It is a linear actuator, but is much more flexible than a pneumatic cylinder. Furthermore, air almost has no weight and low pressure components decrease the total weight of the pneumatic system. Thus, the relatively light weight pneumatic drive system with stored compressed air could be a good choice for this research project.

Comparing the hydraulic system and pneumatic system to the electric drive system, the electric drive system is a lot simpler. In some of the simplest applications, the electric drive system may just refer to the electric actuator. For most common applications, the electric drive system includes electric motor, motor driver, and the power source.

The electric drive system has many advantages. First of all, the electricity is very easy to supply and store. Rechargeable batteries or a disposable battery could be the alternative electric power source too. Besides, the whole system is very simple. Unlike pneumatic systems and hydraulic systems, the electric system doesn't need a generator and a physical valve/piping control system. The light weight microchip can provide all controlling logic for the actuator. For some motors, the entire close-loop system (drive board and sensor) is mounted on them. This compact structure increases the flexibility of the device design. In addition, there are so many different types of electric motors available in the market, such as AC or DC motors, linear or rotational motors, asynchronous or synchronous motors, and etc. Some special motors, like servo motors and stepper motors can provide motions with extremely high resolution. Some high-end motors' revolution could reach 0.02 degree for rotation or 0.001 mm for linear motion. Furthermore, electric actuators are cost effective. Thus, electric drive system is a good choice for robotics.

Both pneumatic drive systems and electric drive systems are feasible for this rehabilitation device project. With the compressed air tank, the entire pneumatic drive system could be portable. However, without the constant pressure supply from the generator, the pneumatic system requires a high pressure air tank with regulator(s) to provide constant relatively lower pressure for a period of time. A good example of such a pneumatic system is the scuba dive system. However in order to hold relatively high pressure, the material of the air tank is usually made of steel increasing the total weight of the system. Furthermore, after regulators

drop the pressure down to ambient pressure (about 15 psi), a typical 18 liter scuba tank with 4000 psi air pressure (about 50 lbs.) can only last about one hour for breathing. Thus, it is clear that a portable compressed air tank last less time for providing constant intermediate pressure (about 100 psi) to the device. Considering design goals like light weight/portable, simple structure, low loads, and low cost, the electric drive system is more proper. Since the rehabilitation device is not a heavy duty application, a small cheap hobby motor is good enough for it. Thus, the electric drive could be considered as the best choice for this research project. Details of motor selection are reported in a later section.

4.2 **Drive Structure Design**

As discussed in chapter 3, the device is driven by cables. However, the push-pull cables are a force transmission mechanism. They cannot generate any force by themselves; therefore the drive mechanism and the structure are needed in order to drive the cables.

Applied force can only be transmitted along the cable, thus mechanisms which can make cables move linearly are needed. In general classification, both rotational motion and translational motion can accomplish the requirement. It is clear that the translational motion from the generator can make cables move longitudinal. As long as the cable is attached on the moving stage of the generator, the cable can transmit longitudinal force and movement. For rotational motion generators, intermediary mechanisms are needed to transform rotational motions to translational motions in which there are so many mechanisms to carry out this purpose. For instance, cables could be twined on the rotatory part of the generator. An example of this is a spool, a drum or a disc with grooves to be the rotatory part of the generator. Cables are untwined or twined on the rotatory part tangentially from fixed outlet(s). This mechanism is very similar to the forearm mechanism which is discussed in chapter 2. In this way, the rotational motion

generator could provide linear motions to cables. Another mechanism that could be used is four-bar linkage mechanism. More specifically, the in-line (or off-line) slider crank four-bar linkage mechanism could transform rotational motion to translational motion. In addition, the rack and pinion mechanism could accomplish the purpose too. Furthermore, the screw mechanism (threaded rod mechanism) can also realize rotational motion to translational motion transformation. There are four most commonly used mechanisms for motion transforming. Some other mechanisms (like the cam mechanism) or derivative mechanism from each category could realize the same motion transforming function too, but they are less common and usually modified or designed for specific applications. Therefore, we will not discuss them in this section. For this research project, some specific modification may be need for the selected mechanism. They will be discussed later if applied. Table 4.1 summarized generators and mechanisms mentioned above with their common advantages/disadvantages and typical applications.

Generator	Linear motor	Rotary motor			
Motion transforming mechanism	No need	Spool	Slider crank four-bar linkage	Rack and pinion	Screw mechanism
Advantages	High accuracy	Simple: Long movement	Heavy duty	Simple; Medium duty	High accuracy; Heavy duty
Disadvantages	Complex; Expensive	Low (no) accuracy	Medium accuracy; None linear	Medium accuracy	Relatively low speed
Typical application(s)	Maglev train; Aircraft launch system	Hoist	Sharper machine; Compressor	Steering mechanism	CNC machine

Table 4.1: Summarization of generators and motion convert mechanisms.

Without any intermediary motion transmission or motion transforming mechanisms, the linear motor can generate translational movements with high accuracy. As mentioned above, some high-accuracy linear motor's resolution can reach 0.001 mm. However, compared to rotary motors with similar load capacity, linear motors are very expensive. Also, it's relatively more complex structure requires very high assembly accuracy to ensure the output accuracy. High accuracy is a big advantage; however, micrometer level accuracy is not needed in this research project. Making a high quality assembly (1-10 micrometers) on a light weight portable device is not an easy job. Besides, the expensive cost involved makes linear motors a less desirable option in this unfunded research project. Therefore, the linear motor was not the best choice for this research project.

With rotary motor, motion transforming mechanisms are needed for providing translational movements. The rotary motor with a grooved rotatory part to twine and untwine cable is a simple method for providing longitudinal cable movements. If the groove is deep enough, the spool can hold a very long cable. This is the biggest advantage of the spool design. However, we cannot expect any accurate cable length control for the spool design. The diameter of the cable is not ignorable, thus the cable has to be twined in a thread-like format. The cable will be twined over previous twined cable if the first layer of the spool is fulfilled. So, there is no accurate linear relationship between the length of the cable have been twined (or released) and the rotatory cycles of the rotary motor. There is a way to solve this problem. If the groove is shallow and narrow enough which can only hole one cable, and the spool rotates less than one cycle, then there is a linear relationship between the length of the cable have been twined (or released) and the rotational angle of the motor. The forearm mechanism discussed in chapter 2 works in this way. There are still some problems for the control structure in this project. First, the spool needs to be big enough for cable movement. This means that the circumference of the

spool needs to be at least twice longer than the stroke distance (cable movement length). Obviously, any big part could increase difficulty for designing a portable device. At the meantime, bigger diameter of the spool causes bigger torque load applied on the motor with the same force. Therefore, a better and stronger motor is needed for operating the mechanism. Usually, a stronger motor is bigger, heavier, and more expensive. None of these changes were expected in this project. As a result, the spool mechanism may not be a good choice for this project.

Slider crank four-bar linkage mechanism is a commonly used mechanism transforming motion in both directions. In other words, it can transfer motions between the linear motion and the rotational motion. A typical linear to rotational motion example is the piston-crank mechanism in internal combustion engines. A compressor application is a good example of rotational to linear motion transformation. One cycle of rotational motion delivers one stroke of linear motion. For an in-line slider crank mechanism, the relationship between the stroke distance and the rotational angle is a standard sine function. For an off-line mechanism, the relationship can be determined with position parameters making this mechanism proper for this project. The only problem is the relationship between the linear stroke and rotational angle is not linear, so the motor needs to be controlled precisely.

From a functional point of view, the rack and pinion mechanism is very similar to the slider crank mechanism. Both of them can transform motions between linear and rotational motion. The biggest difference is that as long as the power source is constant, the slider crank mechanism can transform stroke motion to constant one direction rotational motion in both high and low speed (and vice versa). Unfortunately, the rack and pinion mechanism cannot transform constant stroke motion to a single direction constant rotational motion (and vice versa) and can only be operated in low speed. This is the main reason that the rack and pinion mechanism

cannot be applied in any kind of engine or generator, but it is perfect for a steering mechanism. (Some derivative of the rack and pinion mechanism can transform a constant single direction rotational motion to linear stroke motion, and vice versa. This strengthens the functional similarity claim at the beginning of the paragraph, but its performance is a much worse than a slider crank mechanism. For example, the shock will be generated when changing direction etc. Besides, these derivatives are rarely used. Thus, a special case or special derivative is not considered as the common characteristics of one category of the mechanism.) Another difference which is worthy of mentioning is that the relationship between linear motion of the rack and the rotational motion of the pinion is linear. Since this research application will not involve any high speed motion, and the constant rotational motion input is not necessary, the rack and pinion mechanism could be a good choice for the drive mechanism of the cable.

The screw, (as a simple machine, not as a fastener; also known as threaded rod mechanism), is another very commonly used mechanism for transforming rotational motion to linear motion. The typical pitch of the threaded rod is small enough (i.e. the efficiency ŋ is below 50%) that it cannot transform linear motion back to rotational motion. This refers to the self-locking property of the screw. Another mechanical advantage of the screw is the force amplification, i.e. the force out to force in ratio is larger than 1. The cost of the force amplification is the decrease of moving speed.

Considering the structure of proper mechanisms mentioned above, both the slider crank mechanism and rack and pinion mechanism have perpendicular motion axes. In more detail, the rotational axis of the motor is perpendicular to the longitudinal axis of linear motion. So the motor has to be mounted perpendicular to the linear moving stage. On the other hand, the motor could be mounted in line, because the screw mechanism has coincident axes. . Obviously, the perpendicular structure needs more space than an in-line structure. Thus, the screw mechanism is

better size-wise. Based on the basic principle of the electric motor, it is easier to increase motor's speed than to increase the motor's output torque. (Excepting extremely high speed motors which can reach 100,000 rpm or higher. To these extremely high speed motors, the bottleneck for speed increasing is the speed tolerance of physical bearings. Many research groups are focusing on new types of bearings and their performance.) In order to reduce high rotational speed to relatively low speed, a planetary gearbox or better gearbox is required. Because of this there usually are more relatively high speed motors available in the market than low speed electric motors. Also, because of its force amplification property and self-locking property, the screw mechanism has been used as motion transferring mechanism more often than the slider crank mechanism and the rack and pinion mechanism. So there are many different types of screw shaft and nuts available in the market, and the cost is relatively low compared to the slider crank mechanism or the rack and pinion with similar quality. Actually, most "linear motors" available in the market are the combo of rotatory motion and screw mechanism. Since the screw mechanism is better size-wise, availability-wise, and cost-wise, the screw mechanism was selected for this research project.

4.3 **Motor Selection**

Since the screw mechanism was selected for the drive structure, the electric motor may doesn't need much torque output. Based on the load simulation in chapter 3, the minimum break force was 35 N. It is not necessary for the screw mechanism to provide the break force, but it will increase the capacity margin if the drive mechanism can provide 35 N force or more. So this minimum break force was used as the reference for motor selection.

The principles of operation of both AC motors and DC motors are very similar regarding the interaction of the magnetic field. The only difference is that the AC motors don't need

commutation. There are many different types of AC motors; however, they are usually designed for industrial usage. Thus, they are usually big in size, heavy weight, high cost and for heavy duty jobs. Some industrial AC motors cannot use two-phase low voltage electric power which is supplied for the public. They require three-phase 380 Volt or higher voltage electric power which is only supplied for the industry. In general, there are no or little available AC motors for hobby level application. Therefore, the DC motor would be the better option for such applications.

Based on how the stator magnetic fields are created, DC motors can be classified into two main categories: permanent magnet DC motors and electrically excited DC motors. Furthermore, the electrically excited DC motors are classified into at least three sub-categories: shunt wound, series wound, and compound wound. Comparing electrically excited DC motors, the stator magnetic fields in permanent magnet DC motors are created by permanent magnets, so there is no I2R heating problem. Since the permanent magnets are a lot stronger than field winding with the same size, the permanent magnet DC motors are smaller than other types of DC motor. Usually, the size of the permanent magnet DC motor is about one fourth of the size of equivalent electrically excited DC motor. Since the current and field change direction only in the rotor, rotation direction could be easily reserved by switching the polarity of the applied power. Also, the relationship between torque and speed of the permanent magnet DC motor is linear and simplifies the controlling algorithm. Because of all these benefits, permanent magnet DC motor was selected for this research project.

The permanent magnet DC motor also has three sub-categories: brushed, brushless, and stepper motor. Brushes and commutator are used to reverse the direction of the current. However, the brushless DC motor has a permanent magnet on the rotary and rotational field on the stator. So the rotary doesn’t need the commutator to change the current direction, and the

brush is not needed as the result. It uses transistor to reverse the current. From a maintenance point of view, the brushless DC motor is better because there is no need to replace the worn brush. Also, without the coil in the rotor, the inertia of the rotor is a lot smaller than a brushed DC motor making the control a lot easier. Thus, the brushless DC motor or stepper motor would be a good choice for this research project.

Since the screw mechanism will be used in the drive structure, the selection of the threaded rod should be made at the same time. Since the friction of the threaded rod and nut really depends on its helix angle, the quality of manufacturing and how well it is lubricated, the efficiency of this mechanism cannot be fixed to a certain number. But usually the efficiency is around 15% to 40%. Thus, the analysis here for selection is based on the assumption that the ideal screw mechanism (i.e. it is a frictionless threaded rod and nut) was used.

Because of the frictionless assumption, there is no energy loss. So the work done by input force is equal to the work done by the screw:

$$W_{in} = W_{out} \tag{4.1}$$

Since the work is equal to the product of the force and the distance it acts, so

$$W_{in} = 2\pi r \cdot F_{in} \tag{4.2}$$

$$W_{out} = l \cdot F_{out} \tag{4.3}$$

where l is the lead of the screw. So the ideal mechanical advantage MA_i is equal to the distance ratio:

$$MA_i = \frac{F_{out}}{F_{in}} = \frac{2\pi r}{l} \tag{4.4}$$

and the torque format is:

$$\frac{F_{out}}{T_{in}} = \frac{2\pi}{l} \tag{4.5}$$

As mentioned above, the brushless DC motor or stepper motor could be a good choice for this application. In order to improve the accuracy of motor speed and rotation angle, the stepper motor or servo motor could be used. The servo motor mentioned in this paper is the combo of DC brushless motor and rotational encoder (or rotor tachometer).

However, to maintain high resolution of the motor outputs, a high accuracy (i.e. low backlash) mechanical structure is needed. Typically, the power screws can address the backlash problem by preloading the nut(s). For medium-range lead, the ball screws are usually used to reduce the friction. Thus, the power ball screws are commonly used in CNC machines to keep motors' high resolution and are costly. It should be noted that extremely high accuracy is not necessary for rehabilitation purpose. So the selected screw mechanism is the affordable standard lead screw. The nut's material is medium to low grade bronze, and the screw material is stainless steel. The manufacturing quality of the screw and nut are not very high. Thus, the measured backlash is about 0.5 mm. considering the lead screw only, the 0.5 mm backlash means that the nut may not move even if the screw is rotated about 90 degrees. Therefore, any motor which has a resolution higher than 90 degrees becomes meaningless with this specific lead screw. The ultimate purpose of motor selection is to control the end-effector for providing motion. Therefore, the position or the speed of the end-effector is more important than the motor's speed and position accuracy. Since sensors will be applied directly on the end-effector joints for gathering information, high resolution motors are not necessary in this application.

In order to approve the above analysis, an available 28byj-48 stepper motor was used to rotate the lead screw. Based on the data sheet of the stepper motor, this is a 4 phase unipolar stepper motor. The motor came with a 1/64 ratio speed reduction gearbox. The frequency is 100

Hz, and the stride angle is 5.625°/64. In order to achieve high torque and high resolution, the 1/8th micro-stepping was used to operate it. The sequence is 1, 12, 2, 23, 3, 34, 4, 41. Thus, the output axle's resolution is about 0.7°/step. In theory, the screw nut's position resolution could reach about 0.0039 mm/step. But as expected, the nut cannot provide as fine a position movement as in calculation, and the stepper motor was being used like a normal DC motor while operating. Besides, the low speed of the stepper motor became the biggest disadvantage. Since the frequency of the motor is only 100 Hz, the highest speed the motor could reach is 12.5 cycles/second. Because of the speed reduction gearbox, the output shaft could only reach approximately 0.2 cycle/second, which is about 12 rpm. With speed reduction of the screw mechanism, the nut's maximum moving speed is about 24 mm/min. It is obvious that this speed is way too slow for providing exercise. In conclusion, the high resolution motors are not necessary for this project.

Of course, there are so many high speed and high resolution motors available in the market, and they are suitable for this project. But they usually cost several times more than the standard brushless DC motors. To reduce the cost of this project, the standard brushless DC motors were used.

Based on the availability of the threaded rod/nut and the DC motor, the cost, and other factors, the right-hand, single start, 2 mm pitch, 8 mm diameter lead screw with matching nuts, and 300 rpm, 12 volt, 0.6 amp, DC geared motors were selected for this research project.

Take efficiency ŋ into consideration, $W_{in} = ŋ \cdot W_{out}$. Thus, the real mechanical advantage MAr equal to:

$$MA_r = \frac{ŋ \cdot F_{out}}{F_{in}} = \frac{2\pi r \cdot ŋ}{l} \tag{4.6}$$

The efficiency can be calculated based on the Mechanical Manual. Based on the information above, we know that the static frictional coefficient between bronze and steel with lubricated and greasy surfaces is about 0.16. Using 8 mm screw pitch diameter and 2 mm screw lead for calculating the screw efficiency we get about 32.79%. Applying the efficiency range 30% ~ 35% instead of 32.79% efficiency in the equation x, we know that

$$MA_r = \frac{\eta \cdot F_{out}}{F_{in}} = \frac{2\pi r \cdot \eta}{l} = \frac{2\pi \times 4\ (mm) \times (30\% \sim 35\%)}{2\ (mm)} \approx 3.77 \sim 4.40 \quad (4.7)$$

$$\frac{\eta \cdot F_{out}}{T_{in}} = \frac{2\pi \cdot \eta}{l} = \frac{2\pi \times (30\% \sim 35\%)}{2\ (mm)} \approx 0.94 \sim 1.10\ (1/mm) \quad (4.8)$$

The torque is measured by force sensor. Figure 4.1 shows the Current-Torque curve and Voltage-Speed curve. The speed and the torque were measured on the output shaft of gearbox. The gearbox ratio is 16:1.

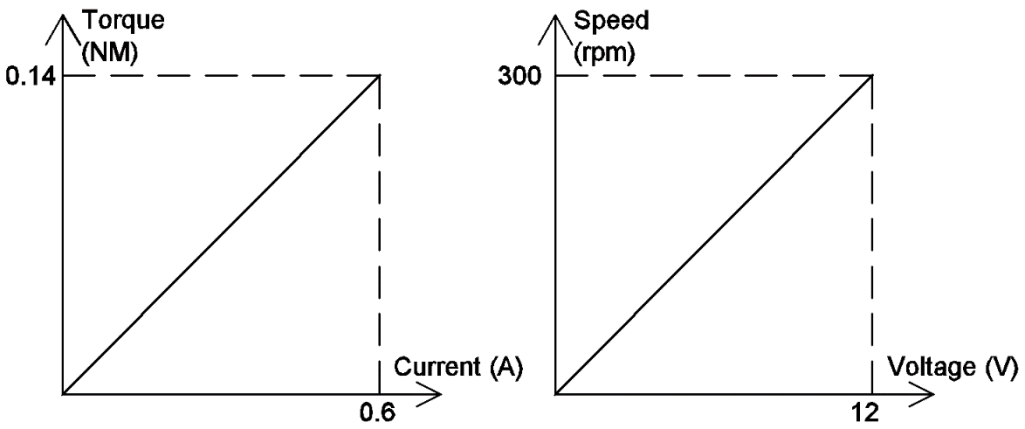

Figure 4.1: Torque-Current curve and Speed-Voltage curve of the selected motor.

With selected motors and threaded rods, the structure of the drive mechanism could be designed. There are four set of screw mechanisms for controlling four degrees-of-freedom. The

length of the threaded rod was determined by the cable's necessary movement distance. Each threaded rod was supported by a set of bearings at both ends. Motors were mounted along the threaded rods. Rigid couplers were used for transferring power from the motors to the threaded rods. Nuts on the threaded rods were used as the moving platform. The Figure 4.2 shows the structure of the drive mechanism.

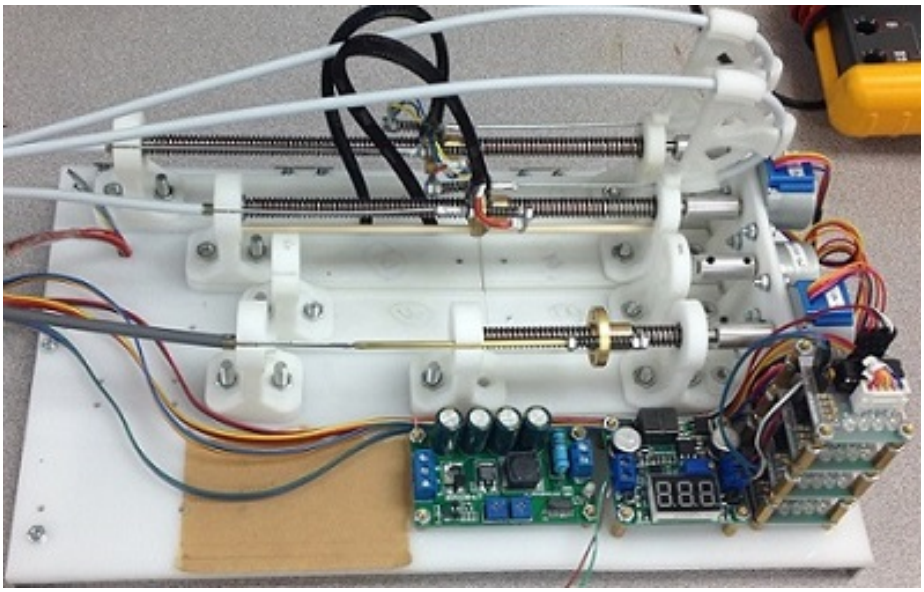

Figure 4.2: Drive mechanism structure.

4.4 **Sensor Application**

Sensors were applied for making the control loop a closed-loop system. At the wrist joint-end, rotational potentiometers were used to measure the angular position of each joint. By calculating the changing rate, rotational speed could also be detected by the potentiometer. Both speed and position information is important in the control loop for decision making.

Hall-Effect proximity sensors were applied in this project too for limiting the range of motions and measuring applied force. Instead of the switch or latch type sensor, the linear analog output type sensors were selected for fulfilling these two purposes. Because of the size of the structure, small straight permanent magnets were used to provide the magnetic field. The value of the analog output of the sensor is linear to the intensity of the magnetic field. Also, the strength of the magnetic field diminishes inversely proportional to the cube of the distance from the magnet (dipole). Therefore, the output of the sensor can indicate the distance between the sensor and the magnet.

For the limiting range of motions purpose, the sensors were mounted on both ends of the screw mechanism and the small magnets were mounted on the nut. By having constant changing values as the input, the controller could know the real-time position of the nut. Thus, the motor could reduce its speed in a relatively far distance to eliminate the shock, which may be created by a sudden stop.

For the force measuring purpose, the sensors and magnets were all mounted on the nut. The spring supported floating platforms from the nut were designed to mount the sensors. Cables were connected directly on the platforms. When the force is applied on the cable, it will also be applied on the floating platform. Then the spring contracts until its force equalizes the applied force. Thus the floating platform will move a small distance. Because of Hooke's law, the force present in distance changes proportionally. Also because of the relationship between the distance and the output of the sensor, the applied force can be measured by the Hall Effect sensor in this way. Figure 4.3 shows the spring supported floating platform on the nut, and Figure 4.4 shows the sensor mounting method on the nut.

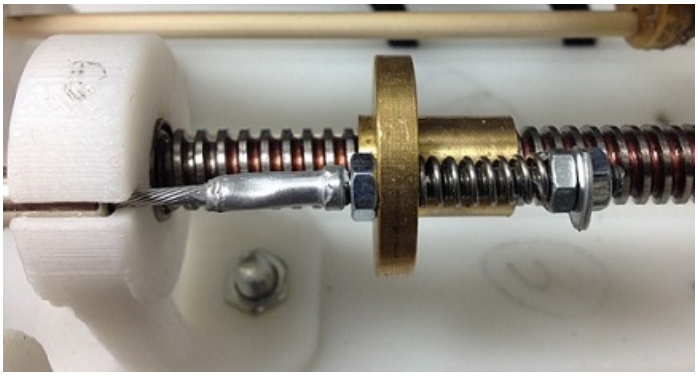

Figure 4.3: Spring supported floating platform.

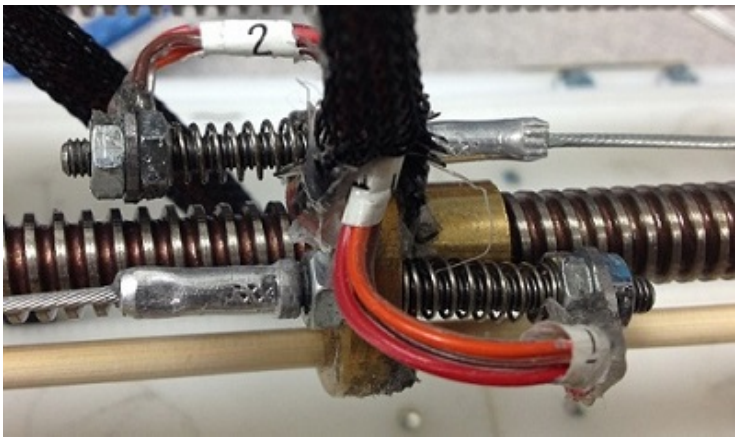

Figure 4.4: Sensor mounting method on the nut.

4.5 **Microchip Selection**

For commercial level products, simple function devices don’t require a complex CPU for functioning. A simple logic hardware circuit is good enough to deliver functions, reduce costs, and improve product's durability. Commonly used non-programmable calculators are good examples. However, for prototype designing, using a programmable microchip is proper for testing and modifying. Thus, the selection of the microchip is reported in this part.

Since the prototype didn't require massive data calculation, the frequency of the CPU is not the most important reference for selection. However, since the device has at least four motors, ten sensors, about ten buttons/switches and LED lights for controlling and indicating, the number of I/O s of the microchip would be the main criteria for selection. Meanwhile, the user friendliness, the programming language, the size and the price are also in consideration.

Based on requirements mentioned above, a single-board microcontroller was a good option. Because of the low cost, the user friendly software, and assembled board option, Arduino boards were chosen for this project. The programming language is C or C++. The following Table 4.2 lists characteristics of several commonly used Arduino boards which may be applied in this project.

Name	Processor	Operating Voltage	Input Voltage	CPU Speed	Analog I/O	Digital I/O (PWM)	Flash (KB)
Uno	ATmega328	5 V	7 - 12 V	16 MHz	6/0	14(6)	32
Due	AT91SAM3X8E	3.3 V	7 - 12 V	84 MHz	12/2	54(12)	512
Leonardo	ATmega32u4	5 V	7 - 12 V	16 MHz	12/0	20(7)	32
Mega 2560	ATmega2560	5 V	7 - 12 V	16 MHz	16/0	54(15)	256
Nano	ATmega168	5 V	7 - 9 V	16 MHz	8/0	14(6)	16
Pro(328)	ATmega328	5 V	5 - 12 V	16 MHz	6/0	14(6)	32
Yun	ATmega32u4	5 V	5 V	16 MHz	12/0	20(7)	32

Table 4.2: Characteristics of several most commonly used Arduino boards.

Since PWM signals are needed for controlling the speed of DC motors, the number of PWM output channels has to be eight or more. Also, all proximity sensors (both potentiometers and Hall Effect sensors) are analog output type. So the number of analog input channels has to be ten or more. Based on these I/O requirements, only Mega 2560 (or Mega ADK) and due are suitable. Since the CPU speed and the analog output are not critical, and higher output voltage is better for motor control, the Mega 2560 board was selected for this project.

4.6 **Motor Drive Circuit Design**

For permanent magnet DC motors, the set drive voltage is the only thing for open loop controlling. The speed of the motor and the output torque are decided by the characteristics of the motor and the load applied on the motor. For closed loop control, adjustable drive voltage is very meaningful. The sensor measures the output speed or torque constantly and sends the signal back to the CPU. The CPU compares the feedback signal with a preset value, and then adjusts the drive voltage trying to eliminate the difference between measured value and preset value. A PID controlling structure is used in the comparison and decision making process. The control algorithm is the software design. Before writing program codes, the hardware circuit design was needed to be designed for making the output drive signal usable to control motors. In this part, the hardware circuit design is reported.

Compared to linear amplifiers control, Pulse Width Modulation (PWM) is a more commonly used speed controlling method for DC motors. It can drive either bipolar transistors or field-effect transistors with very small power dissipation. The basic PWM principle is that the DC power supply voltage is provided with a fixed frequency between two values (in this case is 5v and 0). The asymmetric square waveform has a duty cycle defined as the ratio between the

ON time and the period. By changing the duty cycle, the average current through the motor is changing. As a result, the motor speed or torque changes at the output.

The PWM signal from the CPU may reach 5V at most. However, 5V was not big enough to drive the 12V motor. Thus, a voltage amplifier was needed to amplify the PWM signal to the proper voltage. There were many amplifier circuits available for this purpose. So the right model was needed to be found. If the circuit can realize the same function within the tolerance, a simpler circuit is better. Based on this principle, the basic single-stage bipolar junction transistor (BJT) amplifier was tried first. This basic model is a common emitter circuit. With a pull up resistor, the collector is the output and the base terminal is the input. Typically, the small signal limit caused by low input dynamic range is the major limitation. Exceeding the limitation will cause high distortion. Thus, the input signal is required to be a small signal, and the emitter degeneration and biasing are designed to alleviate the distortion issue.

Based on the availability in lab, the NPN transistor 2N3904 was used to build the common emitter amplifier. Based on its data sheet, the Emitter-Base voltage is 6V. Obviously, the 5V signal didn't exceed the limitation, but it is a relatively big signal. So some distortion was expected without reducing the signal or using emitter degeneration and biasing. However, based on the observation from the oscilloscope, the basic NPN common-emitter circuit did not have much distortion or was not observed. Figure 4.5 shows the PWM signal from the CPU, and the Figure 4.6 shows the amplified voltage by basic common-emitter model. Therefore, the basic model is proper for this application.

Figure 4.5: Output PWM signal (5v) from CPU.

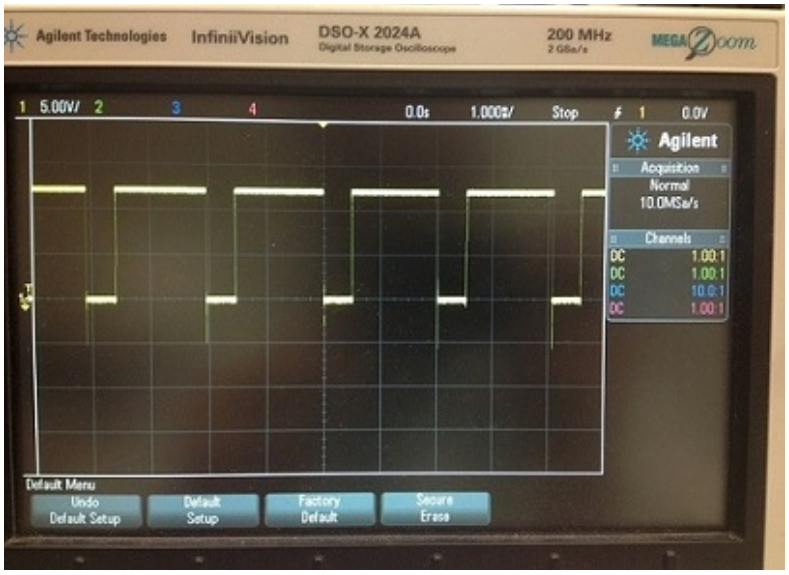

Figure 4.6: Amplified speed control voltage (12v) for motors.

To DC motors, the direction of rotation is related to the direction of the drive current. To change the direction of the motor rotation, the H bridge structure can realize this function without physically changing the polarity of the power supply. It is possible to use BJTs or

MOSFETs to build an H bridge, but it may take a long time to find the right transistor and design the right bias. Thus the l9110s H-bridge chip was used directly. By controlling the input combinations, the direction of output current can be controlled. As a result, the rotation direction of the DC motor can be controlled by program. The Figure 4.7 shows the diagram of PWM speed control and rotation direction control.

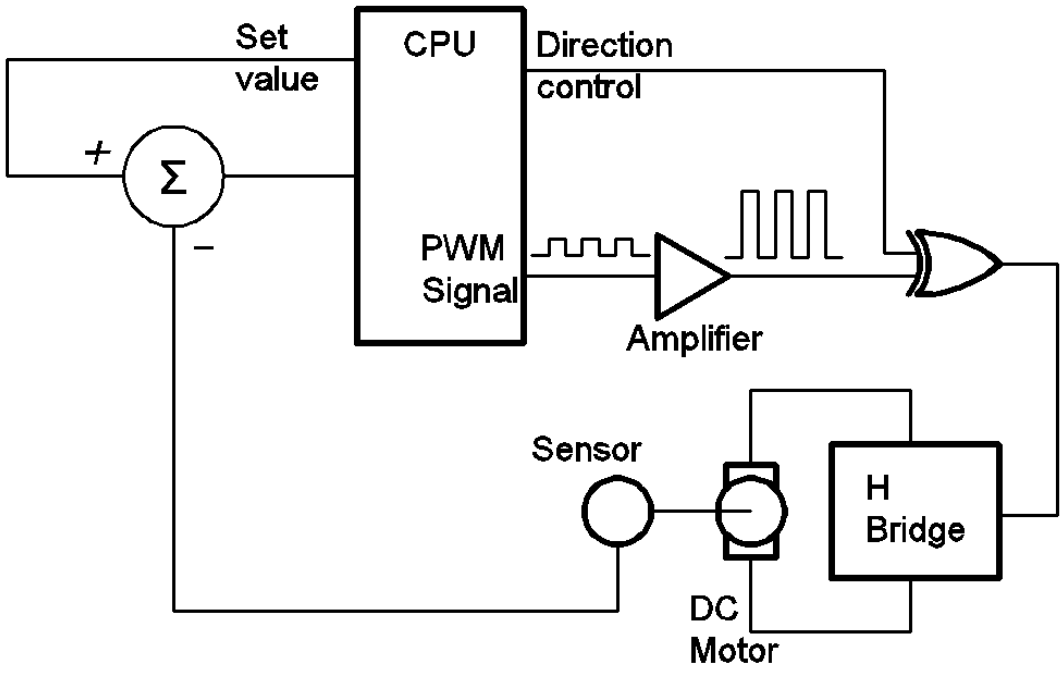

Figure 4.7: PWM speed and direction feedback control diagram.

4.7 PID Control Algorithm

As showed above, the feedback control system was designed. In order to have better speed or position control, the PID controller was decided to use. Theoretically, it is possible to design a PID controller based on the physical device. However, it would take a very long time

for testing. Therefore, the controller design was based on the system model, and the results were calculated by Matlab.

As mentioned in previous chapters, the rehabilitation device is driven by cables. So, the actuators are not controlling the device directly. All mechanics factors (like gravity, friction, loads, noise, etc.) which should be considered in typical parallel robots become the pulling force of the cable. The pulling force on the cable than become the load on DC motor. Based on the torque - speed curve of the DC motor, the load on the motor shaft affect the speed of the motor linearly. In order to provide the output at certain speed, the controller could be designed to adjust the duty cycle of the PWM signal based on the speed – voltage curve of the DC motor. Therefore, the whole system control becomes the motor speed control in this project.

In order to design the controller for the system, the DC motor needs to be modeled first. According to the measurement results and the datasheet of the motor, specifications are listed in Table 4.3.

Specification	Units	Motor
Normal supply voltage	VDC	12
Operation voltage	VDC	1.5 - 13
No load speed	RPM	4800
Peak current	Amps	0.6
Peak torque	N·m	9.38×10^{-3}
Rotor inertia (J)	$Kg \cdot m^2$	1×10^{-6}
Viscous friction constant (b)	N·m·s/rad	1×10^{-6}
Electromotive force constant (Ke)	V/rad/sec	0.024
Motor torque constant (Kt)	N·m/A	0.0156
Terminal resistance (R)	Ohm	6.5
Inductance (L)	H	0.3×10^{-3}

Table 4.3: Specifications of the DC motor.

The modeling of the DC motor in Matlab Simulink was based on equation 4.9 Newton's law and equation 4.10 Kirchhoff's law. The Simulink model of the DC motor is shown in Figure 4.8.

$$J\frac{d^2\theta}{dt^2} = T - b\frac{d\theta}{dt} \xrightarrow{yields} \frac{d^2\theta}{dt^2} = \frac{1}{J}(K_t i - b\frac{d\theta}{dt}) \tag{4.9}$$

$$L\frac{di}{dt} = -Ri + V - e \xrightarrow{yields} \frac{di}{dt} = \frac{1}{L}(-Ri + V - K_e\frac{d\theta}{dt}) \tag{4.10}$$

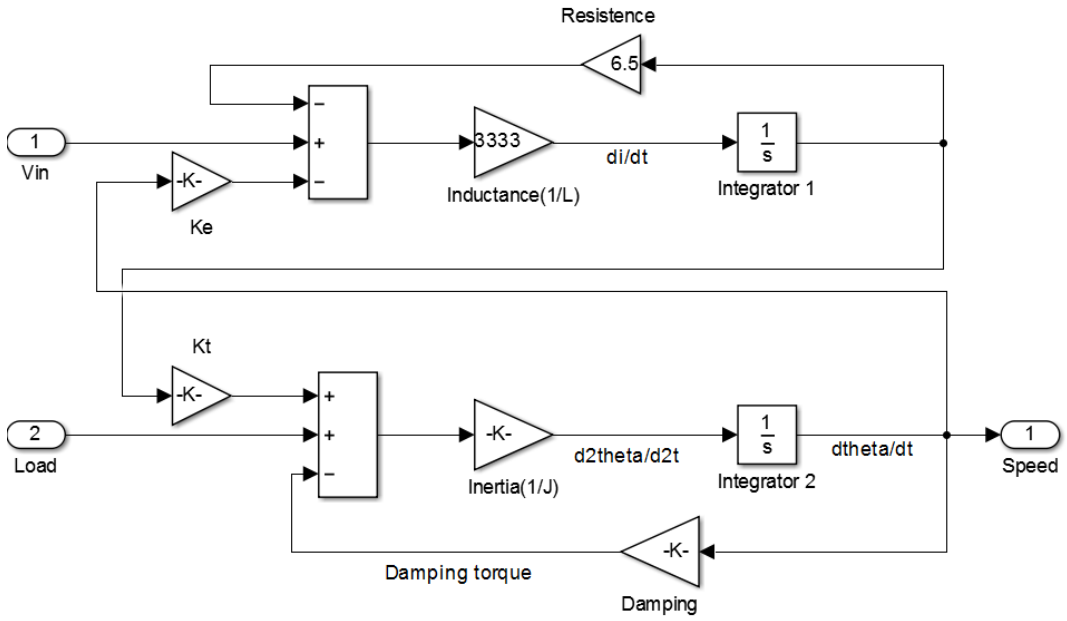

Figure 4.8: Simulink model of the DC motor.

Then the close-loop system with PID controller was modeled in Simulink. Figure 4.9 shows the close-loop system model. Scopes were used to monitor the results. In order to compare results with or without the PID controller in the system, the manual switch was used to let the signal pass through or skip the controller. A random load was applied to the system. The random load signal was limited in ± 1 mN·m. It is about 21% of the stall torque. A 0.1 second

delay was applied to the random load signal. So we could observe the original response of the controller before the random load signal was applied. After several trials, values for PID were set at 0.4540 for proportional (P), 44.23 for integral (I), and – 9.495 for derivative (D).

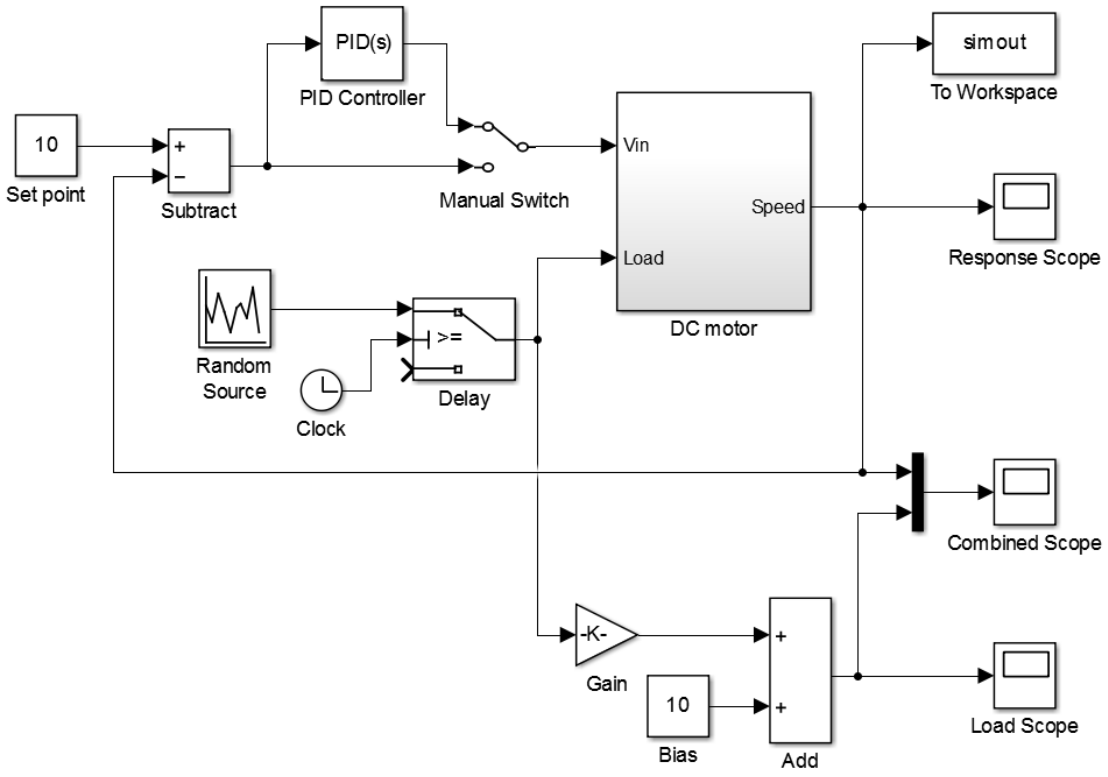

Figure 4.9: Simulink model of the motor speed control system.

The results are showing in following figures. Figure 4.10 shows the output without PID controller. The green line indicates the random load signal versus time (1 second), and the blue line is the output response versus time (1 second). From the result we could see that the output had a big steady state error (0.25). Also, the output affected by the load. The system output cannot maintain the set value (which is the speed for the motor) at all. Figure 4.11 shows the

output with the PID controller. The green line indicates the same random load signal versus time (1 second), and the blue line is the output response versus time (1 second). From the result we could see that the system is stable and the steady state error is very small (about 0.5 x 10-3) after about 0.04 second. The output can keep at the set value after about 0.04 second after load changed. Thus, we could know that the PID controller did functioning as expected. However, the controller also has a limitation. If the frequency of the random signal is higher than 25 Hz, the controller may struggle to control the output.

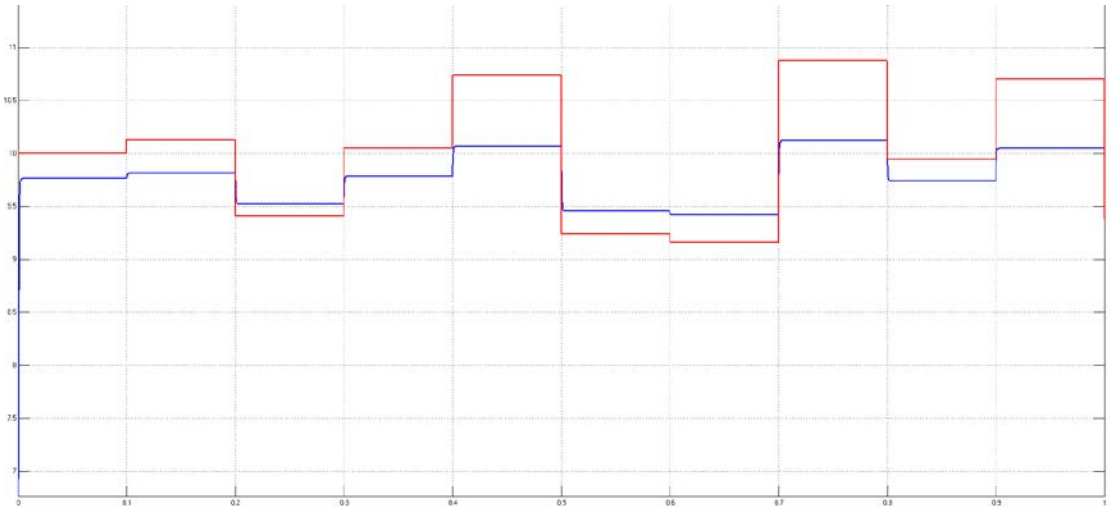

Figure 4.10: Output response without PID controller.

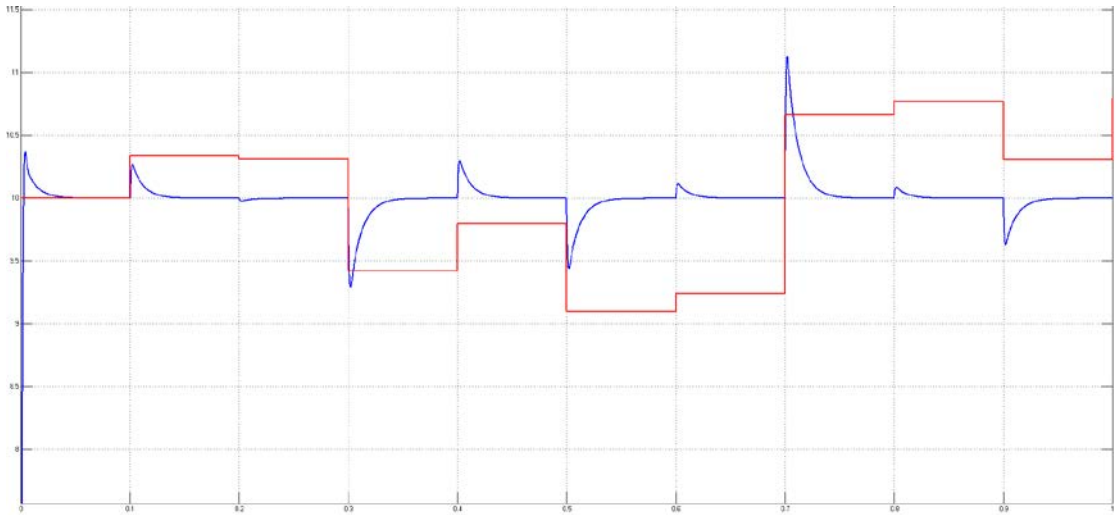

Figure 4.11: Output response with the PID controller.

However, the PID controller seems not necessary based on the simulation results. The main reason is that the screw mechanism reduced the influence of the load for the motor. As explained in previous sections, cables are connected on the nuts and the screws have self-locking property. Thus the load applied on the cable cannot affect the motor, but can only affect the friction force between the nut and the screw. According to the standard friction equation, the friction force equal to the friction coefficient times the normal force. As mentioned in previous section, the friction coefficient is 0.16. Because the pitch of the screw is 2 mm, so 99.5% of the load becomes the normal force in the friction equation. The extra torque applied on the output shaft of the gearbox can be calculated by the friction force times the radius of the screw, which is 4 mm. Since the gearbox ratio is 16, the extra torque applied on the motor is 1/16 of the torque on the output shaft of the gearbox. Take the random load signal generated in simulation as an example, the ± 1 mN·m load on the motor equals to more than 50 N (11.3 lbf.) force at the end-effector.

From the Figure 4.10 we could know that the difference of the output is only about 0.7 V under this load signal. Based on the simulation results of device components in chapter 3, the load capacity is about 35 N. So the load change should be obviously smaller than 10 N under normal operation conditions. In this scenario, the voltage change would be only about 0.1 V without the PID controller. Figure 4.12 shows the output result without PID controller under 10 N force changes on end-effector. 0.1 V change is so small that it could be easily overshadowed by circuit noise and other environment factors.

In conclusion, the PID controller could keep the output at set value as expected. However, since the change of load hardly influent the load of motor because of the screw mechanism and the gearbox, the PID controller is not necessary for the designed rehabilitation device.

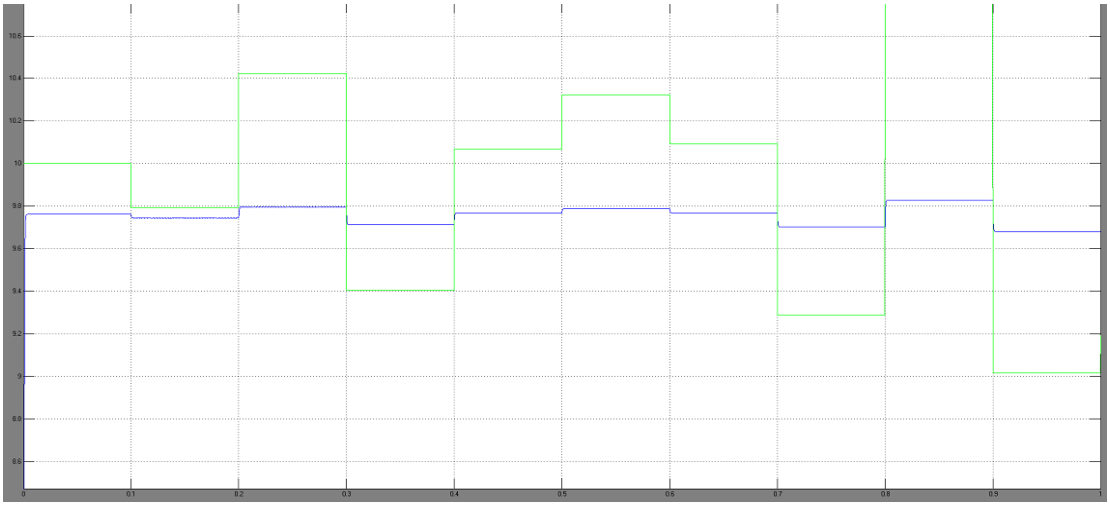

Figure 4.12: Output response without PID controller under 10 N load changes at the end-effector.

5 PERFORMANCE TESTS AND RESULTS

After building the prototype, performance tests were necessary to evaluate the design. In this chapter, the material performance test, device performance tests, and device properties will be reported. All tests were focused on the performance of the device. No data was collected from human subjects.

5.1 **FDM Part Mechanical Performance Test**

5.1.1 Purpose of the test

As mentioned in chapter 3, the Fused Deposition modeling is a rapid prototyping method. It heats the material, extrudes the material along the preset trajectory, and "prints out" the respective part layer by layer. Because it is almost impossible to make semifluid material melt into cooled material, the greatest drawback is the unpredictable low adhesive strength between layers and lines. Furthermore, the unstable environment conditions make the prediction of the weakest location more complicated. Therefore, the simulation reported in chapter 3 which was based off the assumption that the part was made as a solid piece, is not very accurate.

Although the simulation may not have been accurate, this result does not dismiss the simulation’s usefulness in such application. However, the accuracy of the simulation is required and can thus be measured by conducting several mechanical performance tests of each part. The relationship between the mechanical performance of FDM part and simulation result will be identified through this test. Furthermore, this relationship can be used to analyze the simulation result and predict all other FDM parts.

5.1.2 Hypothesis and experiment design

Because the mechanical performance tests are destructive experiments, testing every part would cost too much time and money and make the simulation meaningless. Therefore, only one force component was tested. In this experiment, the upper part of the passive constraint mechanism (shown in Figure 3.5) was selected for testing.

The part selected for testing is made layer by layer, and its layers can be increased along the X, Y, or Z axis. As a result, there are three different ways to "print out" the part. The Figure 5.1 shows the same part made along three different axes. Based on the characteristics of the FDM, the crack should only begin and develop between layers. Specifically, the fracture surface should always be perpendicular to the layers' increasing axis. The fracture will occur at the weakest section (i.e. the smallest contact area if adhesive strength between layers is uniform). Therefore, to increase contact area the part must be strengthen as well. In this case, the part "printed out" along X axis or Z axis should be the strongest, while the part "printed out" along Y axis should be the weakest.

Since the FDM device is capable of making parts hollow or solid, parts with different filling percentages will be tested to verify the hypothesis mentioned above. It is obvious that hollow parts are weaker than solid parts. But with the same filling percentage, the part "printed out" along Y axis should always be weaker than the others. Therefore, the expected curves are relatively flat but have tendency to increase as the filling percentage increases. The curve represents parts built along the X axis and Z axis, which should display larger values compared to parts built along the Y axis. In addition, the Y axis curve should not intersect other curves.

In order to reduce the effect of gross error, four parts made in same way will be tested, and the result will be based on the distribution of each experiment result and the average results of four same experiments. The parts will be made along three different axes with four different

scales of filling percentage. As a result, twelve different groups will be tested to detect the mechanical performance of the FDM part, and each group will have four same specimens to reduce the effect of gross error. All specimens were made under same conditions (same machine, same location, same environment temperature, and same air humidity) to minimize environmental factors that influence the experiment. Six specimens with same filling percentage were created at the same time. Specifically specimens number 1 + 6n to 6 + 6n (n=0, 1, 2, 3, 4, 5, 6, 7) were made at the same time. The table displaying the collected data was designed and is shown in the data collecting section.

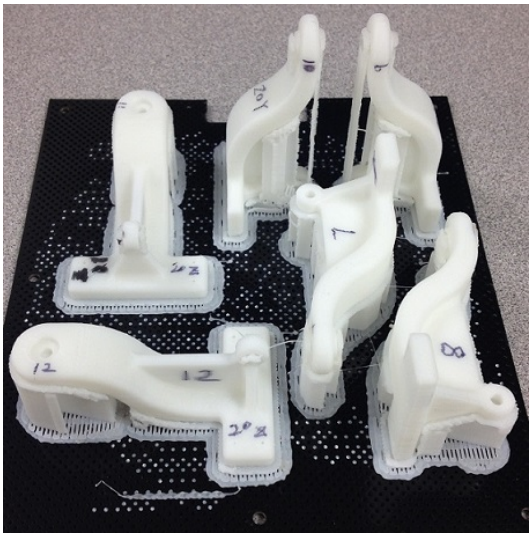

Figure 5.1: The specimens were made along X, Y, and Z axis.

5.1.3 Experiment setup

The specimens are set up on a fixed platform. The connection method used in this experiment is the screw-nut connection, which is the same as the assembly method on the prototype. The pin or screw would be put in the top ring of the specimen. The up-ward force

would be applied through two metal rings which attached to both ends of the pin or screw. The pin or screw was used to provide a uniform force, instead of a point force, to the specimen. The force gauge would be used to measure the force applied on the specimen. The greatest force measured during the testing of the first part will be recorded prior to the breaking of the specimen. Figure 5.2 shows the setup of the experiment. All specimens were tested with same experiment setup and under same conditions.

This test is based on two assumptions: the force gauge is accurate and the force gauge has perfect repeatability.

Figure 5.2: The setup of experiment station for FDM part mechanical performance test.

5.1.4 Data collecting

The data were collected and filled in Table 5.1. The table also displays the average break force and standard deviation of each group. Specimen 47 and 48 did not fail at the connection part, but broke at the pull up ring. Based on results of the simulation and all other specimens, it can be concluded that the ring part should not fail before the connection part. It is speculated that there were some manufacturing defects at the ring part or there were some other unknown defects at other places of both specimen 47 and specimen 48. Therefore, the collected data of these two specimens may not be accurate when comparing the results with other data. Be ensuring that the break force at the connection part should be greater than the measured force, and the standard deviation will be smaller based on above analysis.

The data collected from specimen 47 and specimen 48 are shown in italic and bold in the table below. Chart 5.1 shows the data distribution and the curve of all groups based on the average value in Table 5.1.

Filling percentage	Made along X axis		Made along Y axis		Made along Z axis	
0 (shell)	Specimen 1	1.690 kg	Specimen 3	1.825 kg	Specimen 5	0.960 kg
	Specimen 2	1.875 kg	Specimen 4	1.245 kg	Specimen 6	1.210 kg
	Specimen 25	1.115 kg	Specimen 27	0.735 kg	Specimen 29	1.040 kg
	Specimen 26	1.275 kg	Specimen 28	1.605 kg	Specimen 30	1.125 kg
	Average	1.489 kg	Average	1.353 kg	Average	1.084 kg
	STDEV	0.354 kg	STDEV	0.476 kg	STDEV	0.108 kg
20% (hole)	Specimen 7	2.245 kg	Specimen 9	1.945 kg	Specimen 11	2.045 kg
	Specimen 8	3.025 kg	Specimen 10	1.785 kg	Specimen 12	1.865 kg
	Specimen 31	2.100 kg	Specimen 33	1.545 kg	Specimen 35	2.300 kg
	Specimen 32	2.425 kg	Specimen 34	1.745 kg	Specimen 36	1.945 kg
	Average	2.449 kg	Average	1.755 kg	Average	2.039 kg
	STDEV	0.407 kg	STDEV	0.165 kg	STDEV	0.189 kg
50% (loose)	Specimen 13	2.765 kg	Specimen 15	2.245 kg	Specimen 17	2.925 kg
	Specimen 14	2.685 kg	Specimen 16	2.950 kg	Specimen 18	3.515 kg
	Specimen 37	3.765 kg	Specimen 39	1.435 kg	Specimen 41	3.725 kg
	Specimen 38	1.815 kg	Specimen 40	0.535 kg	Specimen 42	3.635 kg
	Average	2.758 kg	Average	1.791 kg	Average	3.450 kg
	STDEV	0.798 kg	STDEV	1.041 kg	STDEV	0.360 kg
80% (solid)	Specimen 19	2.490 kg	Specimen 21	1.945 kg	Specimen 23	6.245 kg
	Specimen 20	2.835 kg	Specimen 22	1.425 kg	Specimen 24	6.205 kg
	Specimen 43	2.175 kg	Specimen 45	1.610 kg	Specimen 47	***5.425 kg***
	Specimen 44	2.695 kg	Specimen 46	1.070 kg	Specimen 48	***4.950 kg***
	Average	2.549 kg	Average	1.513 kg	Average	***5.706 kg***
	STDEV	0.287 kg	STDEV	0.365 kg	STDEV	***0.630 kg***

Table 5.1: The result of part break force test.

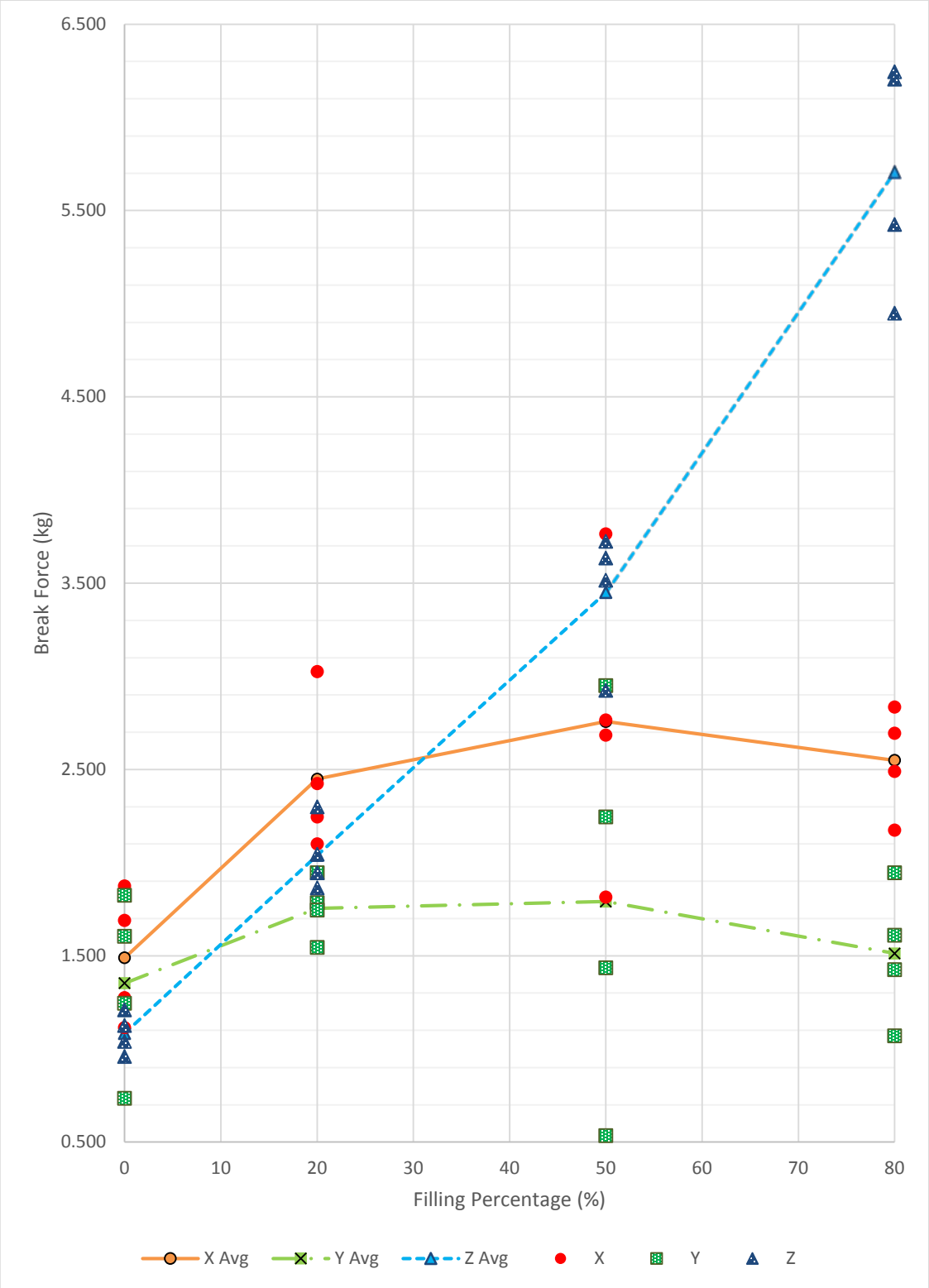

Chart 5.1: The result of part break force test in dots distribution and curves.

5.1.5 Analysis and result

Overall, the results of the test were the same as expected, except the optimal performance of the parts which were built along the Z axis and the tendency of the X and Y curves. A deeper analysis and in-depth discussion will be reported in this section to verify the hypothesis and explain the unexpected mechanical performance of parts that were built along the Z axis.

As explained in chapter 3, there are several random factors that may have affected the mechanical performance of the FDM part. However, the answers to the questions are still being explored: What are the random factors? How do they affect the adhesive strength? How could we avoid these influences? This claim can be verified by the numerically large standard deviation of some groups. The specimen 37 and specimen 38 are good examples that support this claim. The measured break forces for these two specimens were significantly different. The break force of specimen 37 was over twice the break force of specimen 38. However, these two specimens were made at the same time and were tested with same method under the same conditions. The influence of environment factors, machine factors, and method factors were not considered during the mechanical performance test of these specimens. As a result, factors that led to the performance difference are still unknown. In addition, the locations of the fracture surface of the specimens in the same group (i.e. same parts) were different. Figure 5.3 shows specimens 1, 2, 25, and 26 after the experiment. The standard deviation of this group is about 0.35. This is not a big value when compared to other groups. However, four specimens failed at four different positions on the part. Figure 5.4 shows specimens 9 and 10 after the experiment. The standard deviation of this group is only 0.16. This is a very small value. But the specimens failed at different positions. Figure 5.5 shows specimens 17, 18, 41, and 42 after the experiment. The standard deviation of this group is about 0.36. Again, the specimens failed at different

layers. All these specimens in each figure were in same group. The parts in the same group were supposed to be the same (some parts were even made at the same time) and perform similarly. Fracture structures were not supposed to be very similar. However, none of them shared similar fracture structure in similar locations, and the fracture structures shown in the figures are random to the point that they are not predictable. Thus, all these results mentioned above verified the hypothesis that:

1. The fracture or creak would only occur and develop between layers.

2. Failure would occur at the weakest position where the adhesive strength between layers is weakest.

3. The weakest position is unpredictable because of influence of unknown and random factors.

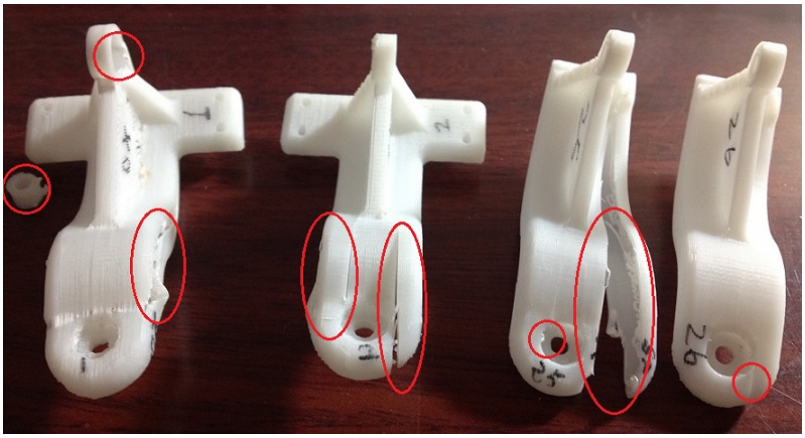

Figure 5.3: Specimens 1, 2, 25, and 26 after the experiment. Failure locations were circled.

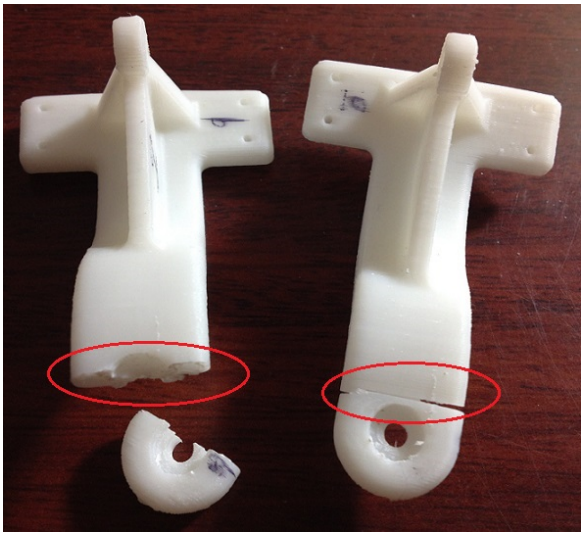

Figure 5.4: Specimens 9 and 10 after the experiment. Failure locations were circled.

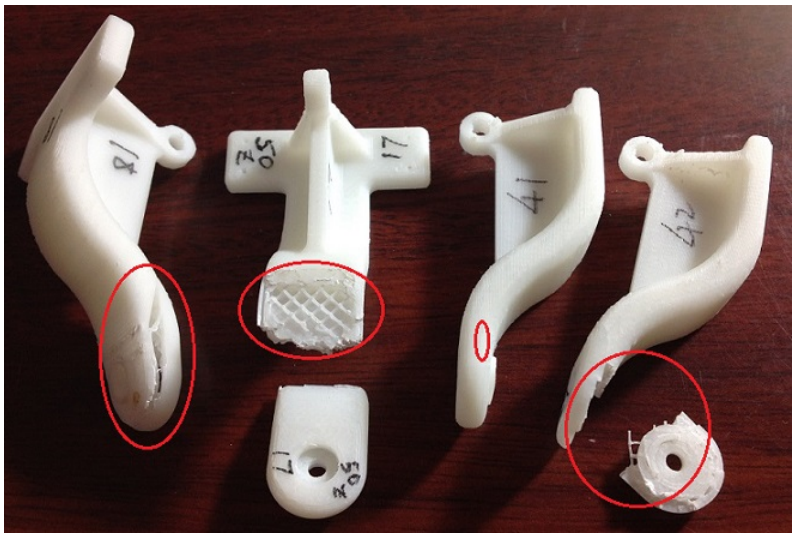

Figure 5.5: Specimens 17, 18, 41, and 42 after the experiment. Failure locations were circled.

As expected, parts built along X axis were stronger than parts built along Y axis. The failure only occurred between layers and the weakest positions were generally at the part which had minimal material (only for tested component in the project). It can be observed that parts

built along the Y axis have the smallest area at the weakest position. Though ABS does not have yield strength, tested FDM parts did not perform like ceramic parts but more like metal parts. They had good ductility. Most tested specimens made along the X and Z axes do not have complete fracture surface. In other word, a main crack or several cracks caused the complete failure of these parts. Based on observation of the fracture structure on all specimens after experiment, the fracture surface of the specimens which were made along Z axis were bigger than others.

From the result we can conclude that with increasing filling percentage, the performance of the part improved. The performance of the parts made along the Z axis increased almost linear to the increasing of filling percentage. However, the performance of parts which made along X axis and Y axis increased very slowly. We believe that the increasing rate of these specimens were so small that the result showed more noise than performance increasing tendency. The main reason behind this result is the several failures that occurred at the connection area of the parts. The 3D printer considered object in two parts: the surface and the body. The surface has a certain thickness. They are 100% filled solid material. The body is the enclosed part inside the surface/shell. Changing the filling percentage can only affect the body. Compared to the main part of specimen, the connection area has a lot of “surface part”. From the cross section along the X axis and Y axis of the screw hole we can observe that the whole area was almost filled by “surface material”. The filling percentage change of the body could not change the total filling percentage too much. Figure 5.6 shows the fracture surface of parts made along the Y axis with different body filling percentage. The fracture structure of the parts made along the X axis was almost the same as parts made along the Y axis. However, from the observation of fracture surface of parts made along the Z axis, we could see that the fracture surfaces were much larger compared to others, and the connection structure did not affect much. Thus, the total filling

percentage of the area depended more on the body filling percentage change. Figure 5.7 shows the fracture surface of parts made along the Z axis with different body filling percentage. Based on the area measurement of the fracture surfaces of specimens, almost 70% of total area were "surface material" to the parts made along the X axis and Y axis. But for parts made along the Z axis, the "surface material" was only about 10%. Chart 5.2 shows the increase in total filling percentage by changing the body filling percentage. Total filling percentage = (surface percentage + (100%-surface percentage) x body percentage) / 100%. Comparing this chart to the experiment result, we can conclude that the total filling percentage increasing rate matches the performance increasing tendency. To specimens made along the X axis, the fracture would extend to the main body. So the performances of these specimens were better than specimens made along the Y axis.

Figure 5.6: The fracture surface of parts made along the Y axis. From left to right, the filling percentages of the body are 0, 20%, 50%, and 80%.

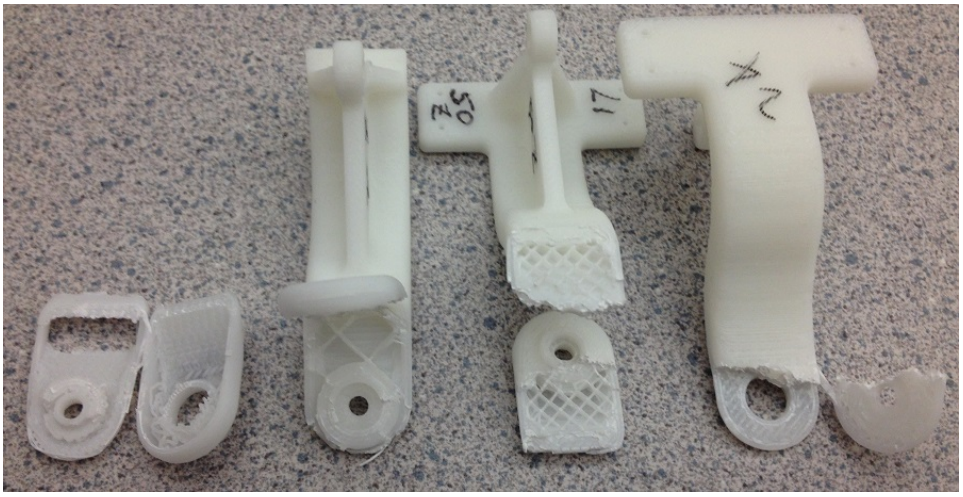

Figure 5.7: The fracture surface of parts made along Z axis. From left to right, the filling percentages of the body are 0, 20%, 50%, and 80%.

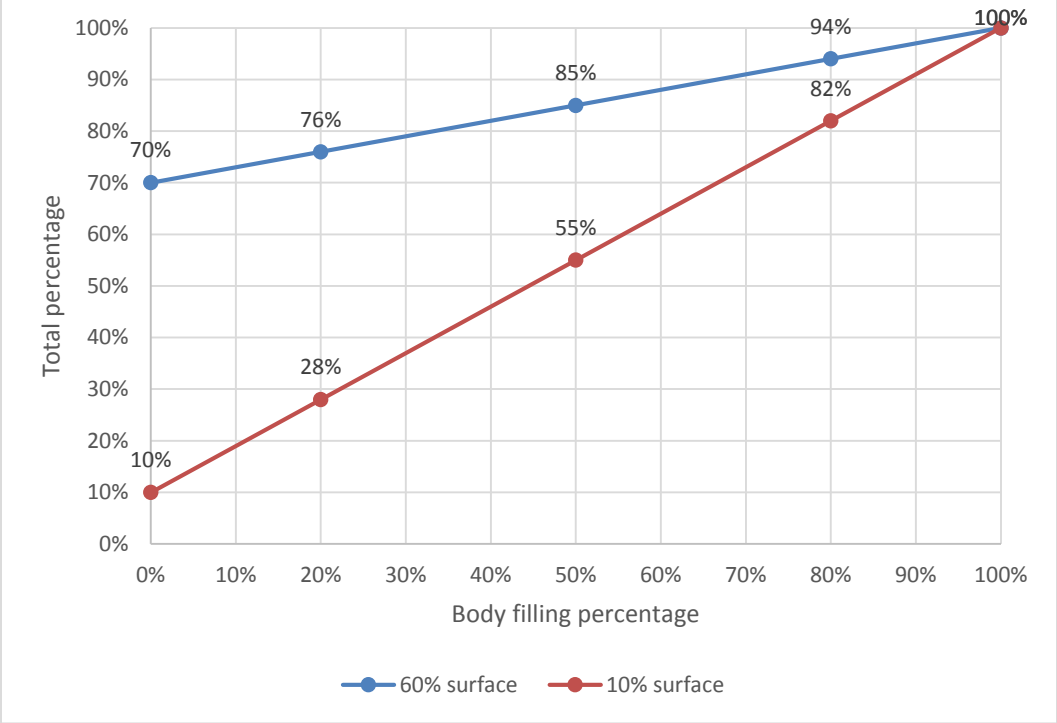

Chart 5.2: The increasing of total filling percentage by changing the body filling percentage.

In conclusion, the fracture would only generate and develop between layers for FDM parts. So the simulation based on uniform material cannot simulate the failure position precisely. Furthermore, there were some unknown and random factors that could have influenced the quality of the part. As a result, the simulation cannot simulate the break force accurately, and the load experiment cannot predict the failure of the same part. This was the main reason that this prototype could not be tested with human subjects. However, the adhesive strength between layers was not small enough to ignore the structure of the part. Therefore, the simulation could still indicate the approximate location and break force of the failure if we could take 3D printing format into consideration. In conclusion, the simulation is still a good reference for FDM parts.

5.2 **Device Backlash Test**

5.2.1 Purpose of the test

The backlash is mainly described as the motion loss in a mechanism caused by gaps between assembled parts. Therefore, it is obvious that the more mechanisms between the actuator and the end-effector, the greater the backlash that will be generated. As a result, the most efficient way to reduce the backlash is to reduce mechanisms between the actuator and the end-effector. One good example for this approach is that CNC lathe usually uses variable speed motor instead of a gearbox, which is commonly used in a manual lathe, to output adjustable speed for the spindle. If the device structure is fixed, the backlash of related mechanisms could be reduced in certain ways. As mentioned in previous section, the standard screw mechanism has a certain backlash that could be minimized by nut(s) with pre-load mechanism(s).

Big backlash, which may cause inaccurate position or speed control, as well as structure instability, can be minimized in a variety of ways. However, backlash reduce mechanisms are usually complex, expensive, and require high quality manufacturing and assembling accuracy.

Therefore, the main purpose of this test is to determine and keep the device backlash under an acceptable level with minimum cost.

5.2.2 Experiment design

In this test, the backlash of the device, not limited to any specific mechanism, was measured. Because the rehabilitation device is not designed for heavy-duty applications and the stall torque of the motor is only about 9 mN·m, there is no force or torque that can cause measureable deformation of components. Thus, the elastic deformation of each component is not considered in backlash tests. Therefore, the backlash was tested without any load on end-effector, and the result would be the total gap between the actuator and the end-effector. Since rigid couplings were used for transferring motions from motors to screws, there is no motion loss from in these sections.

In order to measure the total gap between the actuator and the end-effector, the spring supported floating platforms were removed, cables were fixed on nuts (Figure 5.8), and the screws were held to avoid rotating. The total gap of the device was directly measured from two limit positions of the end-effector. Four motions of the device were tested separately. Ten independent backlash tests were finished for each degree-of-freedom to reduce the measurement error. The table displaying the data collected was designed, is shown in the data collecting section.

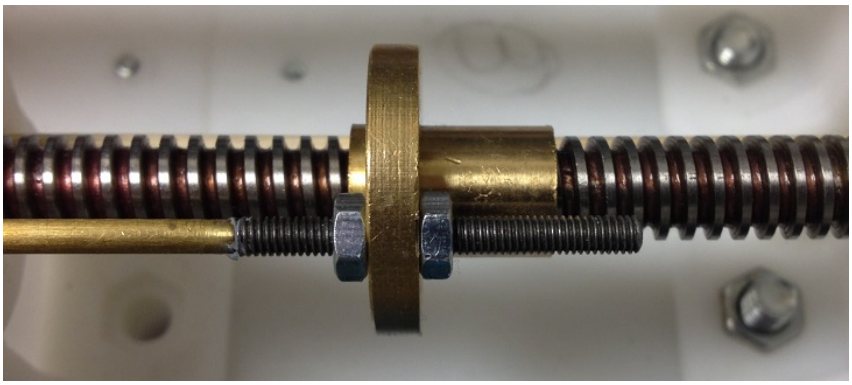

Figure 5.8: Cables were fixed on nuts for backlash tests.

5.2.3 Data collecting

Collected data of the backlash tests are shown in Table 5.2 Recorded numbers were read directly from the digital caliper. Based on observations during tests, the total backlash of each motion is composed of the screw backlash, push-pull cable backlash, and assembled components backlash. The percentage of each composed backlash was recorded in the table based on observation.

Measured backlash	Unit	Wrist flexion/extension	Wrist radial/ulnar deviation	Forearm rotation	Elbow rotation
1	mm	0.56	1.13	1.38	0.89
2	mm	0.57	1.24	1.28	0.74
3	mm	0.59	1.32	1.34	0.78
4	mm	0.55	1.23	1.26	0.78
5	mm	0.54	1.31	1.37	0.71
6	mm	0.54	1.25	1.33	0.72
7	mm	0.56	1.35	1.27	0.72
8	mm	0.51	1.29	1.22	0.76
9	mm	0.55	1.14	1.22	0.78
10	mm	0.52	1.19	1.27	0.74
11	mm	0.56	1.22	1.30	0.80
12	mm	0.51	1.18	1.22	0.75
13	mm	0.57	1.28	1.38	0.79
14	mm	0.52	1.18	1.31	0.88
15	mm	0.51	1.29	1.38	0.85
16	mm	0.59	1.38	1.32	0.78
17	mm	0.55	1.18	1.35	0.76
18	mm	0.55	1.20	1.32	0.74
19	mm	0.53	1.12	1.30	0.84
20	mm	0.56	1.18	1.24	0.77
21	mm	0.58	1.20	1.31	0.76
22	mm	0.54	1.36	1.24	0.75
23	mm	0.53	1.35	1.28	0.73
24	mm	0.56	1.32	1.23	0.76
25	mm	0.51	1.17	1.31	0.83
26	mm	0.58	1.20	1.37	0.71
27	mm	0.59	1.24	1.36	0.82
28	mm	0.58	1.14	1.27	0.79
29	mm	0.51	1.25	1.25	0.85
30	mm	0.55	1.34	1.28	0.86
Average	mm	0.55	1.24	1.30	0.78
Standard deviation	mm	0.026	0.076	0.052	0.051
Screw backlash	%	40	20	15	30
Cable backlash	%	60	80	25	40
Assembly backlash	%	0	0	70	30

Table 5.2: The result of backlash tests of the rehabilitation device.

5.2.4 Analysis and result

From the result we can conclude that most of the system backlash originated from the push-pull cable. The cable's backlash is mainly caused by the size difference between the cable and its hose. The outer diameter of the cable was measured at 1.2 mm, but the inner diameter of the hose was measured at 1.8 mm. Thus, when the cable doesn't have enough tension or enough applied pushing force, it will become very loose inside the hose and will lose some motion as a result. In order to let the cable move smoothly inside the flexible hose, the push-pull cable is designed to accommodate this very loose fit. Therefore, the cable's backlash cannot be reduced by changing higher quality cables, and the backlash will increase as the length of the push-pull cable increases.

The cable's backlash can be minimized only by using it as pulling cable. In this project, both wrist's flexion/extension motion and forearm rotation motion are driven by two cables, and the elbow structure has pre-load mechanisms. Each cable for these motions only provides pulling force while functioning. In addition, only wrist radial/ulnar motion is provided by the push-pull cable. Therefore, the backlash of wrist radial/ulnar motion is greater than other motions, and the cable backlash is the main component. For the forearm motion, the drive mechanism includes more parts than other motions. The parts' slight deformation from 3D printing had greater deviation gaps in assembly than expected in design. Therefore, these gaps generated relatively big backlash in forearm rotation motion. The backlash caused by 3D printing could be easily reduced by changing manufacturing method. Because the 3D printed parts were only used in this prototype, related backlash will be a problem in future appliances.

In general, the average backlash value is about 1 mm, which is an acceptable level of backlash for rehabilitation purposes.

5.3 **Range of Motion Test**

5.3.1 Purpose of the test

The purpose of this project is to cover a greater range of motion for each degree-of-freedom compared to other existing devices. The device's range of motion is restricted by many factors. The main factors include the mechanism limitation, actuators' ability, and passive joints' restrictions. The actuators' ability and passive joints' performance can be easily improved by replacing them with better actuators. However, the limitation to the mechanism's working space cannot be increased after it has been designed. Because it is impossible for manufactured components and the assembly accuracy to be as perfect as simulation, the real limitation of the mechanism must be smaller than designed.

The purpose of this test is to figure out what the real mechanism limitation is after the whole device has been assembled. Without considering the limitation of the 3D printed parts, the designed working space for the proposed mechanism is ±35° wrist radial/ulnar deviation, ±82° wrist flexion/extension, ±80° forearm rotation, and 150° elbow flexion/extension. Since two motions of the wrist are dependent, Figure 5.9 shows the diagram of the proposed wrist mechanism's range of motion. The center line indicates the goal of the project which is set up and reported in chapter 1. The dash line indicates the limitation of the proposed mechanism regardless of the manufacturing method and the assembly accuracy.

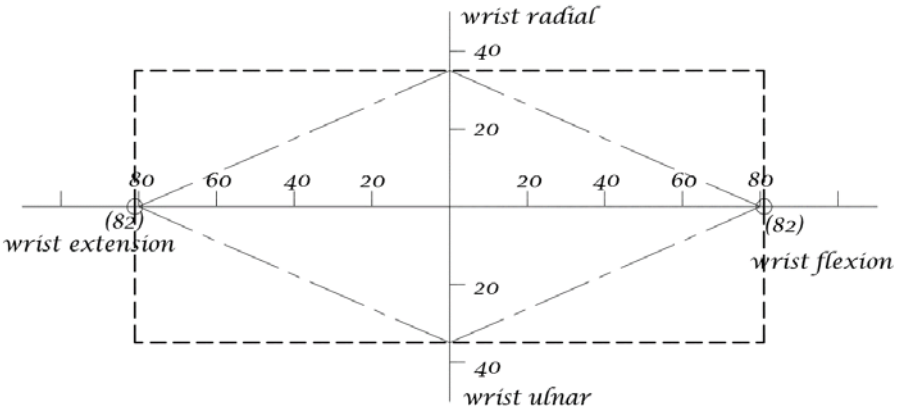

Figure 5.9: Proposed wrist mechanism's range of motion.

5.3.2 Experiment design

The experiment setup was ready after the device had been assembled. Driven cables were pulled by hand. Limitation ranges were measured by a protractor. To determine the wrist mechanism's motion limitation in 2D diagram, more data at different positions were collected. The table collecting the data was designed, and is shown in the data collecting section.

5.3.3 Data collecting

Table 5.3 shows the data collected in the experiment. The accuracy of the protractor is 1°, which indicates that the accuracy of the data is limited to one significant figure. As a result, multiple trials will not improve the measurement accuracy. The table below displays the data limited to one significant figure. In Figure 5.10, the solid line indicates the working space of the measured wrist mechanism's range of motion. The dash line indicates the limitation of the proposed mechanism regardless of the manufacturing method and the assembly accuracy.

	Flexion	Extension
Elbow	128°	0°
	Supination	Pronation
Forearm	158°	158°
	Wrist ulnar deviation	Wrist radial deviation
Wrist flexion 81°	0°	0°
Wrist flexion 75°	5°	5°
Wrist flexion 69°	15°	15°
Wrist flexion 53°	22°	20°
Wrist flexion 45°	28°	20°
Wrist flexion 35°	35°	20°
Wrist flexion/extension 0°	35°	20°
Wrist extension 35°	35°	20°
Wrist extension 45°	28°	20°
Wrist extension 53°	22°	20°
Wrist extension 69°	15°	15°
Wrist extension 75°	5°	5°
Wrist extension 81°	0°	0°

Table 5.3: Measured range of motion.

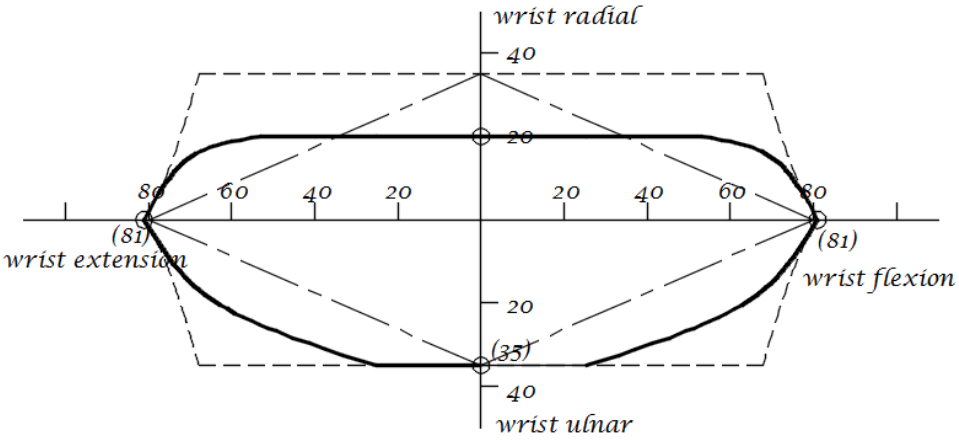

Figure 5.10: Measured range of motions of wrist mechanism in solid line; dash line indicates expected range of the mechanism; center line indicates proposed range.

After the screw mechanism was assembled for controlling the device, the range of motion was fully restricted by the length of the screws. Because the length of the screw would not be limited by any factor, the work space of the mechanism should be maintained. While the screws were under machining, more material waste was created that expected. Furthermore, I did not have access to any CNC lathe, and amateur operation on the new manual lathe resulted to shorter screws than expected. Therefore, the range of motion of the device was further limited by short screw mechanisms. The elbow's motion range was not affected by its length of screw, but the forearm rotational range was limited to 156°. The wrist's motion range was affected as well. Figure 5.11 shows the workspace limitation after driven cables were attached on the screw mechanisms. The screw mechanisms were set up to meet the wrist's radial deviation and flexion range to prove that the mechanism's limitation could be maintained. In order to rebuild the screw mechanism, it would cost a great deal of time and money. The prototype is good enough to demonstrate the functionality of the proposed mechanism and structure, and thus it has been decided not to rebuild the screw mechanisms.

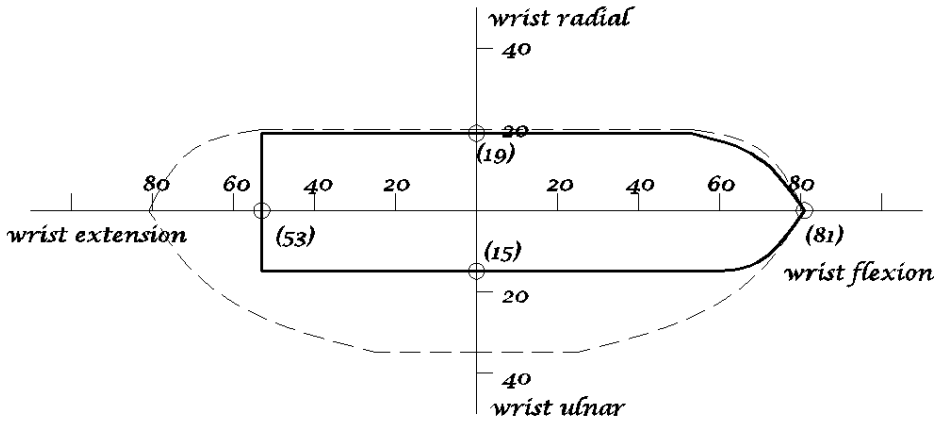

Figure 5.11: Wrist workspace limitations after driven cables were attached on the screw mechanisms.

5.3.4 Analysis and result

Table 5.4 shows the comparison between the range of proposed mechanism (without restriction from the screw's length) and relative joints' range of motion. From the data in the table we can conclude that the proposed mechanism can fully cover each joint's functional range of motion and at least 88% of full range of motion.

	Range of motion (ROM)	Functional range [39], [41], [42], [45]	Mechanism's range
Wrist radial deviation	0 ~ 20°	0 ~ 15°	0 ~ 20°
Wrist ulnar deviation	0 ~ 35°	0 ~ 35°	0 ~ 35°
Wrist flexion	0 ~ 85°	0 ~ 10°	0 ~ 81°
Wrist extension	0 ~ 70°	0 ~ 35°	0 ~ 81°
Forearm supination	0 ~ 85°	0 ~ 50°	0 ~ 153°
Forearm pronation	0 ~ 80°	0 ~ 50°	0 ~ 153°
Elbow flexion	0 ~ 145°	30 ~ 130°	0 ~ 128°

Table 5.4: Comparison between the range of proposed mechanism and relative joints' ROM.

With the proposed mechanism, the range of wrist flexion/extension motion may not be further improved. However, the range of elbow flexion/extension motion and wrist ulnar/radial deviation can be slightly expended. One factor which restricted the range of these two motions is the 3D printed parts. The 3D printed plastic parts have poor mechanical performance compared to any other manufacturing method and its unpredictable failure was verified in previous experiments. The unexpected failure of 3D printed parts originated from its requirement for bigger and thicker designs. Thus, bulky parts limited the space of push-pull rod and relative parts

for wrist radial/ulnar motion, and limited its range of motion as a result. Similarly, the situation for the elbow flexion/extension motion, the forearm ring collided to the upper arm before the rotation mechanism reached its limitation because the rotation part of the mechanism was not capable of being "printed" too long. Figure 5.12 describes this problem. Because all parts were designed for this specific prototype using the 3D printing method, none of these ranges could be further improved in this project. However, if the manufacturing method could be changed to a way which is better than 3D printing, the range of motion should be improved compared than measured with this built prototype. The dash line in Figure 5.13 indicates expected wrist range with the same mechanism but better manufacturing method.

In conclusion, the proposed mechanism performs better than the goal set up in proposal. The prototype assembled with 3D printed parts could fully cover the functional range of motion for each joint and at least 88% of the full range of motion. If there are better ways to make components for future use, the range of motion can be expended slightly with the same mechanism.

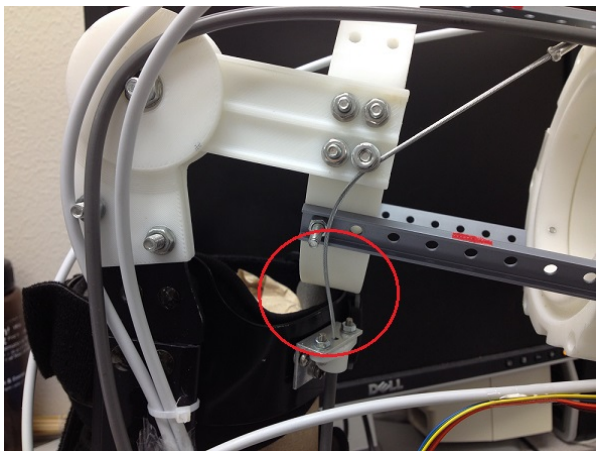

Figure 5.12: The forearm ring collides with the upper arm before the rotational mechanism reaches its limitation.

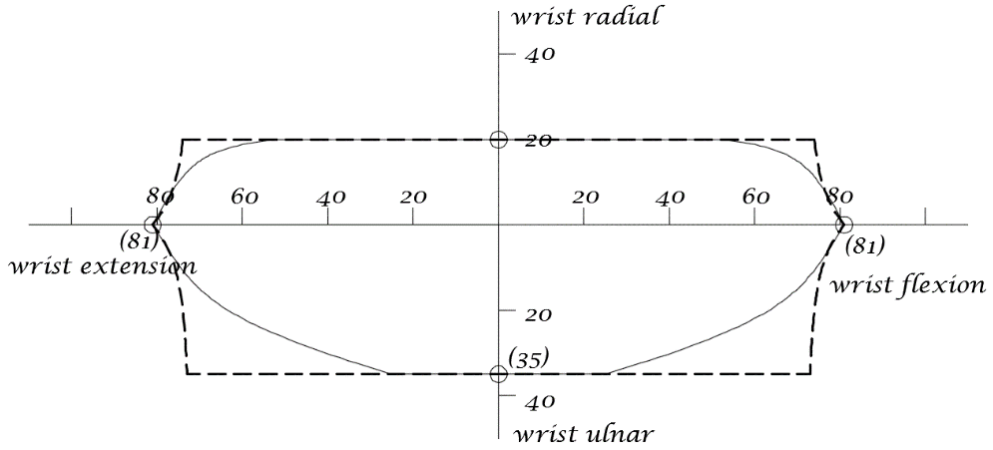

Figure 5.13: Expected wrist range with the same mechanism but better manufacturing method.

5.3.5 Daily activities coverage

With combinations of different motions, the device could provide several typical daily activity exercises. Table 5.5 shows the list of typical daily activity exercises the device could cover based on the measured range of motion for the device. The activities were selected based on information in published papers [39] [41] [42] [45] [46].

Without the motion of shoulder, very limited activities could be finished. However, this project doesn't include shoulder joint. Therefore in the section, the assumption that shoulder could collaborate with elbow and wrist motions on activities was made.

With the limitation of the elbow motion range of this built prototype, neck area cannot be reached. However as mentioned above, this is mainly caused by the big 3D printed part. It is believed that the elbow mechanism's motion range could reach elbow's range if the prototype was made in other material and manufacturing method.

Reach	Head vertex	Do	Pour water
	Chest		Drink/Eat
	Waist		Cut with knife
	Sacrum		Read newspaper
	Shoe		Rise from a chair
			Open a door
			Open a bottle
			Turn steering wheel
			Use screw driver
			writing

Table 5.5: Typical daily activity exercises which could be covered by the device.

5.4 **Accuracy and Repeatability Test**

5.4.1 Purpose of the test

Accuracy and repeatability of the robot are two important parameters. The purpose is to detect the accuracy and the repeatability of the device as a whole system. The experiment should be finished with fully assembled device which fully controlled by designed system.

5.4.2 Experiment design

The device has four degrees-of-freedom, so the experiments include tests for each degree-of-freedom and whole device. In experiments, each degree-of-freedom will be preset at a certain angle. In other words, the device will stop when the sensor reaches its pre-set value. The device will try to reach pre-set angle from any other position. The dial indicator will be used to measure the small distance from the reference position to the stop position in each experiment. The experiment will be repeated 25 times for each setup. The table collecting the data was designed, and is shown in the data collecting section.

5.4.3 Experiment setup

In experiments, the device is attached to a stand and fully controlled by its control system. The setup for these experiments is just to find a good position for placing the dial indicator. Figure 5.14 shows the dial indicator's position for elbow joint's experiments. Figure 5.15 shows the dial indicator's position for wrist joint's experiments. Experiments involve all degrees-of-freedom has the same setup as wrist joint's experiments. Using dial indicator for forearm rotation experiments is not appropriate. The caliper is used to measure the distance. Figure 5.16 shows the setup for forearm rotation experiments.

The resolution of the dial indicator is 0.001 inch. The resolution of the caliper is 0.01 millimeter. All results will be reported in millimeter.

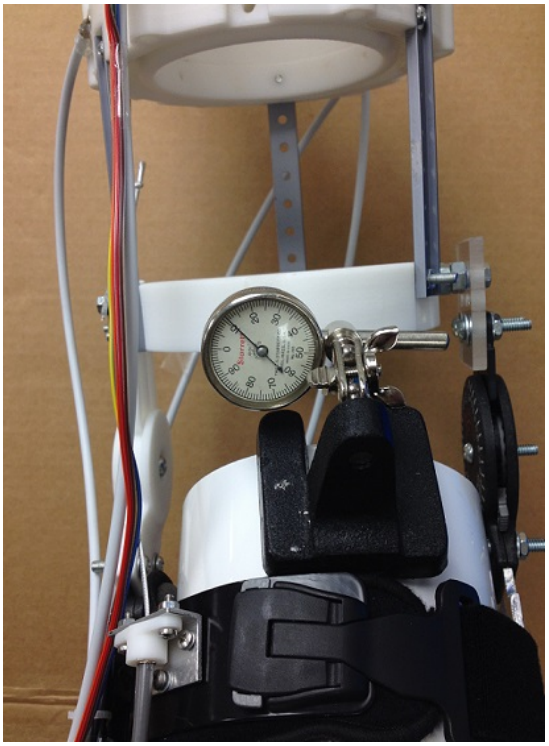

Figure 5.14: The dial indicator's position for elbow joint's experiments.

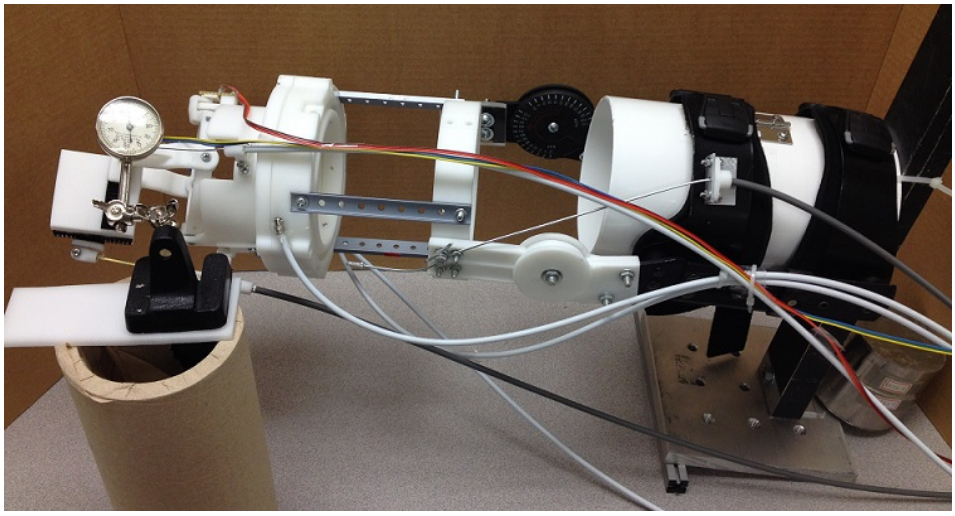

Figure 5.15: The dial indicator's position for wrist joint's experiments.

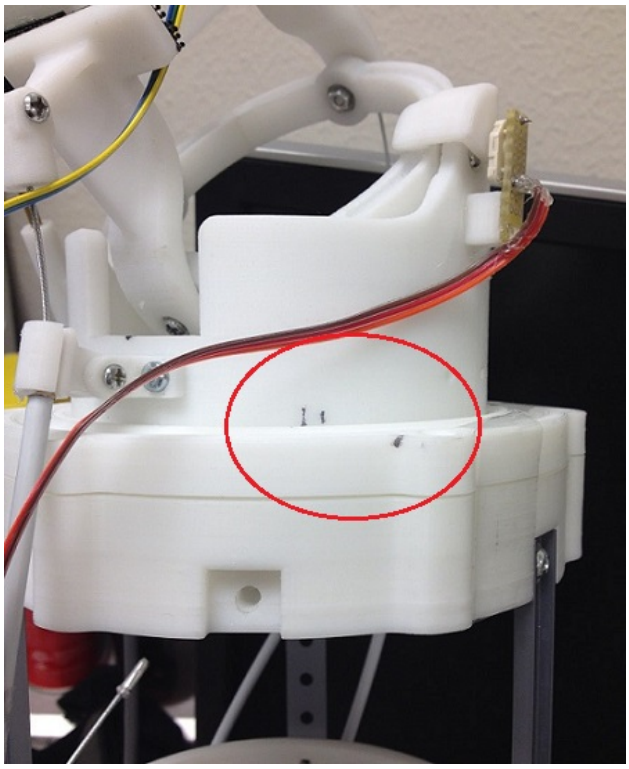

Figure 5.16: The setup for forearm rotation experiments.

5.4.4 Data collecting

Following Table 5.6 shows the collected data.

Experiment	Unit	Elbow	Wrist flexion	Wrist ulnar deviation	Forearm	Whole device
1	mm	0.21	0.03	0.58	0.78	-0.57
2	mm	0.32	- 0.28	0.68	0.74	0.25
3	mm	-0.28	0.68	0.65	-0.35	0.31
4	mm	0.28	-0.27	-0.38	-0.20	-0.90
5	mm	0.15	-0.01	-0.65	0.80	-0.62
6	mm	-0.07	0.58	0.33	0.62	0.46
7	mm	0.26	-0.10	-0.46	0.68	0.12
8	mm	0.23	0.40	0.06	-0.22	-0.40
9	mm	-0.02	0.33	0.21	-0.87	0.79
10	mm	0.17	-0.58	-0.61	0.19	-0.56
11	mm	-0.26	0.21	0.64	-0.84	-0.35
12	mm	-0.14	0.05	-0.29	-0.48	0.20
13	mm	0.23	0.24	-0.57	0.47	-0.18
14	mm	-0.14	-0.22	0.25	-0.10	-0.94
15	mm	0.25	-0.09	0.35	-0.46	0.50
16	mm	0.14	0.62	0.06	0.33	-0.21
17	mm	-0.07	-0.09	-0.07	-0.82	-0.76
18	mm	-0.26	0.13	-0.30	0.86	-0.11
19	mm	-0.01	-0.31	-0.57	0.47	0.23
20	mm	-0.30	0.72	-0.11	0.41	0.36
21	mm	-0.33	0.57	0.01	-0.43	0.55
22	mm	0.19	-0.42	0.55	-0.74	-0.12
23	mm	-0.30	-0.57	0.23	0.84	-0.55
24	mm	-0.07	0.53	-0.16	-0.20	-0.65
25	mm	0.05	-0.20	0.40	0.41	-0.12
Max	mm	0.32	0.72	0.68	0.86	0.79
Min	mm	-0.33	-0.58	-0.65	-0.87	-0.94
Average	mm	0.01	0.08	0.03	0.08	-0.13
STDEV	mm	0.217	0.395	0.432	0.593	0.491

Table 5.6: The result of accuracy and repeatability experiments.

5.4.5 Analysis and result

In Table 5.6, the maximum number and the minimum number represent the accuracy of the each set of experiments. The standard deviation represents the repeatability of each set of experiments.

From the results we could know that the accuracy is just slightly bigger than backlash except the elbow joint. Therefore the backlash is the main reason cause the inaccuracy of the device. Table 5.7 shows the comparison of backlash and accuracy. As mentioned in backlash experiments report, the backlash could be minimized if by pre-load the system. The elbow joint's accuracy results perfectly supported this claim. The elbow joint is pre-loaded by the weight of the device. So the backlash is minimized and the measured accuracy is smaller than backlash. Also, the repeatability of the elbow joint is much better than any other's.

Position sensors used in the system are analog output, so the resolution of these sensors is essentially infinite. Besides, the frequency of the microchip is 16 MHz; the time delay in control system can is negligible. Other possible causes for inaccuracy could be the deformation of components and measurement error.

	Unit	Wrist flexion/extension	Wrist radial/ulnar deviation	Forearm rotation	Elbow rotation
Average backlash	mm	0.55	1.24	1.30	0.78
Accuracy	mm	1.30	1.33	1.73	0.65
Backlash/Accuracy percentage	%	42.3	93.2	75.1	120

Table 5.7: Comparison of backlash and accuracy tests result.

5.5 **Device Properties**

Following Table 5.8 shows general properties of the device.

	Unit	Value
Overall size on arm	mm (L) x mm (W) x mm (H)	500 x 160 x 160
Weight on arm	g	843

Table 5.8: Device properties.

6 CONCLUSION AND FUTURE WORK

6.1 **Conclusion**

As mentioned in chapter 1, robotic therapy has proved to be effective. Thus many rehabilitation robots have been developed to provide designed exercises. Narrowing the Scope down to upper arm rehabilitation only (shoulder motions are not included), most existing rehabilitation devices are based on grounded serial robots which can only control the posture of its end-effector. Therefore, the status of each joint cannot be precisely controlled and the huge robot makes the robotic therapy inflexible for therapy schedules and location. Several exoskeleton-type rehabilitation robots for forearms have been developed recently, and they can precisely control the status of the covered joint(s). Some of them are light weight, so their portability allows the user to receive therapy whenever and wherever they want. However, these exoskeleton-type rehabilitation robots either cannot cover all four degrees-of-freedom on a forearm or cannot provide enough range of motion (up to 60% of full range of motion) because of their mechanisms or structural limitation(s).

A new mechanism was proposed to cover all four degrees-of-freedom on forearm (wrist radial/ulnar deviation, wrist flexion/extension, forearm supination/pronation, and elbow flexion/extension) and at least 90% of full range of motion of each degree-of-freedom. The proposed mechanism was developed based on the spatial orientation parallel robot with a passive constraint mechanism. The designed mechanism provides motions at a range of 35°/35° for wrist radial/ulnar deviation, 82°/82° for wrist flexion/extension, 158°/158° for forearm supination/pronation, and 128°/0° for elbow flexion/extension. The whole device was designed to be driven by cables. Therefore, all actuators and power transmission mechanisms can be removed from the device to reduce the weight on user's arm, and increased the portability of the

device as a result. DC motors and the screw mechanisms were selected to provide motions for drive cables. Therefore, the proposed structure includes two main parts: the wearable cable driven rehabilitation device on user's arm, and the control part which could be carried like a backpack. The prototype was made to test out the functionality of the proposed mechanism and structure. Due to the manufacturing method limitations for this project, the prototype was made mainly with 3D printed plastic parts. After the device was assembled, a sensor based control system was reported for controlling the rehabilitation device so the device could provide exercise based on pre-programmed moving patterns. The built prototype weight is about 800 grams on the user's arm, and the overall size is about 160 mm (W) x 160 mm (H) x 500mm (L). The length can be adjusted based on the length of user's forearm.

Because of the special characteristics of the 3D printing method, the mechanical performance experiments for a typical 3D printed part on the device were finished to predict the mechanical performance of the device. Based on the results, the failure of the 3D printed parts is unpredictable, and the mechanical performance would be affected significantly if the same part was printed in a different way. Thus, the simulation based on the assumption that the part is made with solid and uniform material is inaccurate. However, the simulation is still a good reference. To better understand the performance of the device, backlash tests were conducted. The average backlash of the device is about 1 mm. This result is very good for this prototype and for rehabilitation applications. Additionally, tests to determine the range of motion of the assembly were completed. In general, the prototype's workspace could reach the design. However, because of bulky 3D printed parts, the space for wrist radial/ulnar deviation was restricted. Also due to the manufacturing errors and assembling errors, the workspace of the assembly was reduced to 20°/35° for wrist radial/ulnar deviation, 81°/81° for wrist flexion/extension, 153°/153° for forearm supination/pronation, and 128°/0° for elbow

flexion/extension. Based on the measured results, the prototype fully covers the functional range of each joint, and covers the full range of motion of wrist radial deviation, wrist extension, and forearm supination/pronation; about 88% of full range of motion of elbow flexion/extension and wrist ulnar deviation; about 95% of full range of motion of wrist flexion. It is necessary to mention that due to some mistakes that had been made while machining the screws using a manual lathe, the screws are shorter than expected. Therefore, the prototype's workspace is further limited by the length of the screws. Since the functionality of the proposed mechanism's performance had been proven, the screws were not remade. The accuracy of the device is about 1.5 mm and the standard deviation (repeatability) is about 0.5.

In summary, the prototype proved that the proposed new mechanism and structure could reduce the overall size and the weight on user's arm, and increase the portability as a result. Also, the proposed mechanism can cover all four degrees-of-freedom with full coverage of their functional range of motion and at least 88% of their full range of motion.

6.2 **Future Work**

In this project, the prototype was never tested on human subjects. In order to further test out the reliability of the rehabilitation device, exercise providing tests based on human subjects would be an important step. However, due to unstable mechanical performance and unpredictable failure of 3D printed parts, the built prototype would not be recommended to use for human subject experiments. A newer version of the rehabilitation device made with metal parts or high density plastic parts would be strongly recommended for testing on humans. By using metal parts or high density plastic parts, the size and the weight of the device would be further reduced because metal parts and industrial level high density plastic parts have superior mechanical performance to 3D printed parts.

On another note, the drive cables used on the built prototype are considered to be much stronger than necessary. As a result, the hoses of these push-pull cables are too stiff. While doing experiments, hoses often have slight interference between each other, so some motions may not be occur smoothly. Also, hoses colliding ruined one connection on the device when doing device performance tests. From a functional point of view, a very thin nylon rope is good enough to accomplish this application. However, there was no push-pull type nylon rope available in market while this project was processing, and the selected cable was the best choice at that time as explained in a previous chapter. Therefore, finding a better flexible light weight Bowen cable or similar rope to replace the current steel cable would be one of the most meaningful improvements.

In addition, a sensory feedback intelligent decision making system will be the future direction of this research. Such system which may detect the status of the patient during training and adjust its output based on feedback signals will make the rehabilitation robots smarter and more user friendly than current prototype.

REFERENCES

[1] H. Fischer, . L. Kahn, . E. Pelosin, H. Roth, J. Barbas, W. Z. Rymer and D. Reinkensmeyer , "Can Robot-Assisted Therapy Promote Generalization of Motor Learning Following Stroke?: Preliminary Results," in *Biomedical Robotics and Biomechatronics*, Pisa, Italy, 2006.

[2] J. W. Krakauer, "Motor learning: its relevance to stroke recovery and neurorehabilitation," *Current Opinion in Neurology*, vol. 19, no. 1, pp. 84-90, 2006.

[3] W.-w. Liao, C.-y. Wu, Y.-w. Hsieh, K.-c. Lin and W.-y. Chang, "Effects of robot-assisted upper limb rehabilitation on daily function and real-world arm activity in patients with chronic stroke: a randomized controlled trial," *Clinical Rehabilitation,* vol. 26, p. 111–120, 2012.

[4] N. G. Kutner, . R. Zhang, A. J. Butler, S. L. Wolf and J. . L. Alberts, "Quality-of-Life Change Associated With Robotic-Assisted Therapy to Improve Hand Motor Function in Patients With Subacute Stroke: A Randomized Clinical Trial," *Physical Therapy,* vol. 90, pp. :493-504, 2010.

[5] S. E. Fasoli, H. I. Krebs, J. Stein, W. R. Frontera and N. Hogan, "Effects of robotic therapy on motor impairment and recovery in chronic stroke," *Archives of Physical Medicine and Rehabilitation,* vol. 84, no. 4, p. 477–482, 2003.

[6] Y.-w. Hsieh, C.-y. Wu, W.-w. Liao, K.-c. Lin, K.-y. Wu and C.-y. Lee, "Effects of Treatment Intensity in Upper Limb Robot-Assisted Therapy for Chronic Stroke A Pilot Randomized Controlled Trial," *Neurorehabilitation and Neural Repair,* vol. 25, pp. 503-511, 2011.

[7] P. S. Lum, C. G. Burgar, P. C. Shor, M. Majmundar and M. Van der Loos, "Robot-assisted movement training compared with conventional therapy techniques for the rehabilitation of upper-limb motor function after stroke," *Archives of Physical Medicine and Rehabilitation,* vol. 83, no. 7, p. 952–959, 2002.

[8] M. A. Finley, S. E. Fasoli, . L. Dipietro, J. Ohlhoff, L. MacClellan, . C. Meister, . J. Whitall, R. Macko, C. T. Bever, H. I. Krebs and N. Hogan, "Short-duration robotic therapy in stroke patients with severe upper-limb motor impairment," *Journal of Rehabilitation Research & Development,* vol. 42, p. 683–692, 2005.

[9] L. Dipietro, H. I. Krebs, B. T. Volpe, J. Stein, C. Bever, S. T. Mernoff, S. E. Fasoli and N. Hogan, "Learning, Not Adaptation, Characterizes Stroke Motor Recovery: Evidence From Kinematic Changes Induced by Robot-Assisted Therapy in Trained and Untrained Task in the Same Workspace," *Neural Systems and Rehabilitation Engineering,* vol. 20, no. 1, pp.

48 - 57, 2012.

[10] R. Colombo, F. Pisano, S. Micera, . A. Mazzone, C. Delconte, M. C. Carrozza, . P. Dario and G. Minuco, "Robotic Techniques for Upper Limb Evaluation and," *Neural Systems and Rehabilitation Engineering,* vol. 13, no. 3, pp. 311 - 324, 2005.

[11] L. E. Kahn, M. Averbuch, W. Z. Rymer and D. J. Reinkensmeyer, "Comparison of Robot-Assisted Reaching to Free Reaching in Promoting Recovery From Chronic Stroke," in *7th International Conference on Rehabilitation Robotics*, Evry, France, 2001.

[12] M. Shimodozono, . T. Noma, . Y. Nomoto, N. Hisamatsu, K. Kamada, . R. Miyata, . S. Matsumoto, A. Ogata, . S. Etoh, J. R. Basford and . K. Kawahira, "Benefits of a Repetitive Facilitative Exercise Program for the Upper Paretic Extremity After Subacute Stroke: A Randomized Controlled Trial," *Neurorehabilitation and Neural Repair,* pp. 1-10, 2012.

[13] L. E. Kahn, M. L. Zygman, W. Z. Rymer and D. J. Reinkensmeyer, "Effect of robot-assisted and unassisted exercise on functional reaching in chronic hemiparesis," in *Engineering in Medicine and Biology Society*, Istanbul, Turkey, 2001.

[14] L. E. Kahn, P. S. Lum, W. Z. Rymer and D. J. Reinkensmeyer, "Robot-assisted movement training for the stroke-impaired arm: Does it," *Journal of Rehabilitation Research & Development,* p. 619–630, 2006.

[15] N. Hogan, H. I. Krebs, J. Charnnarong, P. Srikrishna and A. Sharon, "MIT - MANUS : aworkstation for manual therapy and training II," in *Telemanipulator Technology*, Boston, MA, 1992.

[16] H. I. Krebs, M. Ferraro, S. P. Buerger, . M. J. Newbery, . A. Makiyama, . M. Sandmann, D. Lynch, B. T. Volpe and N. Hogan, "Rehabilitation robotics: pilot trial of a spatial extension for MIT-Manus," *Journal of NeuroEngineering and Rehabilitation,* 2004.

[17] M. J. Johnson, K. J. Wisneski, J. Anderson, D. Nathan and R. O. Smith, "Development of ADLER: The Activities of Daily Living Exercise Robot," Pisa, Italy, 2006.

[18] R. Q. Van der Linde, P. Lammertse, E. Frederiksen and B. Ruiter, "The HapticMaster, a new high-performance haptic interface," *Proc. Eurohaptics*, pp. 1-5, 2002.

[19] R. Loureiro, F. Amirabdollahian, M. Topping, B. Driessen and W. Harwin, "Upper Limb Robot Mediated Stroke Therapy—GENTLE/s Approach," *Autonomous Robots,* vol. 15, no. 1, pp. 35-51, 2003.

[20] M. Takaiwa and T. Noritsugu, "Development of Wrist Rehabilitation Equipment Using Pneumatic Parallel Manipulator," in *Robotics and Automation*, Kyoto, japan, 2005.

[21] J. Oblak, I. Cikajlo and . Z. Matjacic, "Universal Haptic Drive: A Robot for Arm and Wrist Rehabilitation," *Neural Systems and Rehabilitation Engineering*, vol. 18, no. 3, pp. 293 - 302, 2010.

[22] G. Rosati, P. Gallina and . S. Masiero, "Design, Implementation and Clinical Tests of a Wire-Based Robot for Neurorehabilitation," *Neural Systems and Rehabilitation Engineering*, vol. 15, no. 4, pp. 560 - 569, 2007.

[23] G. Rosati, P. Gallina, S. Masiero and A. Rossi, "Design of a new 5 d.o.f. wire-based robot for rehabilitation," in *Rehabilitation Robotics*, Chicago, IL, 2005.

[24] P. S. Lum, C. G. Burgar, M. Van der Loos, P. C. Shor, M. Majmuudar and R. Yap, "MIME robotic device for upper-limb neurorehabilitation in subacute," *Journal of Rehabilitation Research & Development*, vol. 43, p. 631–642, 2006.

[25] A. Toth and I. Ermolaev, "Robots with patients," *Engineer IT*, pp. 60-62, 2006.

[26] S. J. Spencer, J. Klein, K. Minakata, V. Le, J. E. Bobrow and D. J. Reinkensmeyer, "A low cost parallel robot and trajectory optimization method for wrist and forearm rehabilitation using the Wii," in *Biomedical Robotics and Biomechatronics*, Scottsdale, AZ, 2008.

[27] E. J. Koeneman, R. S. Schultz, S. L. Wolf, D. E. Herring and J. B. Koeneman, "A pneumatic muscle hand therapy device," in *Engineering in Medicine and Biology Society*, San Francisco, CA, 2004.

[28] K. Xing, Q. Xu, J. He, Y. Wang, Z. Liu and X. Huang, "A Wearable Device for Repetitive Hand Therapy," in *Biomedical Robotics and Biomechatronics*, Scottsdale, AZ, 2008.

[29] T. T. Worsnopp, M. A. Peshkin, J. E. Colgate and D. G. Kamper, "An Actuated Finger Exoskeleton for Hand Rehabilitation Following Stroke," in *Rehabilitation Robotics*, Noordwijk, Netherlands, 2007.

[30] D. J. Williams, H. I. Krebs and . N. Hogan, "A robot for wrist rehabilitation," in *Engineering in Medicine and Biology Society*, Istanbul, Turkey, 2001.

[31] T. Nef, M. Mihelj, G. Colombo and R. Riener, "ARMin - robot for rehabilitation of the upper extremities," in *Robotics and Automation*, Orlando, FL, 2006.

[32] T. Nef, M. Mihelj, G. Kiefer, C. Pemdl, R. Muller and R. Riener, "ARMin - Exoskeleton for Arm Therapy in Stroke Patients," in *Rehabilitation Robotics*, Noordwijk, Netherlands, 2007.

[33] A. Frisoli, L. Borelli, A. Montagner, S. Marcheschi, C. Procopio, F. Salsedo, M. Bergamasco, M. C. Carboncini, M. Tolaini and B. Rossi, "Arm rehabilitation with a robotic exoskeleleton in Virtual Reality," in *Rehabilitation Robotics*, Noordwijk, Netherlands,

2007.

[34] T. G. Sugar, J. He, E. J. koeneman, J. B. Koeneman, R. Herman, H. Huang, R. S. Schultz, D. E. Herring, J. Wanberg, S. Balasubramanian, P. Swenson and J. A. Ward, "Design and Control of RUPERT: A Device for Robotic Upper Extremity Repetitive Therapy," *Neural Systems and Rehabilitation Engineering,* vol. 15, no. 3, pp. 336 - 346, 2007.

[35] H. Kobayashi and K. Hiramatsu , "Development of muscle suit for upper limb," in *Robotics and Automation*, New Orleans, LA, 2004.

[36] A. Gupta and M. K. O'Malley, "Design of a haptic arm exoskeleton for training and rehabilitation," *Mechatronics, IEEE/ASME Transactions on,* vol. 11, no. 3, pp. 280 - 289, 2006.

[37] A. Gupta, M. K. O'Malley, V. Patoglu and C. Burgar, "Design, Control and Performance of RiceWrist: A Force Feedback Wrist Exoskeleton for Rehabilitation and Training," *The International Journal of Robotics Research,* vol. 27, pp. 233-251, 2008.

[38] A. U. Pehlivan, S. Lee and M. K. O'Malley, "Mechanical design of RiceWrist-S: A forearm-wrist exoskeleton for stroke and spinal cord injury rehabilitation," in *Biomedical Robotics and Biomechatronics*, Rome, Italy, 2012.

[39] B. F. Morrey, L. J. Askew and E. Y. Chao, "A Biomechanical Study of Normal Functional Elbow Motion," *The Journal of Bone & Joint Surgery,* vol. 63, no. 6, pp. 872-877, 1981.

[40] F. Lacquaniti and J. Soechting, "Coordination of arm and wrist motion during a reaching task," *The Journal of Neuroscience,* vol. 2, no. 4, pp. 399-408, 1982.

[41] A. P. Vasen, S. H. Lacey, M. W. Keith and J. W. Shaffer, "Functional Range of Motion of the," *The Journal of Hand Surgery,* vol. 20, no. 2, p. 288–292, 1995.

[42] J. Ryu, W. P. Cooney, L. J. Askew, K.-N. An and E. Y. Chao, "Functional ranges of motion of the wrist joint," *The Journal of Hand Surgery,* vol. 16, no. 3, p. 409–419, 1991.

[43] C. Neu, J. Crisco and S. Wolfe, "In vivo kinematic behavior of the radio-capitate joint during wrist flexion–extension and radio-ulnar deviation," *Journal of Biomechanics,* vol. 34, no. ELSEVIER, pp. 1429-1438, 2001.

[44] K. O. Matsuki, K. Matsuki, S. Mu, T. Sasho, K. Nakagawa, N. Ochiai, K. Takahashi and S. A. Banks, "In vivo 3D kinematics of normal forearms: Analysis of dynamic forearm rotation," *Clinical Biomechanics,* vol. 25, no. ELSEVIER, pp. 979-983, 2010.

[45] R. H. Brumfield and J. A. Champoux, "A Biomechanical Study of Normal Functional Wrist Motion," *Clinical Orthopaedics and Related Research,* vol. 187, pp. 23-25, 1984.

[46] D. J. Magermans, E. Chadwick, H. Veeger and F. v. d. Helm, "Requirements for upper extremity motions during activities of daily living," *Clinical Biomechanics*, vol. 20, no. ELSEVIER, pp. 591-599, 2005.